THE DIRT ON PALEOSOLS: SEDIMENTOLOGY AND PALEOCLIMATE INDICATORS WITHIN THE UPPER TRIASSIC CHINLE FORMATION, PARIA, UTAH

by

Megan Lynn Crocker

A thesis submitted to the faculty of
The University of Utah
in partial fulfillment of the requirements for the degree of

Master of Science

in

Geology

Department of Geology and Geophysics

The University of Utah

August 2012

The University of Utah Graduate School

STATEMENT OF THESIS APPROVAL

The thesis of **Megan Lynn Crocker**

has been approved by the following supervisory committee members:

Cari Johnson	, Chair	**6/12/12** Date Approved
Randall Irmis	, Member	**6/14/12** Date Approved
Erich Petersen	, Member	Date Approved

and by **Kip Solomon** , Chair of the Department of **Geology and Geophysics**

and by Charles A. Wight, Dean of The Graduate School.

ABSTRACT

The supercontinent Pangea was at its maximum subaerial exposure during the Late Triassic, causing an extreme paleoclimatic state. Seasonal, potentially monsoonal weather patterns affected the supercontinent and influenced depositional environments. The Upper Triassic Chinle Formation in Paria, Utah within Grand Staircase-Escalante National Monument provides an excellent exposure of rocks, mostly paleosols, which contain paleoclimatic indicators. This research presents an interpretation of Late Triassic depositional history and paleoclimate in southern Utah using stratigraphy, sedimentology, clay mineralogy, and QEMSCAN analyses from the Chinle Formation at Paria, Utah. The stratigraphic section was divided into three lithostratigraphic intervals based on outcrop descriptions, combined with petrographic, mineralogical, and geochemical analyses. The lowermost unit, interval 1 (0-68.8 m) contains low chroma paleosols with a relative abundance of the clay mineral kaolinite, reducing features and trace amounts of sand. Bk and k-horizons (pedogenic carbonate which forms from the repeated wetting and drying of soils) are present only in the upper 10 m of this interval. Interval 1 represents a more humid environment than the upper intervals, and potentially correlates to the Blue Mesa and Sonsela members of the Chinle Formation. The Bk and k-horizons in the lowermost interval may indicate that seasonality became more pronounced near the upper part of the section. Compared to interval 1, interval 2 (68.8-170.3 m) has fewer reducing features and an increase in pedogenic carbonate and slickensides, indicating climatic seasonality

was still present. Interval 2 probably correlates to the Petrified Forest Member of the Chinle Formation. Interval 3 (170.3-237.4 m) contains an increase in sand from fluvial deposits such as sandstone and conglomerates, and may correlate to the Owl Rock Member of the Chinle Formation. This change in deposition is most likely related to either avulsing river systems or ephemeral stream deposits. Overlying the Chinle Formation in Paria is the Wingate/Moenave Formations that contain eolian dune deposits in addition to fluvial and lacustrine environments indicating more prolonged aridity. The Chinle Formation at Paria, UT thus appears to support existing regional interpretations of a regional paleoclimatic shift from wetter to drier conditions as Pangea drifted northward through the Late Triassic.

TABLE OF CONTENTS

ACKNOWLEDGEMENTS

I am most grateful to Dr. Cari Johnson, who has given me guidance and support over the past 3 years. In addition I would like to thank my committee members, Dr. Randall Irmis and Dr. Erich Petersen for their advice and guidance. Also, I would like to thank Dr. William Parry and Dr. Allan A. Ekdale for all of their advice. Many thanks go to the Bureau of Land Management and Grand Staircase-Escalante National Monument for my research permit and permission to conduct fieldwork. I would also like my financial contributors, ExxonMobil, the Geological Society of America, and the University of Utah Geology and Geophysics Department. To all my field assistants, Ian Semple, Jared Gooley, Casey Kidney, Warren Schaub, and Carrie Levitt, without your help I would not have been able to accomplish what I did! Last but not least, I would like to thank my family for their continued support of all my endeavors. Without their love and support I would not be where I am today.

INTRODUCTION

Non-marine depositional systems are complex but potentially informative about landscape evolution and paleoclimate (Kraus, 1999). The Upper Triassic Chinle Formation is of particular relevance to nonmarine systems and paleoclimate: it consists of fluvial and minor lacustrine depositional environments with extensive exposures throughout the Colorado Plateau (Stewart et al., 1972; Blakey and Gubitosa, 1983; Dubiel, 1987; Matthews et al., 2007). Despite many decades of research on the Chinle Formation, critical questions remain regarding paleoclimate and depositional environment, particularly in the chosen study area of southern Utah, and the long-term evolution of alluvial systems as related to various controlling factors such as climate.

The purpose of this study is to use sedimentology, paleosol morphology, detailed petrography, and clay mineralogy/geochemistry to reconstruct the depositional history and paleoclimate of the Chinle Formation in south-central Utah. This research focuses on the Chinle Formation near Paria, Utah, in Grand Staircase-Escalante National Monument, in order to: a) document stratigraphy and sedimentology with a focus on clay mineralogy of paleosols; b) attempt to provide stratigraphic correlations for a better regional picture of Chinle Formation evolution; c) relate these findings to the broader topics of ancient non-marine records of changing landscapes and climate; and d) compare different approaches to mineralogical investigations of fine grained rocks, specifically using x-ray diffraction (XRD) and QEMSCAN, an automated SEM-based mineral characterization

system (Pirrie et al., 2003). I hypothesize that alluvial successions and paleosols in the study area contain paleoclimatic indicators that reveal a monsoonal climate that intensified near the end of the Late Triassic and caused more widespread aridity into the Jurassic (Parrish, 1993; Tanner, 2000).

Paleoclimate studies are important given the modern context of global warming. Anthropogenic forces are commonly cited as having massive impacts on earth systems (Wilkinson, 2005), including changes in atmospheric carbon dioxide that drive global warming (Karl and Trenberth, 2003; Mitchell et al., 2006). Sedimentary rocks and ancient depositional systems provide a critical context for modern climate change, because of the unique 'deep time' insight that can be gained only from the geologic record (McCarthy, 2000; Freeman, and Goldhaber, 2011; Erwin et al., 2012). In addition to the deep time perspective, the Late Triassic is a time of increased levels of carbon dioxide (Prochnow et al., 2006), which makes it even more relevant to modern global warming. Recent observations of the modern and the Holocene do not provide thorough information regarding climatic responses to massive, rapid input of CO_2. In order to understand this, a proper analogue needs to be a time period(s) where CO_2 concentrations were as high or higher than today (Zachos et al., 2008).

Although paleoclimate studies are critically important, interpreting ancient climate from the rock record is nontrivial, involving the interpretation of various proxies for environmental and climatic change. For example, the isotopic composition of soil carbonate is a potential indicator of atmospheric partial pressure of carbon dioxide (pCO_2), and this can be determined by studying the $\delta^{13}C/^{12}C$ isotopic ratios of organic carbon in paleosols (Cerling, 1991; Elliot 1997; Tanner, 2001; Cleveland et al., 2008a).

Similarly, the depth of carbonate from the paleo-surface in a paleosol is related to mean annual precipitation. The oxygen isotope composition within the pedogenic carbonate is determined by precipitation; therefore pedogenic carbonate isotopes can estimate mean annual precipitation (MAP) (Retallack, 2005; Prochnow et al., 2006; and Breecker, 2010). Soil clay mineralogy is also influenced directly by temperature and rainfall. Authigenic clays such as halloysite, sepiolite, kaolinite and smectite are generally more useful in interpreting paleoclimate than derived clays such as vermiculite, illite/smectite (I/S) clay, illite, and chlorite (Curtis, 1990).

Nonetheless, paleoclimate indicators are proxies, and therefore diagenetic and other effects must be carefully considered. For example, volcanic glass is unstable at near surface environments and will readily alter to montmorillonite, a smectite clay (Schultz, 1963). Smectite can also give indications of a seasonal climate if the clay is formed *in situ* in a paleosol (Schaetzl and Anderson, 2005). In order to determine if the smectite is derived from a volcanic source, is authigenic, or affected by diagenesis, analyses in addition to x-ray diffraction (which only identifies the clay species) must be performed. A thin section or epoxy plug needs to be viewed to understand the interactions of the grains, textures, diagenetic effects, etc. Without proper analytical techniques, interpretations regarding paleoclimate and smectite clays may be misleading and incomplete. Similarly, isotopic compositions can be modified during diagenesis, carbonate nodules that contain sparry calcite are excluded from studies due to the high likely of being recrystallized disguising the true $\delta^{13}C/^{12}C$ values needed to estimate the pCO_2 (Cleveland et al., 2008).

The Upper Triassic Chinle Formation of southern Utah contains exposures that may give indications of how paleoclimate influenced landscape evolution over time. This rock unit is particularly relevant to the issue of changes in climate, in part because its deposition records a major latitudinal shift that may result in changing paleoclimate signals (Whiteside et al., 2011) (i.e., development and then intensifying of monsoonal conditions; see Dubiel, 1989) in a nonmarine succession. The Chinle Formation near Paria, Utah in Grand Staircase-Escalante National Monument (Figure 1) is understudied compared to many other Chinle Formation exposures in the region. The study area is also ideal for studies of depositional environments and paleoclimate because it includes a relatively thick succession (~240 m) of exposed rock, mainly mudstone and siltstones of stream and floodplain origin, which spans most of the Chinle Formation depositional record, from the basal Shinarump Member to the Owl Rock Member (Blakey, personal communication, 2011).

Figure 1. Inset: Map of Utah, SLC = Salt Lake City. Small black box is the general location of the field area, expanded to the right in a Google Earth image. Outcrop of study is located within the larger black box. Highway 89 is in red with connecting access road in black.

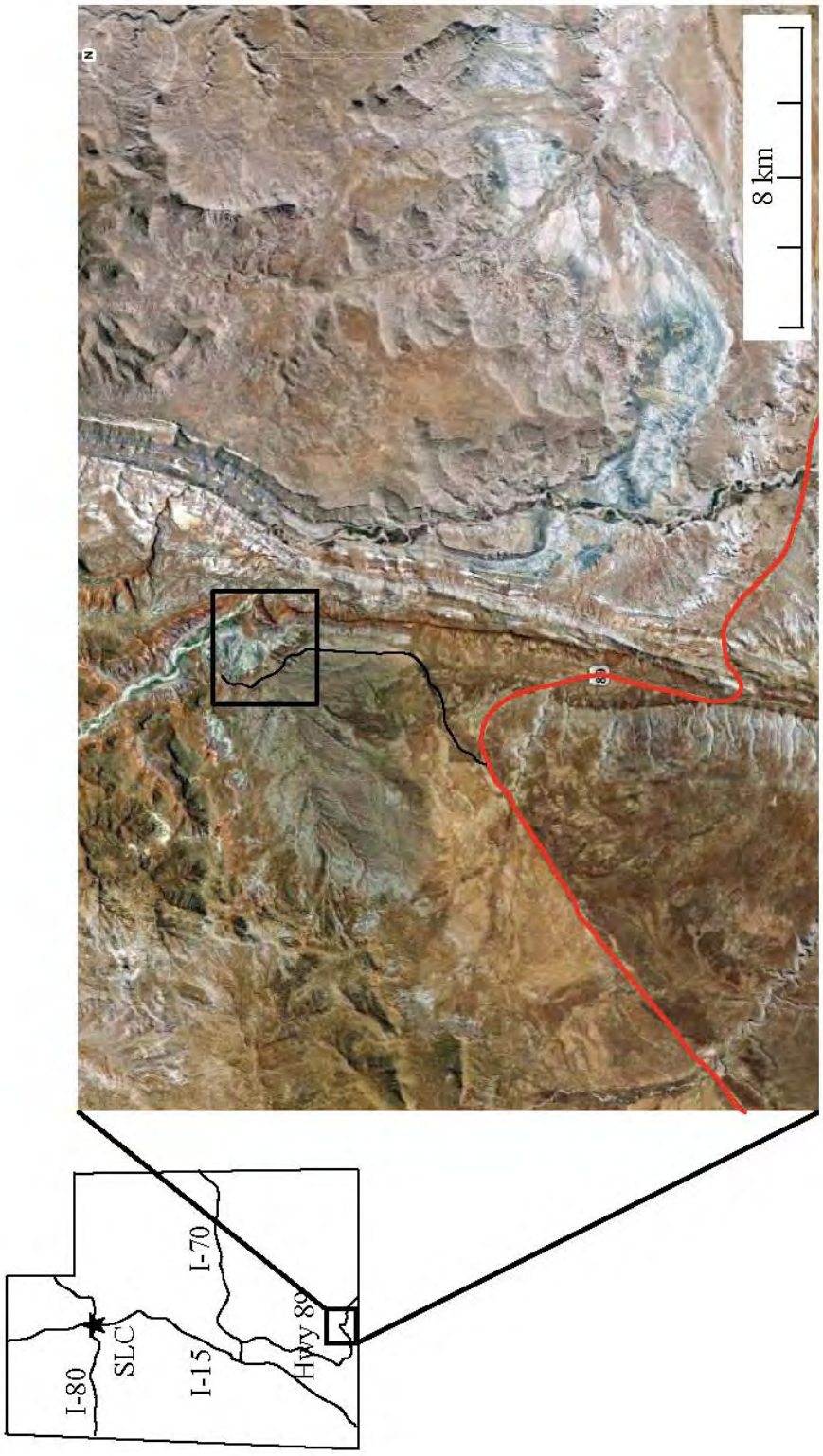
8 km
I-80
SLC
I-15
I-70
Hwy 89

GEOLOGIC SETTING

Paleogeography

The Chinle Formation was deposited on the western edge of the supercontinent Pangea during the Late Triassic (Blakey and Gubitosa, 1983). The Chinle Formation basin was a nonmarine continental backarc basin bound by the Ancestral Rockies to the east and the Cordilleran arc to the west and south (Figure 2 and Figure 3) (Blakey and Gubitosa, 1983). The basin migrated from about 5-15 degrees north of the paleoequator during deposition of the Chinle Formation (Figure 4) (Van der Voo et al., 1976; Kent and Olsen 1997; Kent and Irving, 2010).

The active Cordilleran arc provided some input for the volcaniclastic material present in the Chinle Formation (Stewart et al., 1986). However the fluvial deposits of the Chinle Formation show dominantly north or northwest paleocurrent directions indicating a southerly source as well (Blakey and Gubitosa, 1983). Pebbles and cobbles >25 cm, some comprised of altered vitric tuffs that altered to clays were deposited in the conglomeratic layers in the lower Chinle Formation suggesting they could not have traveled far (Stewart et al., 1986; Riggs et al., 1993; Basdekas, 1993). Volcanic lithics in the study area of Paria, Utah are particularly pumaceous and therefore also suggest a more local source (Basdekas, 1993). The Mogollon Highlands may represent this source area (Figure 2), but the U-Pb isotope geochronology of volcanic rocks found in southern Arizona and northern Sonora may indicate that this source is too young (~25 million

years) to have influenced Chinle Formation-aged rocks (Stewart et al., 1986). The Mogollon Slope is potentially a better termed used for this region because the highlands did not fully form until later in the Jurassic and into the Cretaceous (Bilodeau, 1986), although more recent authors still include the Mogollon Highlands on paleogeographic maps of the Triassic (e.g., Dickinson and Gehrels, 2008). Chinle Formation sedimentation ceased when Laurentia (the North American craton) drifted into desert paleolatitudes and Jurassic age sedimentation began (Dickinson and Gehrels, 2008).

Stratigraphy

The Chinle Formation is up to 520 meters (~1,700 feet) thick in east-central Arizona and west-central New Mexico, and decreases in thickness to the north and northeast (Stewart et al., 1972). It is fully nonmarine due to tectonic uplift during the Late Triassic (Blakey and Gubitosa, 1983). The Chinle Formation lies unconformably above the Early to Middle Triassic Moenkopi Formation, the Tr-3 unconformity (Figure 5), (Pipiringos and O'Sullivan, 1978) or the Permian Cutler Group (Stewart et al., 1972). The late Middle Triassic and early Upper Triassic rocks were either not deposited or were eroded away before Upper Triassic rocks were deposited (Dubiel, 1994). The Lower Jurassic Wingate and Moenave Formations unconformably overlie the Chinle Formation (the J-0 unconformity; Figure 5) (Pipiringos and O'Sullivan, 1978; Dubiel, 1991).

Radioisotopic age constraints on Chinle deposition are sparse, due to lack of widespread volcanic units suitable for dating (Mundil, 2007). Recent research has shown that the Chinle Formation deposition is probably mostly Norian (~227-228 Ma) and Rhaetian and that the Norian may have spanned upwards of 20 Ma (Muttoni et al., 2004; Furin et al., 2006; Irmis et al., 2011). The Blue Mesa Member found in Six Mile Canyon

of western New Mexico contains U-Pb zircon dates of ~218 Ma (Ramezani et al., 2011; Irmis et al., 2011) so at least the beginning of the Chinle Formation deposition is before 218 Ma. The end of the Triassic is an important date to constrain due to the decline in biodiversity and flood basalt volcanism (Morton and Hesselbo, 2008; Schoene et al., 2010). Recent dating of the end of the Triassic to Jurassic boundary is ~201.6 Ma, determined from zircon bearing volcanic tuffs in northern Peru (Schalteggar et al., 2008; Schoene et al., 2010). However it is not clear that the Chinle Formation reached the Triassic-Jurassic boundary and it is more likely that the Moenave Formation contains the transition from the Triassic to the Jurassic (Donohoo-Hurley et al., 2007, 2010).

The Chinle Formation as a whole consists of a basal sandstone/conglomerate, and overlying strata are predominantly sandstones and variegated mudstones (Stewart et al., 1972; Blakey et al., 1986) (Figure 5). In general, the lower units of the Chinle Formation are typically bentonitic claystone, clayey sandstones, and thin widespread sandstones and conglomerates, whereas the upper Chinle Formation units are predominantly siltstone/claystone red-beds with sandstones and minor conglomerates (Stewart et al., 1972).

Petrified Forest National Park in Arizona is one of the most thoroughly studied regions for the Chinle Formation (Figure 6 and 7). The lithostratigraphy of the Chinle Formation in this area has been debated and refined in more recent literature, in part because outcrops are found throughout the length of the park but are not continuous (Murray, 1990; Heckert and Lucas, 2002; Woody, 2006; Martz and Parker, 2010) despite their excellent exposure. Due to the discontinuity and large extent of Chinle Formation outcrops regionally (Figure 7), it is difficult to correlate specific member terminology

across regions; this is a challenge in the study area of Paria, UT. Fewer studies focus on the Chinle Formation strata in Utah; the main areas of previous study are within Canyonlands National Park of southeastern Utah (Figure 6) (Blakey and Gubitosa, 1993); the Paradox Basin (Prochnow, 2005, Prochnow, 2006; Matthews, 2007); Lisbon Valley of southeastern Utah (Dubiel, 1993, Hazel, 1994); the San Rafael Swell of eastern Utah (Abdel-Gawad and Kerr, 1963; Beer, 2005); the Circle Cliffs of southern Utah (Dubiel, 1987; Brown, 2003; Beer, 2005) and near Vernal, Utah (Stewart et al., 1972, Dubiel, 1992). Thus the Chinle Formation of southwestern Utah, specifically near Paria, is especially important because few studies have been concentrated there beyond basic stratigraphic work (Stewart et al., 1972; Blakey and Gubitosa, 1983; Basdeskas, 1993; Parker et al., 2006).

A significant challenge in conducting regional correlations of the Chinle Formation involves the existing stratigraphic nomenclature. Member nomenclature has been informally assigned to some of the exposures in Paria but distinct member lines are difficult to define because the type sections are found much further away and do not correlate well. A loosely defined nomenclature for the Paria area is used in this study (Ron Blakey, personal communication) (Figure 8) the details of which are found in the interpretations section. A cross-section from Paria to Lisbon Valley, Utah shows the Shinarump, Petrified Forest, and Owl Rock Members located in Paria, Utah (Figure 9) (Blakey and Gubitosa, 1983). Two additional members, the Blue Mesa and Sonsela, have been recognized in the area more recently (Blakey, personal communication, 2011).

Paleoclimate

The Permian-Triassic interval is considered to represent an extreme paleoclimatic state (Dubiel et al., 1991). Pangea's extent reached from 85° N to 90° S paleolatitude (Zielgler et al., 1983); therefore the continent cut across and disrupted every zone of atmospheric circulation (Dubiel, 1991). In addition, sea level was low (Vail et al., 1977: Haq et al., 1987). The large exposure of land, especially in the low mid-latitudes, and the warm seaway provided a source of moisture and maximized summer heating in the circum-Tethyan part of the continent (Parrish, 1993; Sellwood and Valdes, 2006). Figure 10 highlights the central portion of Pangea during the Late Triassic to highlight Walter's Biomes that were modeled by Sellwood and Valdes, 2006. The location of the field area borders between summerwet-tropical humid and desert-subtropical arid.

The western North American climate during the Late Triassic has long been debated. A widely accepted interpretation cites a monsoonal climate, e.g., a climate with strongly seasonal influences (Kutzbach and Gallimore, 1989; Dubiel, 1989; Hasiotis and Dubiel, 1994; Tanner and Lucas, 2006). A monsoonal climate is not only defined by seasonality, it is caused by the cross-equatorial flow circulation resulting from the thermal and pressure contrasts of the winter and summer hemispheres (Dubiel et al., 1991). The monsoonal climate hypothesized for the Triassic was originally based on the global distribution of Triassic aged rocks that were red-beds and evaporites (Robinson, 1971). A red-bed is considered to be a mudstone, siltstone, or sandstone that consists of detrital grains in a reddish-brown mud matrix or cemented by reddish-brown ferric oxide precipitates (Van Houten, 1964). Red-beds are important in interpreting paleoclimate because the reddening of alluvial and fluvial deposits occurs from the alternating of wet

and dry climates. During wet cycles, iron can be easily leached from iron-bearing minerals (Parrish, 1993). Some authors have used the term “megamonsoonal” to describe the Pangean climate (Kutzman and Gallimore, 1989; Dubiel et al., 1991; Parrish, 1993; Curtin and Parrish, 1999; Smith and Swart, 2002). Although there is disagreement regarding if Pangea really had a megamonsoonal climate, many workers think there was likely a monsoonal climate or at least an increase in seasonality over the duration of the Late Triassic (e.g., Dubiel, 1991; Tanner, 2000).

By the end of Chinle Formation deposition, the Owl Rock, Church Rock, and Rock Point Members are hypothesized to reflect the increasing seasonality of the climate during the Late Triassic (Blakey and Gubitosa, 1983; Dubiel, 1989). Capping these members are the Triassic/Jurassic-aged Wingate Sandstone and/or the Moenave Formations that represents large amounts of wind-blown sand that buried any remaining Chinle Formation streams under an eolian sand sea (Blakey and Gubitosa, 1983; Clemmensen et al., 1989).

Paleoecology

Paleontological evidence aids in the interpretation of paleoclimate due to the fact that some organisms are adapted for very specific environments. Flora, fauna, and ichnofossils have been found stratigraphically throughout the Chinle Formation but are most prolific in members such as the Petrified Forest (Parrish, 1989). A listing of major flora groups in the Chinle Formation includes fungi, lycopods (tree), sphenophytes (horsetails), ferns, conifers, ginkos, and bennettitaleans, mainly from below the Sonsela Sandstone in Petrified Forest National Park in Arizona (Ash, 1972; Ash 2005). Abundant vertebrate fossils have been found in the Petrified Forest Member at Ghost Ranch, NM,

predominantly *Coelophysis bauri*. Over a thousand individuals of this small theropod have been found at this quarry (Schwartz and Gillette, 1994). Ichnofossils within the Chinle Formation include *Scoyenia* (deposit feeding insect larvae)*, Koupichnium* (horseshoe crab), *Camborygma* (crayfish), *Cylindricum* (bee trace) found in the Petrified Forest National Park (Hasiotis and Dubiel, 1994). These organisms represent specific niches they can survive which indirectly indicates the prevailing paleoclimate conditions.

In southern Utah, sphenopsids, ferns, conifers, and benettitaleans are found within the Shinarump and Temple Mountain Members (Ash, 1975; Ash, 1987; Ash, 2001; Ash, 2003). Also, in the upper portion of the Chinle Formation, fragmentary ferns, bennettitaleans, and sphenophytes occur within fallen blocks of either the Owl or Church Rock members (Milner, 2006). Within the Circle Cliffs of Grand Staircase-Escalante National Monument, a bed within the Petrified Forest Member contains abundant fossil wood from the species *Araucarioxylon arizonicum* and *Woodworthia arizonica.* The Shinarump, Monitor Butte, Moss Back, and Petrified Forest members contain vertebrate fossils that are fragmentary and are identified from more complete skeletons in other regions. These include phytosaurs*,* small archosaurs, and metoposaurid amphibian (Parrish and Good, 1987). Vertebrate fossils found more recently in Utah for the first time include the aetosaur *Desmatosuchus* and a *Paratypothorax*-like species (Parker et al., 2006). Even less attention has been given to the Chinle Formation of southwestern Utah, and only fragmentary fossils have been described from this area (Dubiel and Brown, 1993; DeBlieux et al., 2006).

Fossil flora has importance when interpreting paleoclimate because plants can give indications of paleoenvironmental conditions (Ash and Creber, 1992). Growth rings

in trees, for example, reflect the climate in which it grew (Creber and Chaloner 1985; Ash, 1992). Trees that grow in current monsoonal systems have poorly developed or totally lack growth rings (Fahn and Werker, 1990; Ash, 1992). The paleoclimate of the Petrified Forest National Park has been interpreted through fossil trees and was originally deemed to be without periodic seasonal influence (Ash and Creber, 1992). Subsequent work indicates that fossil ferns found in the park lived under a humid subtropical to tropical climate (possibly monsoonal), in part based on the present-day occurrence of living relatives in wet/monsoonal climates in Asia (Ash, 2001). However, plants growing in riparian environments within incised valley-fill sequences have an increased likelihood of being preserved compared to plants on fluvial floodplains. Thus the impacts of local hydrologic conditions must be addressed in addition to regional climate (Demko et al., 1998).

Ichnofossil tiering of trace fossils in paleosols can have direct relationship to paleoclimate if their post depositional paleohydrologic conditions are favorable to preservation. Controlling factors to trace fossil preservation as well as organism distribution include soil moisture content and the paleo-water table. The paleohydrologic system that the tiering records can be compared locally and regionally to reconstruct the amount of water in the substrate which shows the seasonal and annual precipitation trends of Pangea (Hasiotis and Dubiel, 1994).

Figure 2. Paleogeographic map of western North America during the Late Triassic. Local source areas for the Chinle Formation include the Ancestral Rockies Highlands, the Mogollon Highlands, and an unnamed regional source from New Mexico and Texas. Modified from Dickinson (1981), Blakey and Gubitosa (1983), and Prochnow et al. (2006).

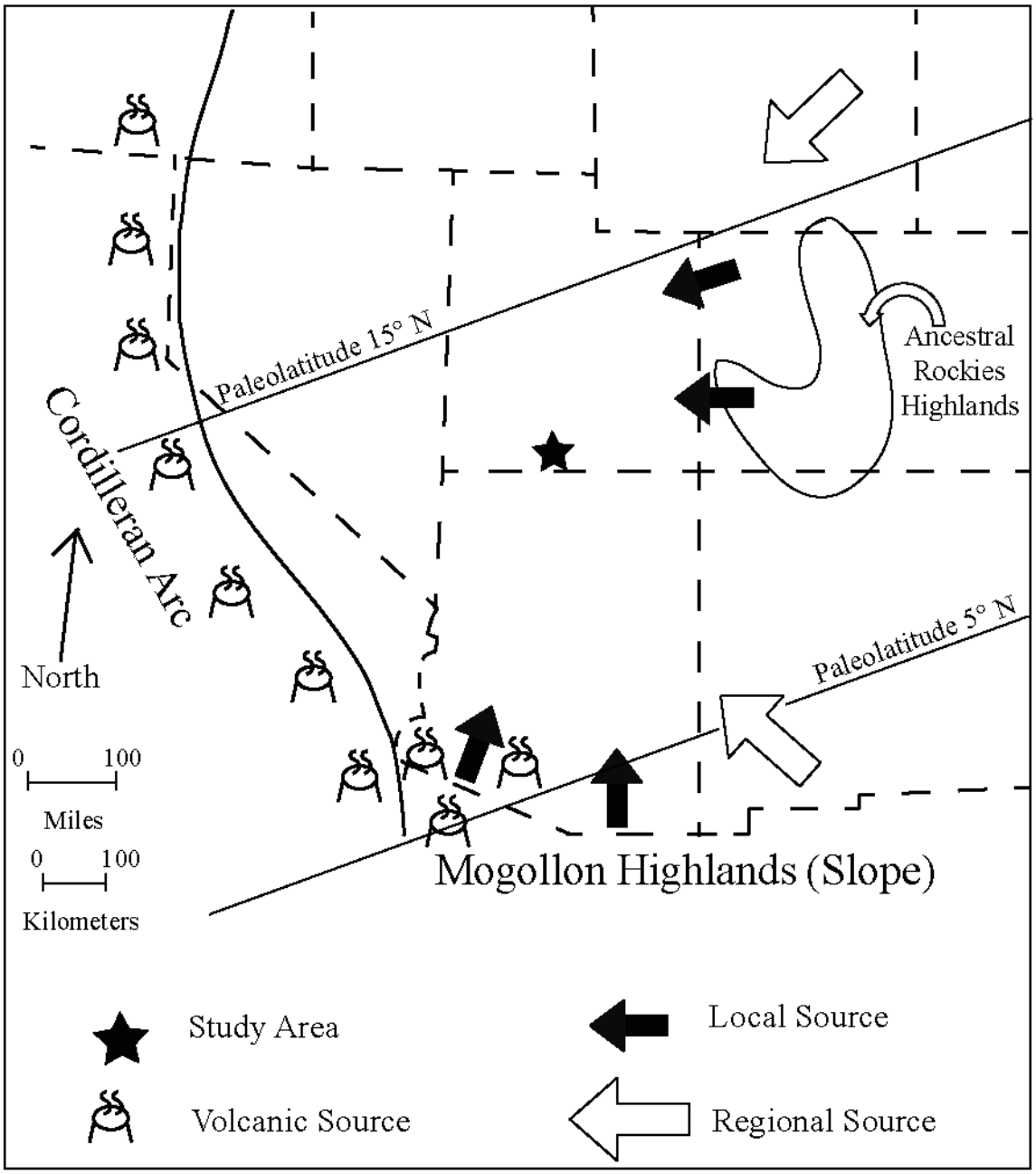
Paleolatitude 15° N
Ancestral
Rockies
Highlands
Cordilleran Arc
North
Paleolatitude 5° N
0 100
Miles
0 100
Kilometers
Mogollon Highlands (Slope)
Study Area
Local Source
Volcanic Source
Regional Source

Figure 3. Above: Late Triassic paleogeographic reconstruction of the world. Inset is enlarged on the right with the black star showing the approximate location of study area. Adapted from Blakey (2011).

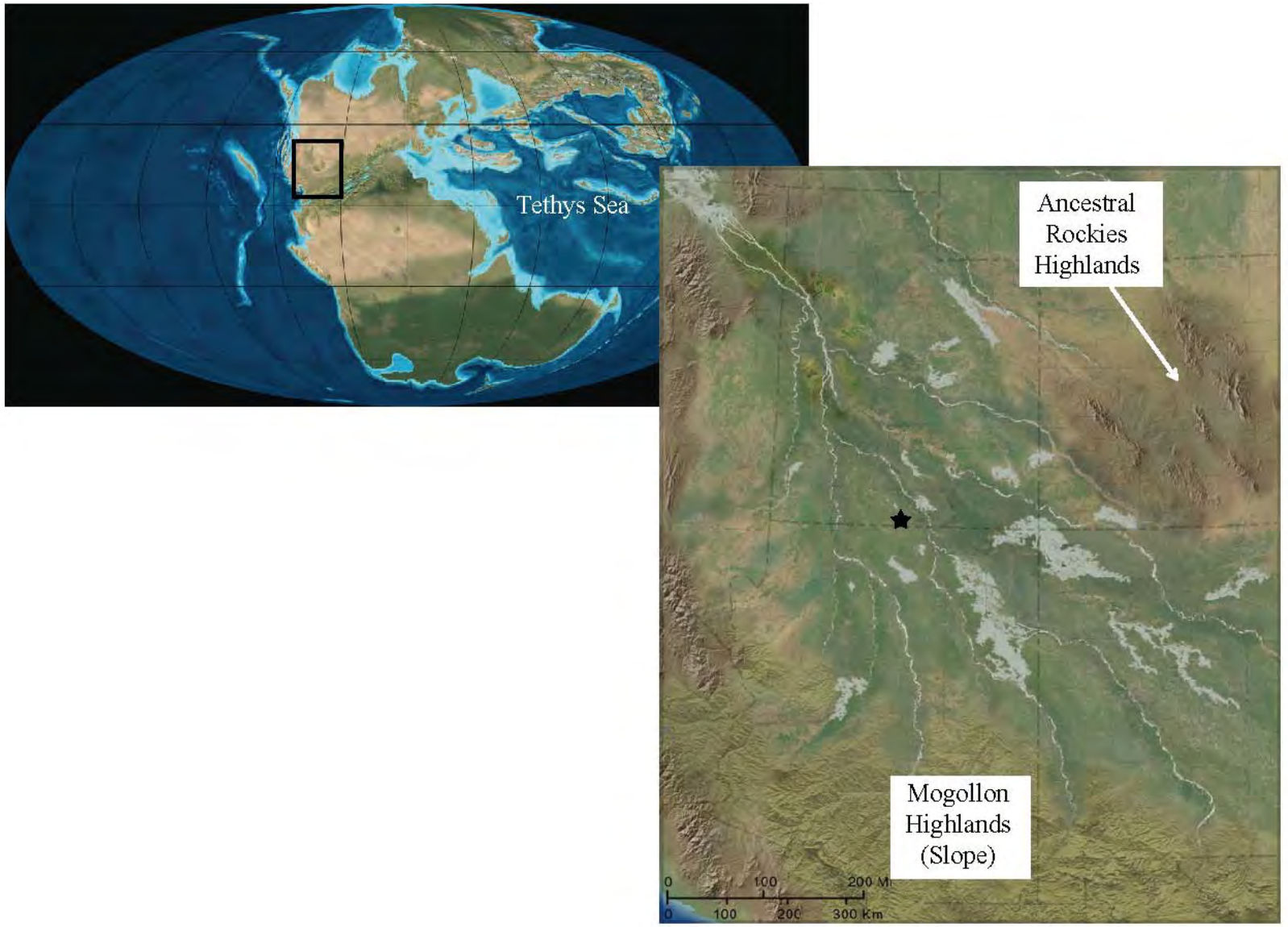
Tethys Sea
Ancestral
Rockies
Highlands
Mogollon
Highlands
(Slope)
0
100
200 M
0
100
200
300 Km

Figure 4. Paleogeographic reconstruction of the area above and below the equator (0) of Pangea. The red star represents the approximate location of Paria, Utah as it migrated latitudinally from the Early to Middle Triassic to the Early Jurassic. Images modified from Blakey (2012).

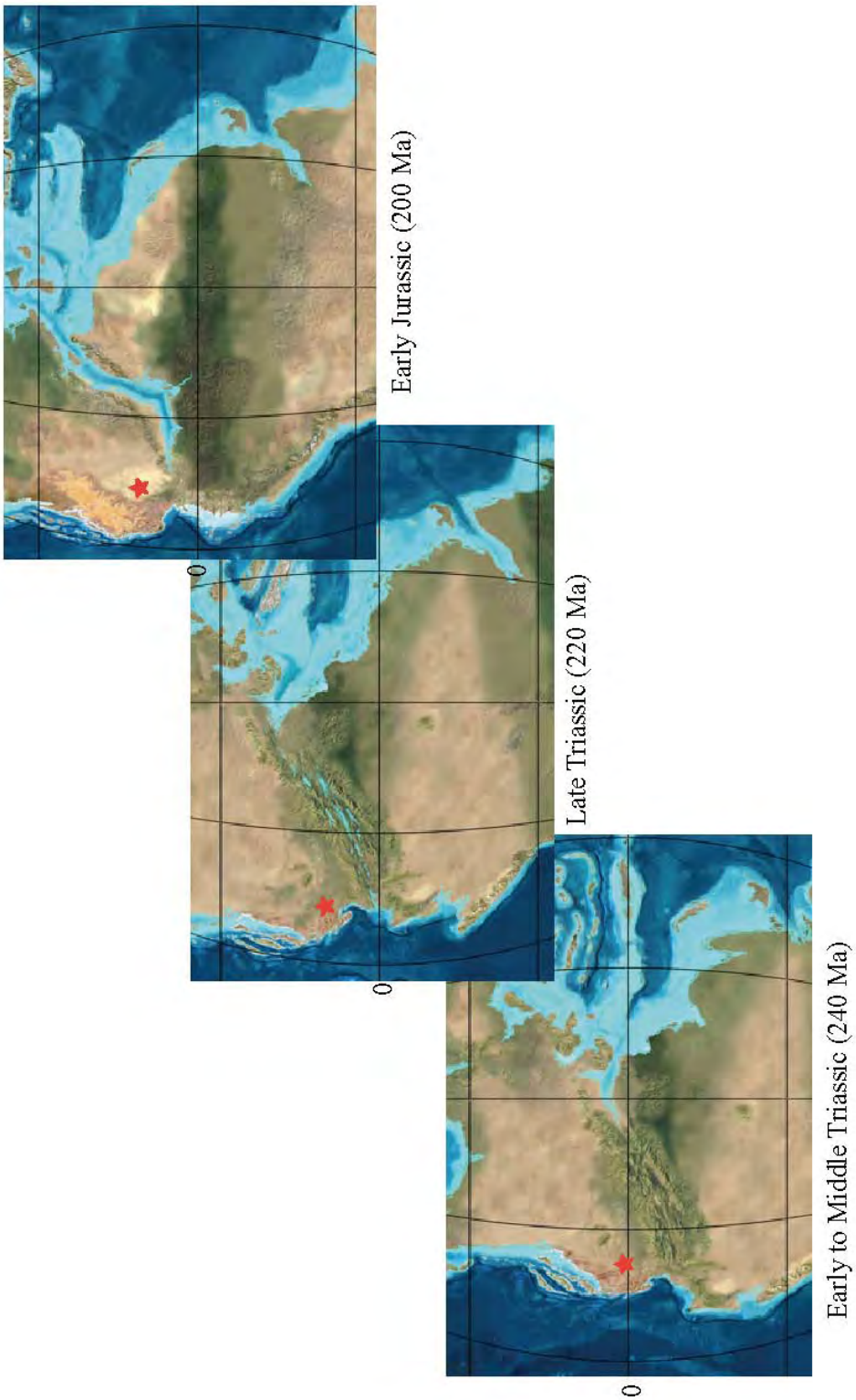
Early Jurassic (200 Ma)
Late Triassic (220 Ma)
Early to Middle Triassic (240 Ma)
0
0
0

Figure 5. Triassic and Jurassic Stratigraphy of the Smoky Mt. 30'x 60' Quadrangle. Adapted from Doelling and Willis (2006).

System and Series		Formation	Member	Symbol	Thickness (m)	Lithology
Jurassic	Lower	Moenave Formation	Springdale SS	$^{J}T_{R}m$	90-134	
			Dinosaur Canyon			
Triassic	Upper	Chinle Formation	Upper	T_{Rcu}	150-200	J-0 unconformity
			Lower	T_{Rcl}	0-47	
			Shinarump			Tr-3 unconformity
	Lower	Moenkopi Formation	Upper Red	T_{Rmu}	38	
			Shnabkaib	T_{Rms}	67	
			Middle Red	T_{Rmm}	113	
			Lower Red/ Virgin Limestone	T_{Rml}	76	
			Timpoweap	T_{Rmt}	6-37	

Figure 6. The main areas of previous studies (see text) of the Chinle Formation in Utah and the field area of this study, Paria.

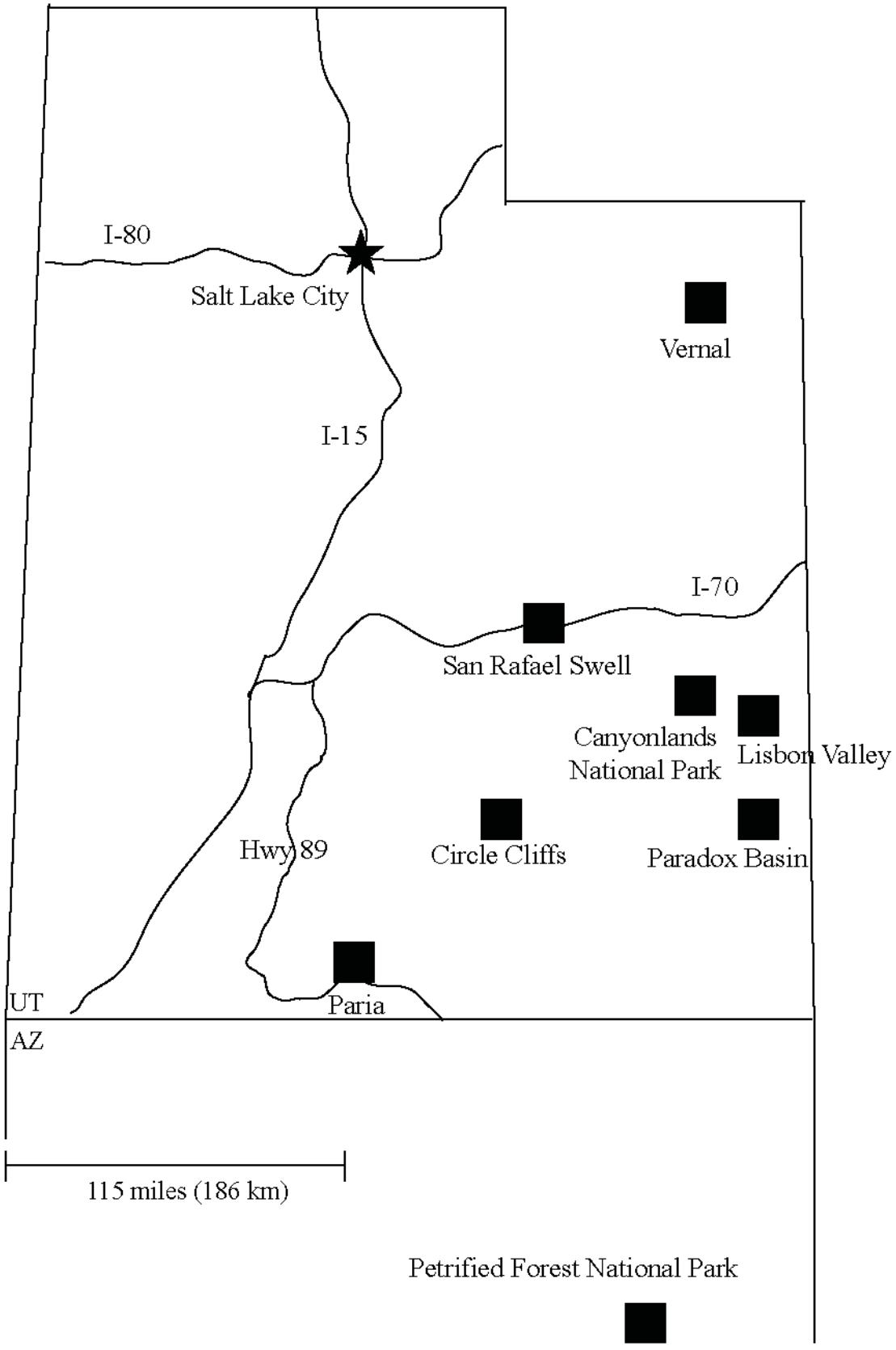
I-80
Salt Lake City
Vernal
I-15
I-70
San Rafael Swell
Canyonlands
National Park
Lisbon Valley
Hwy 89
Circle Cliffs
Paradox Basin
Paria
UT
AZ
115 miles (186 km)
Petrified Forest National Park

Figure 7. Distribution of Chinle aged outcrops in the four corners region. Red star is the location of this study. Blue star is the Petrified Forest National Park (PFNP). Adapted from Tanner and Lucas (2006) and Stewart et al. (1972).

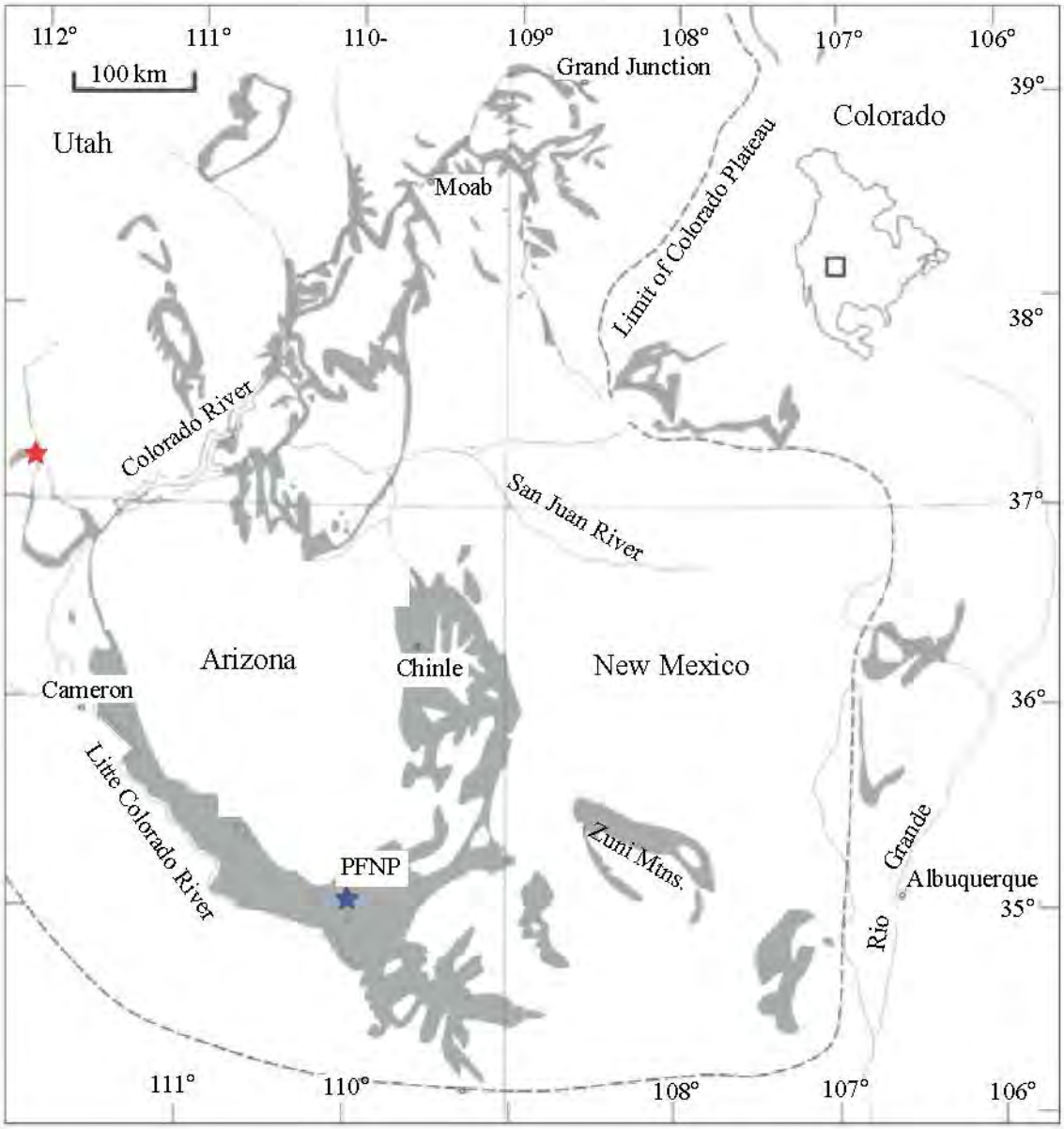
112°
111°
110-
109°
108°
107°
106°
100 km
Grand Junction
39°
Utah
Colorado
Moab
Limit of Colorado Plateau
38°
Colorado River
San Juan River
37°
Arizona
Chinle
New Mexico
Cameron
36°
Little Colorado River
PFNP
Zuni Mtns.
Rio Grande
Albuquerque
35°
111°
110°
108°
107°
106°

Figure 8. Triassic rocks found in Paria, Utah with the informal intervals from this study labeled on the outcrop photo below. Stratigraphic section adapted from Doelling and Willis (2006) and Blakey (2010).

System and Series		Formation	Possibily Correlative Members	Informal Interval	Thickness (m)	Lithology
Triassic	Upper	Chinle Formation	Owl Rock	3	150-200	
			Petrified Forest	2		
			Sonsela	1	100	
			Blue Mesa			
			Shinarump	n/a		

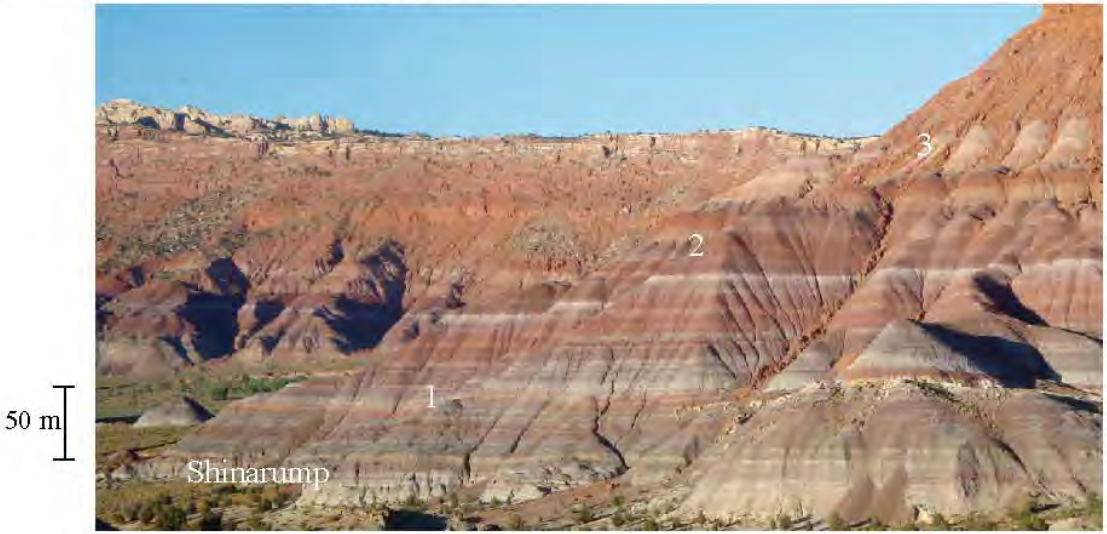

Figure 9. Generalized stratigraphic cross-section from Paria, Silver Falls, Jacobs Chair, and Lisbon Valley, southern Utah. Towns of Escalante and Monticello, Utah, and Page, AZ for reference. Adapted from Blakey and Gubitosa (1983).

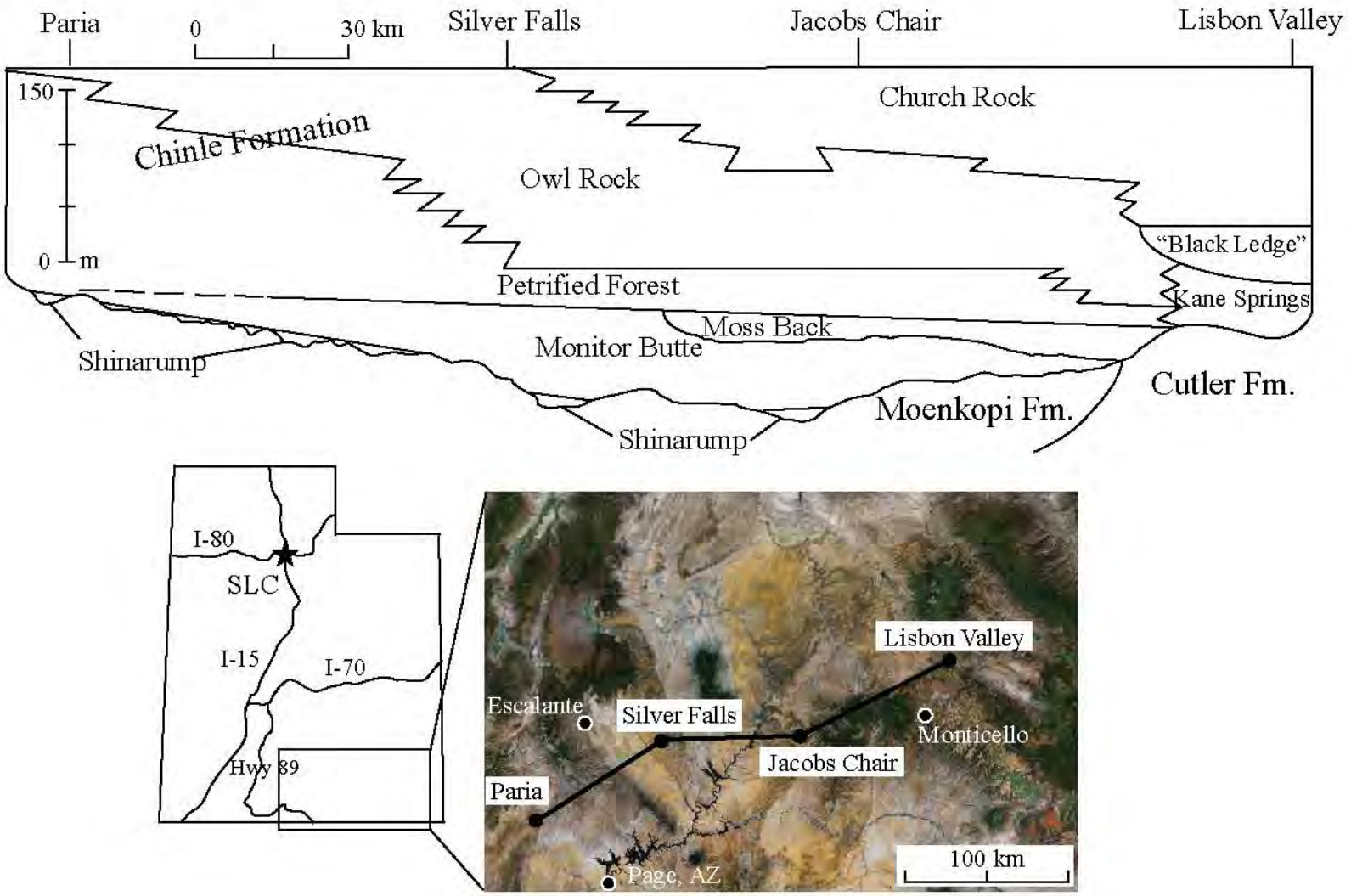
Paria
0
30 km
Silver Falls
Jacobs Chair
Lisbon Valley
150
0
m
Chinle Formation
Church Rock
Owl Rock
"Black Ledge"
Petrified Forest
Kane Springs
Moss Back
Monitor Butte
Shinarump
Cutler Fm.
Moenkopi Fm.
Shinarump
I-80
SLC
I-15
I-70
Hwy 89
Lisbon Valley
Escalante
Silver Falls
Monticello
Jacobs Chair
Paria
Page, AZ
100 km

Figure 10. The Walter biome zones as modeled by Sellwood and Valdes (2006, adapted) using precipitation and temperature with subsequent legend.

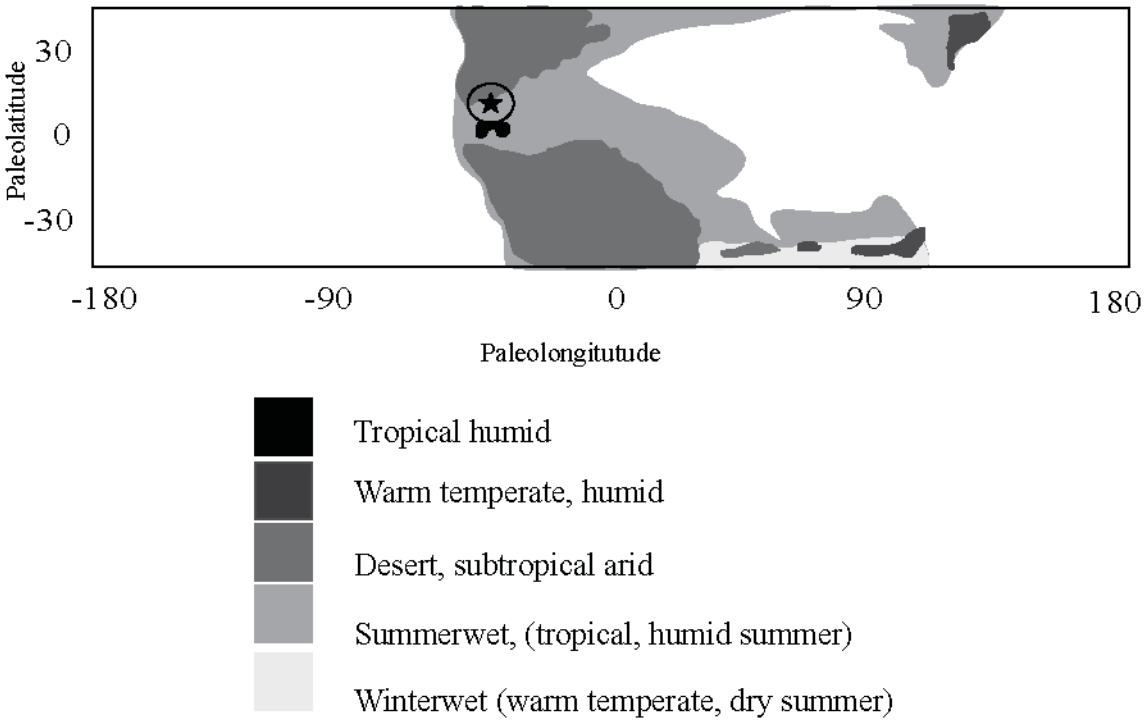
30
0
-30
Paleolatitude
-180
-90
0
90
180
Paleolongitutude
Tropical humid
Warm temperate, humid
Desert, subtropical arid
Summerwet, (tropical, humid summer)
Winterwet (warm temperate, dry summer)

METHODS

The main goal of this study is to determine if paleoclimatic interpretations can be made from studying the Chinle Formation paleosols at Paria, Utah. In order to accomplish this, a detailed sedimentologic analysis of the paleosols was performed in the field with periodic sampling. Twenty eight samples were analyzed using x-ray diffraction (XRD) analysis and 16 samples were analyzed using Quantitative Evaluation of Minerals by SCANning electron microscopy (QEMSCAN). Another aspect of this research is to determine if QEMSCAN can accurately identify clay minerals, and to discuss the benefits and shortcomings of the method in this context.

Stratigraphic Analysis

One 240 m section was measured using a 2-m long Jacob staff with 10 cm increments at Paria, Utah. Grain size was determined using a grain size card. Color was determined using a Rock Color Chart (Goddard et al., 1979). Mottling, plant, vertebrate, invertebrate fossils, nodules (carbonate or other), carbonate cement, and slickensides, pedogenesis, and anything else of interest were noted. Samples were taken periodically and/or at horizons that have interesting features not normally seen throughout the earlier part of the section. Three thin sections total were also used for petrographic descriptions, one per interval.

The paleosol classification system used in this paper is the US Soil Taxonomy as initially explained in Retallack (1990) with modifications by Mack (1993), and their

definitions for paleosols are used (Table 1). In this study, horizons containing root traces or burrows are identified as A-horizons. K horizons are more resistant units that are formed from coalescing carbonate nodules. A Bk horizon contains carbonate nodules as well, but not in a resistant layer like a K horizon. Bt horizons have accumulation of clays. Bc horizons contain concretions or nodules while Bg horizons are gleyed and contain pyrite or siderite nodules. Lastly, Bz horizons contain an accumulation of salts or salt crystal casts. Each of these is noted in the Appendix A for each paleosol horizon.

These horizons were then grouped into the types of soils depending on their color and sedimentary features. Gleysols contains low chroma colors, may contain root traces and trace fossils in either A or B horizons, and lack in accumulations of carbonate. Vertisols were more often variations of reds, purples, and browns; they may contain trace fossils and often contain accumulations of carbonate as in a Bk horizon. Calcisols contain distinct carbonate rich horizons (K horizons).

Sample Preparation for Clay Extraction

To analyze clay minerals, ~100 g of sample was gently crushed into a coarse sand-sized fraction in a mortar and pestle. The crushed sample, about 5 ml of a 5% CALGON solution, and 1.5 centrifuge tubes (150 mL) of deionized water (DI) were added to a blender. The components were mixed in a blender to disperse the clays for about 2 minutes. About 125 ml of slurry was decanted into two 100 ml centrifuge tubes. The tubes were balanced together using DI water when necessary. Tubes were loaded across from each other in a four slot centrifuge and centrifuged for 5 minutes at 1000 RPM (time and speed determined by Stokes Law) to remove the >2 μm fraction. The supernate from both tubes were decanted into four, 75 ml centrifuge tubes. Each set of

tubes was balanced on the scale using DI water and loaded into an eight-slot centrifuge. The remaining 2 μm-0.001 μm was settled at 4000 rpm for 5 minutes. All supernate was discarded and the remaining paste at the bottom of the tubes was removed with a spatula and spread on a prelabeled glass slide. Sediment was smoothed over about 60% of the slide to evenly cover and let air dry.

Analysis using X-Ray Diffraction

Samples were analyzed with the Rigaku XRD, DMAX 2000 located at the Department of Geology and Geophysics at the University of Utah, from 2-30°2θ at 4° 2θ/minute. After analyzing the air-dried sample, the sample was placed in a closed container saturated with ethylene glycol vapor. The container was heated in an oven for >8 hours at 60° C (or overnight). The glycol saturated samples were analyzed by XRD from 2-30° at 4°/minute within 2 hours of removal from the glycol chamber. Samples are glycolated in order to expand the air-dried smectite peak that ranges from 12 Å to 15 Å, to 17.2 Å (Parry et al., 2002). Glycolation will also usually sharpen and increase the peak intensity. Select samples were baked to further distinguish clay species (the smectite peak will collapse all together under heating). These samples were put into a muffle furnace for 1 hour at 300° C and then reanalyzed immediately. Relative clay % was determined using the semi-quantitative method by Moore and Reynolds, (1989).

Sample Preparation for QEMSCAN

Selected samples of different facies were prepared as 25 mm epoxy plugs and polished in kerosene to prevent samples with abundant swelling clays (smectites) from

adsorbing water and falling apart. After polishing, the mounts were photographed using a an Olympus camera on a binocular microscope and then carbon coated to about 400 μm.

Analysis by QEMSCAN

Sixteen samples were analyzed with the QEMSCAN instrument at the Energy and Geoscience Institute at the University of Utah. QEMSCAN is an automated instrument that uses nondestructive micro-analysis of minerals, rocks, and man-made materials (Haberlah et al., 2010). An electron beam steps across the surface of the sample with a predetermined spacing and x-ray energy spectra for each pixel is acquired. The measured spectra are immediately compared to spectra in a reference database and each measurement is classified as a phase. The output consists of a digital "mineral image" in which each measurement is represented by a pixel. A "false" color codes for the phase assigned to the pixel (Pirrie et al., 2004, Allen et al., 2012 in press). Nine epoxy plugs were loaded and analyzed at a time and a subset of the plug was used for analysis to maximize information recorded. Different analytical parameters were used for each sample, depending on its grain size range (Table 2).

After analysis, the measured energy spectra were reclassified using the program iDiscover 5.2 with the Oil and Gas Species Identification Protocol (SIP) produced by the company FEI. The Oil and Gas Species SIP is a collection of energy spectra that are specifically helpful to sedimentary rocks for the oil and gas industry. SIP's can be edited and further refined for a particular projects needs. Once edited, these SIP's are proprietary and are not public. For this study, the SIP was not further refined.

Some samples had large amounts of minerals classified as "Other". The clay minerals are the predominant source of this "Other" (see next section for discussion).

Phases representing less than 0.5% were not included due to them being a very minor constituent of the sample. The minerals that were above 0.5% were then normalized to 100%. Background was not included in the data plots but can be seen mapped out across the samples when applicable in Appendix C. The data from the identified clays of smectite, illite, and kaolinite from QEMSCAN were calculated to determine the clay portion of the sample and compared to the XRD clay mineral relative amount percentages.

X-ray diffraction data are compared to the QEMSCAN data in this study in part to see how accurate the Oil and Gas SIP 5.2 is at identifying clays. It should be noted that the clay samples were prepared for the bulk clay mineralogy of the sample brought back to the lab. QEMSCAN samples were chosen for the most part as bulk samples but in some cases, the analysis area was chosen to highlight specific features within the rock, such as different colors, grain sizes, etc. Therefore QEMSCAN samples cannot be directly compared, but portions of the QEMSCAN sample do represent the bulk sample.

Table 1. Paleosol Definitions

Master Horizons	Description	Found in Paria, UT
O	Surface accumulation of organic materials (peat, lignite, coal) ovelying clayey or sandy part of soil	
A	Usually has roots, organic and mineral matter, forms the surface of a paleosol horizon that does not contain an O horizon	✓
E	Found below an O or A horizon and appears bleached because lighter colored, less organic, less sesquioxidic or less clayey than material below	
B	Underlies an A or E horizon and is enriched in some material compared to overlying and underlying horizons (because darker colored, more organic, more sesquioxidic or more clayey) or more weathered than other horizons	✓
K	Subsurface horizon that is saturated with carbonate that forms a massive layer	✓
C	Subsurface horizon that is slightly more weathered than fresh bedrock, lacks properites of other horizons, shows mild mineral oxidation, limited accumulation of silica, carbonates, soluble salts, or moderate gleying	✓
R	Consolidated and unweathered bedrock	

Subordinate descriptors specifically for Paria, UT rocks		
c	Concretions or nodules	✓
g	Evidence of strong gleying, such as pyrite or siderite nodules	✓
k	Accumulation of carbonates, less than a K horizon	✓
s	Illuvial accumulation of sesquioxides	✓
t	Accumulation of clay	✓
z	Accumulation of other salts or salt crystal casts	✓

Adapted from Retallack (1990)

Table 2. QEMSCAN Parameters

Interval	Depth (m)	Analysis Time (min)	Field Size $(um)^2$	Point Spacing (um)	# of Fields
1	0.0	25	1000	5	7
	2.0	41	1000	2.5	3
	2.9	40	1000	2.5	3
	6.1	49	1000	3	5
	38.0	16	1000	4	3
	61.9	51	1000	4	9
2	84.6	28	1000	4	5
	114.2	25	1000	5	7
	129.2	16	1000	4	3
	139.6	12	1000	6	5
	139.8	33	1000	5	6
	142.5	39	1000	2.5	3
3	172.3	30	1000	3	3
	173.4	39	1000	4	7
	179.3	17	1000	5	5
	190.9	37	1000	3	5

RESULTS

Stratigraphy

Two stratigraphic sections were measured in Paria, Utah: one 63 m thick south-facing outcrop consisting of the Shinarump Member, and another 240 m thick outcrop down-dip of the Shinarump on the western facing side of Gingham Skirts Butte (Figure 11). On initial visual inspection there are three intervals across the butte that are noted by a change in colors as seen on outcrop and on the digital elevation model (DEM) with hillshading and orthoimagery (Figure 12). The first interval is characterized by low chroma grays, blues, and greens from 0 m to 68.8 m; the second is reds and browns 68.8 to 170.3 m; and the third interval is predominantly pinks, reds, and tans (informally called “candyland” and above) from 170.3 to 237.4 m. Once trenched, these colors change slightly (representing fresh exposures) but still show a distinct change at those boundaries.

The first stratigraphic section begins in the upper portion of the Lower to Middle Triassic Moenkopi Formation to document the transition to the Shinarump Member of the Chinle Formation. The Shinarump Member erosionally truncates the Moenkopi Formation (Figure 13). Pleistocene (?) conglomerate overlies the top of the Shinarump Member at the location of stratigraphic section one. The rocks in this area dip to the east and the same sandstone from the first stratigraphic section can be correlated across the wash to the second stratigraphic section. Ten paleocurrents were measured on trough

cross beds from the sandstone below the second stratigraphic section (Figure 14) and have a northwesterly direction, which is in broad agreement with previous studies (Blakey and Gubitosa, 1983). The second section starts at the top of the sandstone unit in Figure 11 and a photograph of the section is shown in Figure 15. Each interval of the second stratigraphic section will be described individually, below. The detailed spreadsheet description can be found in Appendix A and the diagrammatic stratigraphic section can be found on Figure 16, with sample locations on Figure 17.

Interval 1 (Figure 18) consists mainly of mudstone with one layer that is made up of fine sandstone; the generalized colors include grays, reds, and a minor portion of browns. Most of interval 1 is not calcareous; only carbonate nodules react with acid as well as one fine sandstone layer that has a carbonate cement (38.0 m, Figure 16). Meniscate backfilled unbranching burrows are present in samples 6.1 m (Figure 19 for a burrow in thin section), 22.3, and 24.6 m. Root traces are found in this interval at 6.1 m (Figure 18) and are evidenced by the yellowish sections of the sample. The thin section shows evidence of root structures and burrows. The thin section sample is predominantly composed of clays with sporadic silt (~10%). Mottling is abundant in the outcrop. Interval 1 consists of A, Bk, Bc, Bt, C and K horizons (Table 2 for definitions). The latter three soil horizon types are only sporadically found in this section.

Interval 2 (Figure 20) contains mudstones, sandstones and conglomerates (with clasts up to a couple centimeters in diameter). The colors range from mostly reds and browns with a minor amount of gray. Predominantly, the carbonate nodules react with acid but some green mottles react to acid as well, in addition to carbonate cement in the matrix. Burrows are found at 84.6 m (bottom right photo of Figure 20 and in Figure 21

and Appendix C) and mottling is abundant (Green dots in 77.2 in Figure 20). Root traces were found at 80 m. Interval 2 contains A, Bc, Bk, Bt, Bz, and Bs horizons. The thin section sample from 84.6 m is illite rich as noted by the high pleochroism using cross-polarized light and rotating the stage (Figure 21). The photo of the 137.3 m stratum in Figure 20 shows the 10 m thick channel sandstone with conglomeratic layers.

Interval 3 (Figure 22) contains claystone, siltstone and sandstone (fine to very coarse) that are red, brown, and minor amounts of gray in color. Paleosol horizons present include A, Bk, Bt, Bs, and K. Carbonate nodular layers (K) are found in interval 3 and the green mottles react to acid as well as the matrix in a few samples. Burrows are found at 196.0 m in association with large (~1/2 m) slickensides. There is an abundance of sand within interval 3. Some of the sand rich layers are very resistant (185.5 m) whereas others are very friable and break apart in your hand (191.6 m and 229.6 m). The sandy intervals contain trough cross bedding and reduction occurs within specific layers (see photographs labeled 191.6 m and 229.6 m in Figure 22). See Appendix A for detailed descriptions. The thin section sample from 190.9 m is a muddy sandstone with an abundance of rounded quartz grains. It also contains feldspar and volcanic rock fragments, in addition to clay-rich rip-up clasts upwards of 2 mm in thin section, some of which are laminated, found throughout the sample (Figure 23).

Clay Mineralogy

Twenty-eight samples were analyzed by XRD after air-drying and again after glycolation, the raw data can be viewed in Appendix B. A sample of a XRD pattern can be seen in Figure 24 at 24.6 m. All XRD patterns are combined into one plot to show the changes throughout the section (Figure 25). The relative clay % is shown in Figure 26.

Interstratified illite and smectite (I/S) is present in three samples throughout the section at 6.1, 51.9 and 216.3 meters but do not contain the correct peak to calculate relative percent. Therefore the three samples with I/S are omitted in Figure 26. Four samples were baked in an oven to assure that smectite was being correctly identified in the samples. Of the four samples chosen, the main smectite peak collapsed in each of them.

Smectite is mostly absent at the base of the section until 4.8 m and ranges from 18 to 34% up until 84.6 m (Figure 26). From 110.6 to 151.5 m, smectite ranges from 70 to 100%. From 170.3 to 237.4 m, smectite ranges from 7 to 31% except for one sample that is 90% at 178.0 m. Kaolinite ranges from 28 to 66 % from 0 to 51.2 meters. From 76.5 until the top of the section, kaolinite ranges 5 to 23 % except for 110.65, 170.3, 173.4, 179.3, 190.9 and 237.4 m where it is completely absent. Illite is highly variable throughout the section, ranging from 53 to 72% in the first 4.8 m of section, 0 to 28% in the 22.3 to 51.2 m interval, and within 76.5 to 84.6 m it ranges 58 to 72%. Illite is mostly absent from 110.6 until 151.5 m except for 129.2 m where it is 6%. From 170.3 m until the top of the section, illite ranges from 57 to 93% except for its absence at 178.0 m. Sample 6.1 m is omitted on the clay relative % plot (Figure 26) because there are no illite peaks to calculate the relative % of I/S. This sample does contain kaolinite in addition to I/S, but calculations could not be determined.

Overall, smectite is a minor portion of samples in interval 1 while illite and/or kaolinite are much more abundant. Smectite is the dominant portion of samples in interval 2 while kaolinite is a minor constituent and illite is mostly absent. Interval 3 contains mostly illite with minor smectite and kaolinite.

QEMSCAN

Fifteen samples were analyzed for specific features within the epoxy plugs; see Appendix C for detailed photographs and data. Table 3 shows the sample depths and rock types. An example of the data from a QEMCSAN sample at 6.1 m can be seen in Figure 27. Figures 28 and 29 highlight the data for the sandstone samples and for the paleosol samples. Of the seven samples that are paleosols, calcite is only present in samples 129.2 (3%), 172.3 (25%), and 173.4 (34%) (Figure 29). Regarding the plot of all fifteen samples, calcite is a minor (21% or less) portion of samples below 139.6 m and becomes a more major part of the samples up until sample 190.9 m (Figure 30). Smectite is a constituent of all samples in varying amounts of 1 to 45%. Smectite is present in the fine-grained silts and clays as well as the fine sandstones and conglomerate samples. Illite is in the samples in varying amounts (3-30%) throughout the section but is absent at 6.1 m. Kaolinite ranges from 0 to about 7% throughout the entire section. Above 129.2 m, kaolinite is in three of the seven samples with less than 1%. 'Other' is the grouping where the elemental information gathered does not fit into any classified grouping. Other varies with no apparent pattern from 2 to 17.6%. The group "other silicates" in the fine-grained samples ranges from 1.5 to about 13% and for the samples other than the paleosols it ranges from 0 to about 4%. Plagioclase in the paleosol samples ranges from 1.5 to about 9.5% whereas in nonpaleosol samples it ranges from about <1 to 8%. In the nonpaleosol samples, only the 190.9 m sample contained more than a minor amount of apatite at 1.26%. Amphiboles were only identified in two paleosols, 172.3 and 173.4 m and were about 12.5 and 14.5 %. Dolomite was identified in two paleosol samples as well, 172.3

and 173.4 m at about 3%. Siderite was identified in minor quantities in two samples, 6.1 m at 0.7% and 139.6 at 1.37%.

The samples that are fine to coarse sandstones show an increase in calcite which therefore decreases the relative amount of quartz in the sample (Figure 28). The paleosol samples analyzed with QEMSCAN also show an increase in calcite up-section which agrees with my stratigraphic field observations (Figure 29). There seem to be no trends evident in any of the other minerals in either the paleosol samples or the sandstones.

Paleosol textures can be seen in Figure 31. Samples 2.0 and 2.9 meters have a siltier component to them and the silt-sized alkali feldspar grains in the sample show illite rimming the grains. Sample 6.1 m has a finer grained texture than the first two samples and shows siderite concentrated in specific areas. Sample 61.9 m contains a black carbonate nodule that has few inclusions (mainly illite and some minor quartz) in it. The matrix is predominantly illite with some silt-sized quartz grains and minor calcite dispersed throughout. Sample 84.6 m contains a mixture of illite and smectite with the smectite in more or less concentrated lenses as well as dispersed throughout. 129.2 m contains alkali feldspars with illite rimming the grains as well. Samples 172.4 and 173.4 m contain a large portion of calcite (20-30%) that is dispersed throughout the sample with amphibole and quartz. The calcite appears to be pore-filling.

Clay QEMSCAN Data

With regards to the clay portion of the QEMSCAN data, Table 3 shows the % of clay per sample as well as the % clay normalized to 100 and Figure 32 shows the clay portion of the QEMSCAN data normalized to 100%. Smectite is 26 to 45% from samples 0 to 2 m. Samples from 6.1 to 142.5 m range from 55 to 93% of the clays in the sample.

Smectite range from 21 to 42% from samples 172.3 to 190.9 m. Illite is found from 0 to 2 m from 24 to 37%, it is absent in samples 6.1 and 38 m. Illite ranges from 15 to 44% in samples from 84.6 to 142.5 m. Samples 172.3 to 190.9 m range from 57 to 70%. Kaolinite is more abundant at the base of the section, 20 to 48% in the first 2 and decreases to 6.5% in samples 6.1 and 38 m. Kaolinite is absent at 84.6 and 139.8 m. It is about 1.3 to 2.7% from 114.4 to 139.6 m. Sample 172.3 m has kaolinite of about 8% and then is absent in samples 173.4 to 190.9 m.

The overall trend of the clays as identified by QEMSCAN show that smectite is an increasingly dominant portion of the clays in intervals 1 and 2 and a minor portion of interval 3. Kaolinite shows a decreasing influence upsection as well with the most amount in interval 1, fluctuating amounts in interval 2, and barely any in interval 3. Illite fluctuates in intervals 1 and 2 while it is a dominant portion of interval 3.

Clays Mineralogy Using XRD and QEMSCAN

Eleven samples were analyzed with QEMSCAN and XRD, and Figure 33 highlights the similarities and differences between the methods. The most obvious difference is that XRD identified I/S in sample 6.1 m (but relative % could not be calculated) and QEMSCAN will not ever be able to identify I/S. Overall, the samples show similar trends such as an increase in smectite in interval 2 and a substantial decrease of smectite in interval 3.

Figure 11. View North showing the correlation of stratigraphic sections 1 and 2 with the three visible possibly correlative members shown, the basal Shinarump, the Blue Mesa, and the base of the Sonsela Members. Distance from stratigraphic section 1 to 2 is about 400 meters (0.25 miles).

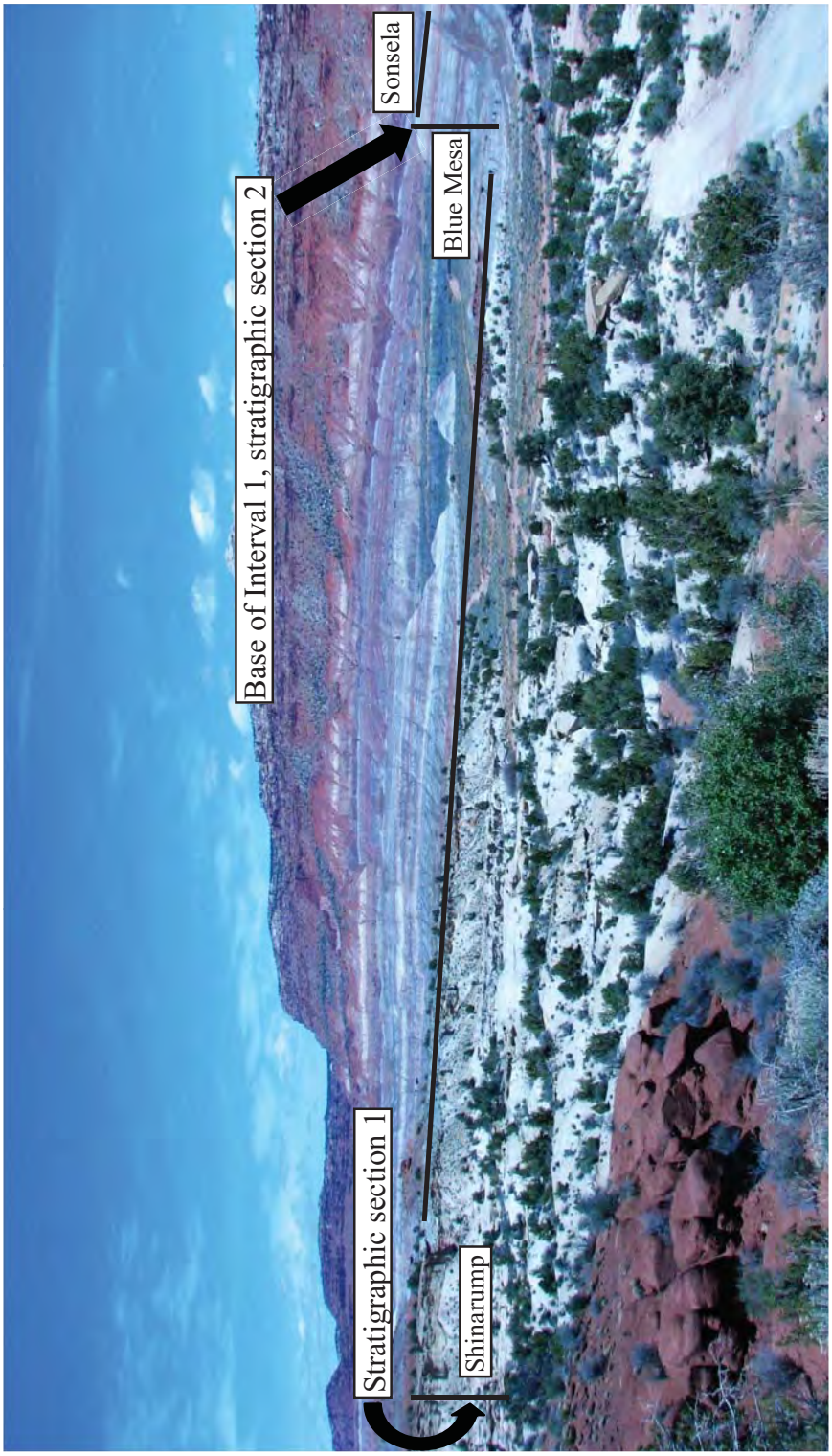
Sonsela
Blue Mesa
Base of Interval 1, stratigraphic section 2
Stratigraphic section 1
Shinarump

Figure 12. DEM with hillshading and orthoimagery of the study area with the stratigraphic section transect in purple with the 3 intervals of major changes outlined and labeled. Area is about 1000 m by 1000 m (0.63 miles x 0.63 miles). Data from seamless.usgs.gov. Bottom right corner is latitude 37.232898 and longitude -111.959761 in decimal degrees.

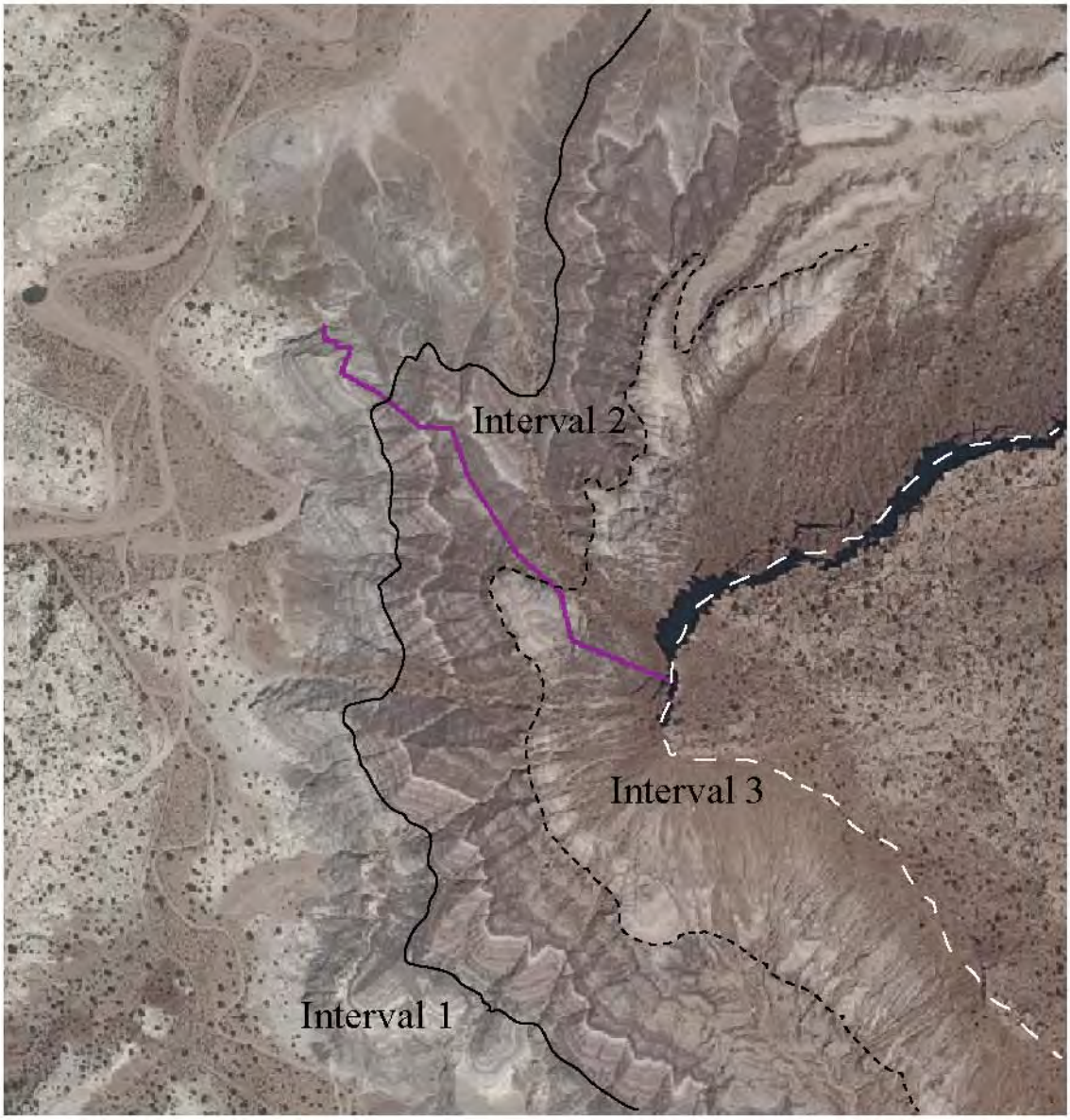
Interval 2
Interval 3
Interval 1
Stratigraphic section transect
North

Figure 13. The Shinarump Member unconformably overlies the Moenkopi Formation and represents a braided stream complex. The location of stratigraphic section 1 is shown by the vertical line (60 m).


Shinarump
Member
Moenkopi
Formation

Figure 14. Stratigraphic section 1: Shinarump Member with the contact between the Moenkopi Formation and Pleistocene(?) conglomerate. Rose diagram of 10 paleocurrent directions measured on trough cross beds in the basal Shinarump Member. Diagram shows a northwesterly flow. Outcrop photo within the vicinity of measured paleocurrents, jacob staff is 1.5 m. Photograph at top right is a close-up of ripples found in this outcrop, arrow on card is 10 cm tall.

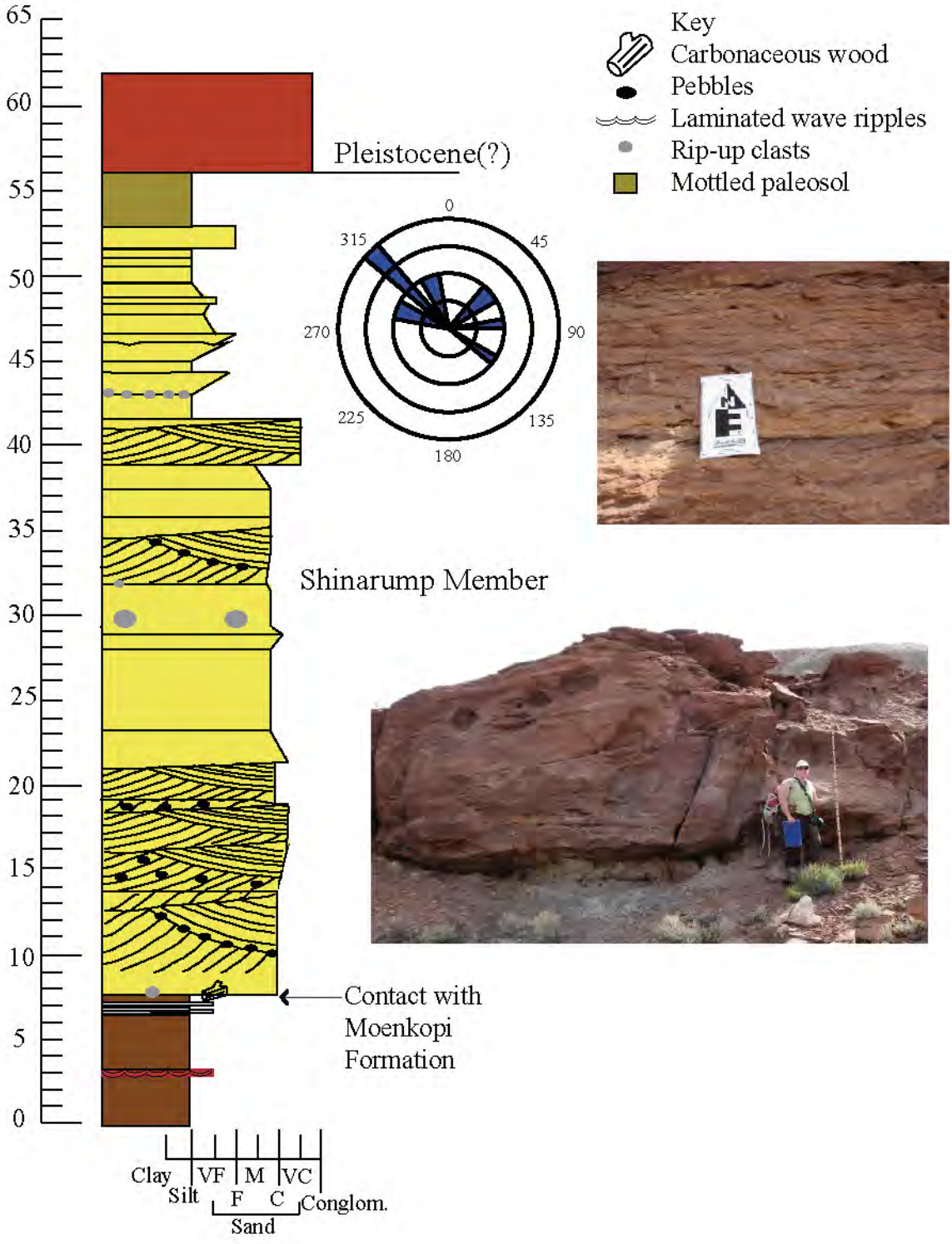
Key
Carbonaceous wood
Pebbles
Laminated wave ripples
Rip-up clasts
Mottled paleosol
Pleistocene(?)
Shinarump Member
Contact with
Moenkopi
Formation
65
60
55
50
45
40
35
30
25
20
15
10
5
0
0
45
90
135
180
225
270
315
Clay
Silt
VF
F
M
C
VC
Conglom.
Sand

Figure 15. Stratigraphic section 2 outcrop photo of Gingham Skirts Butte. Transect represents 240 m in stratigraphic thickness. Intervals 1-3 are labeled. The uppermost line is the contact between the Chinle Formation and the Jurassic Wingate/Moenave Formations.

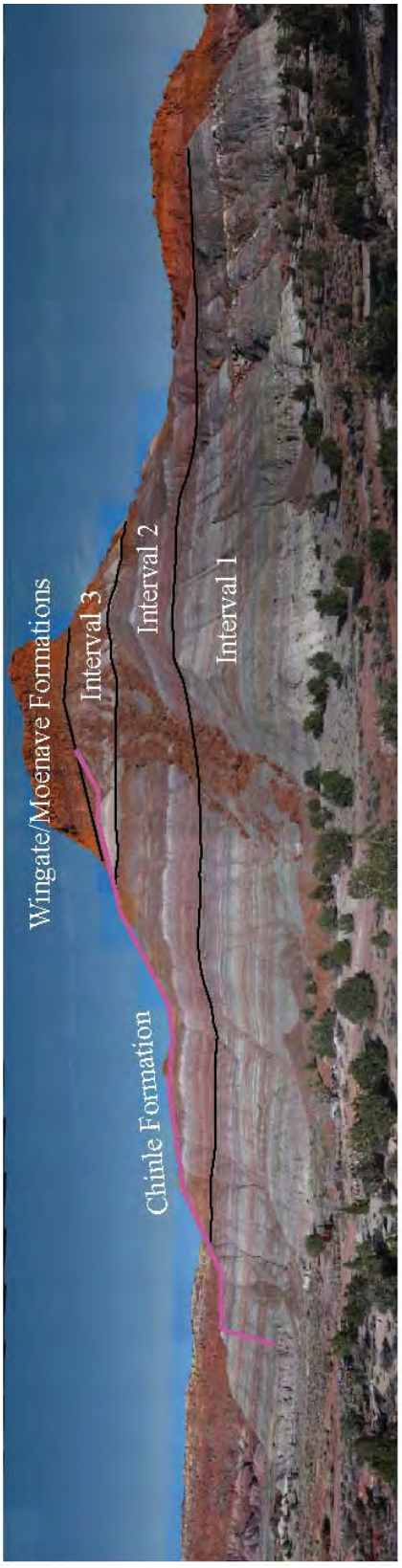
Wingate/Moenave Formations
Interval 3
Interval 2
Interval 1
Chinle Formation
Stratigraphic section transect

Figure 16. Stratigraphic section 2. The general color represents multiple rock colors. To view the exact colors in the stratigraphic section, see Appendix A.

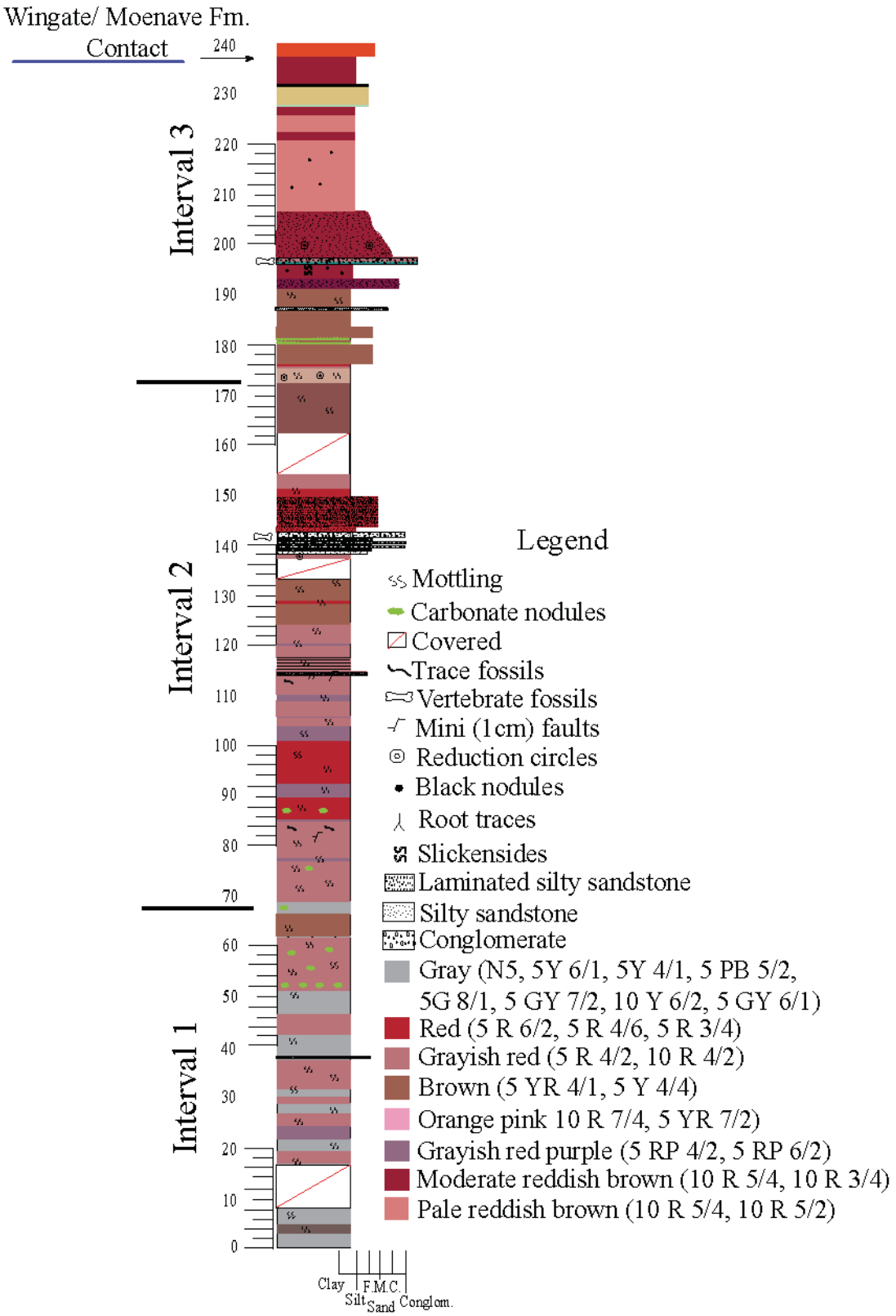
Wingate/ Moenave Fm.
Contact
240
230
220
210
200
190
180
170
160
150
140
130
120
110
100
90
80
70
60
50
40
30
20
10
0
Interval 3
Interval 2
Interval 1
Legend
Mottling
Carbonate nodules
Covered
Trace fossils
Vertebrate fossils
Mini (1cm) faults
Reduction circles
Black nodules
Root traces
Slickensides
Laminated silty sandstone
Silty sandstone
Conglomerate
Gray (N5, 5Y 6/1, 5Y 4/1, 5 PB 5/2, 5G 8/1, 5 GY 7/2, 10 Y 6/2, 5 GY 6/1)
Red (5 R 6/2, 5 R 4/6, 5 R 3/4)
Grayish red (5 R 4/2, 10 R 4/2)
Brown (5 YR 4/1, 5 Y 4/4)
Orange pink 10 R 7/4, 5 YR 7/2)
Grayish red purple (5 RP 4/2, 5 RP 6/2)
Moderate reddish brown (10 R 5/4, 10 R 3/4)
Pale reddish brown (10 R 5/4, 10 R 5/2)
Clay
Silt
F.M.C.
Sand
Conglom.

Figure 17. Stratigraphic section 2 with sample locations. See Figure 15 for legend. C = Clay mineralogy, Q = QEMSCAN, T = Thin sections.

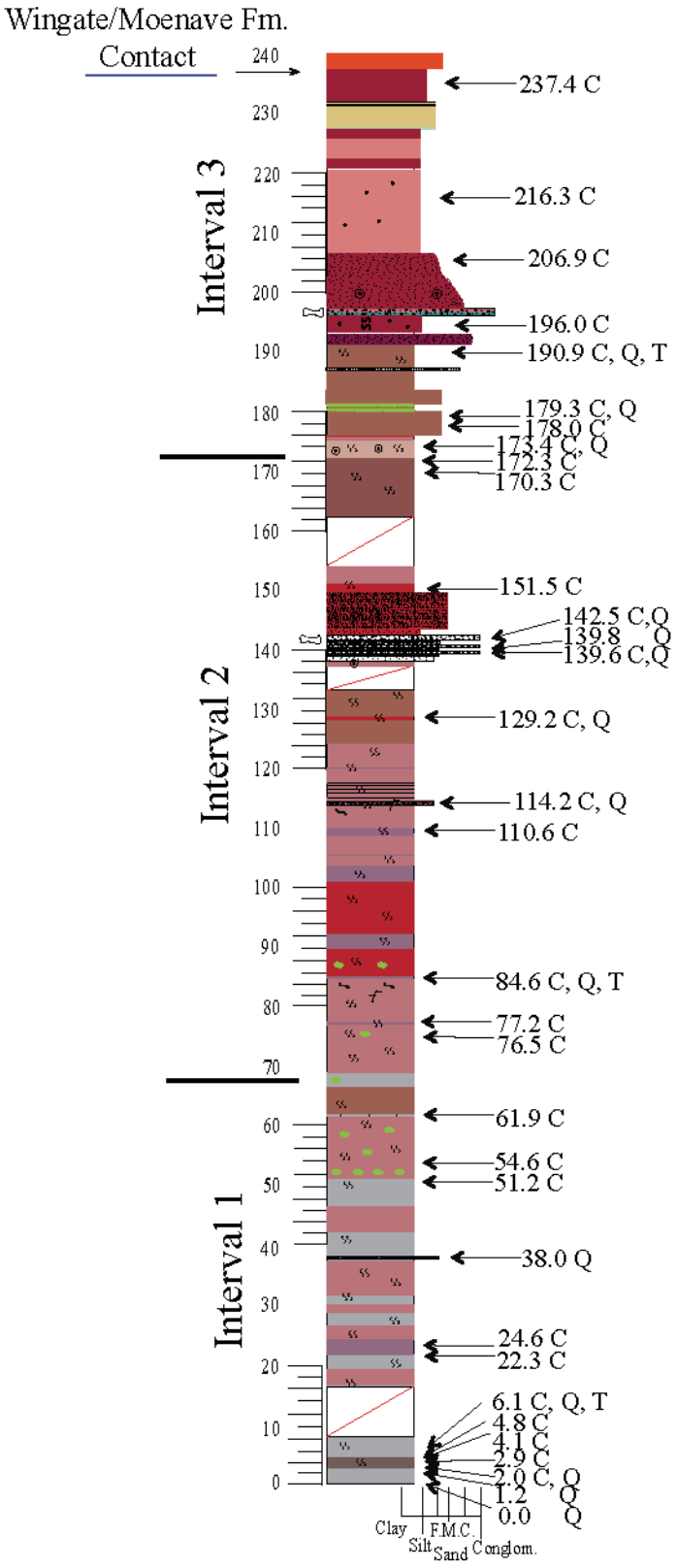
Wingate/Moenave Fm.
Contact
240
230
220
210
200
190
180
170
160
150
140
130
120
110
100
90
80
70
60
50
40
30
20
10
0
Interval 3
Interval 2
Interval 1
237.4 C
216.3 C
206.9 C
196.0 C
190.9 C, Q, T
179.3 C, Q
178.0 C
173.4 C, Q
172.3 C
170.3 C
151.5 C
142.5 C,Q
139.8 Q
139.6 C,Q
129.2 C, Q
114.2 C, Q
110.6 C
84.6 C, Q, T
77.2 C
76.5 C
61.9 C
54.6 C
51.2 C
38.0 Q
24.6 C
22.3 C
6.1 C, Q, T
4.8 C
4.1 C
2.9 C
2.0 C, Q
1.2 Q
0.0 Q
Clay
Silt
F.M.C.
Sand
Conglom.

Figure 18. Interval 1 stratigraphic section and photos. A) Detailed stratigraphic section for Interval 1. B) A Bt horizon with yellow mottles throughout, pencil is about 10 cm long. C) An A horizon with root traces and burrows, the rectangle is approximately 2.54 cm tall and is the location of the epoxy plug. The yellow areas are the roots and the burrows are the thicker red/yellow elongate features. D) A Bt horizon with a general color of grayish red with green hued mottles. E) A 10 cm thick fine sandstone bed. See Figure 15 for Legend.

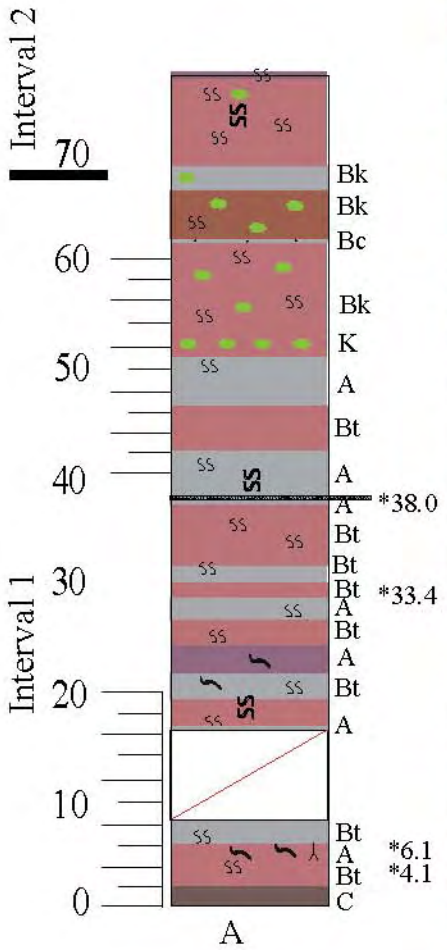
Interval 2
70
60
50
40
Interval 1
30
20
10
0
A
Bk
Bk
Bc
Bk
K
A
Bt
A
A
*38.0
Bt
Bt
Bt
*33.4
A
Bt
A
Bt
A
Bt
A
*6.1
Bt
*4.1
C

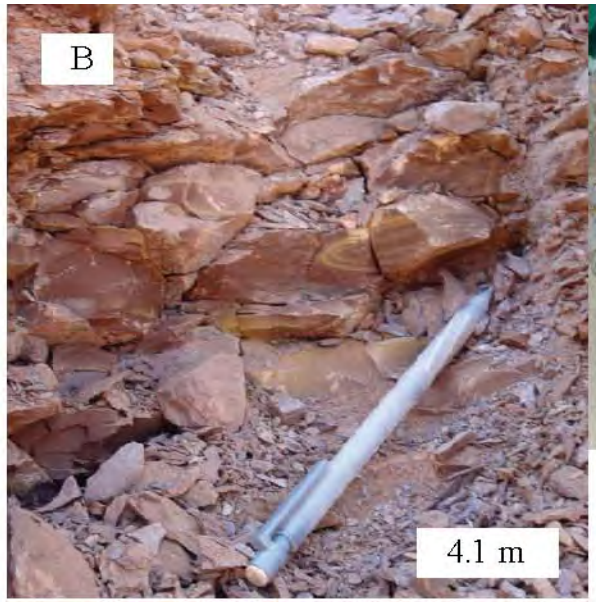
B
4.1 m


C
6.1 m

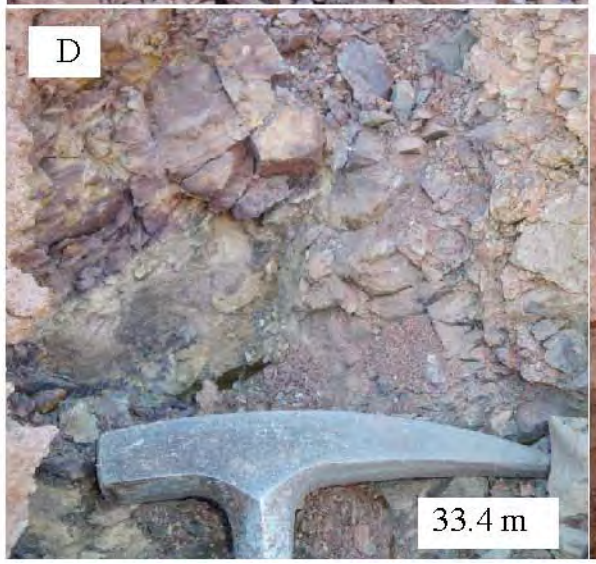
D
33.4 m

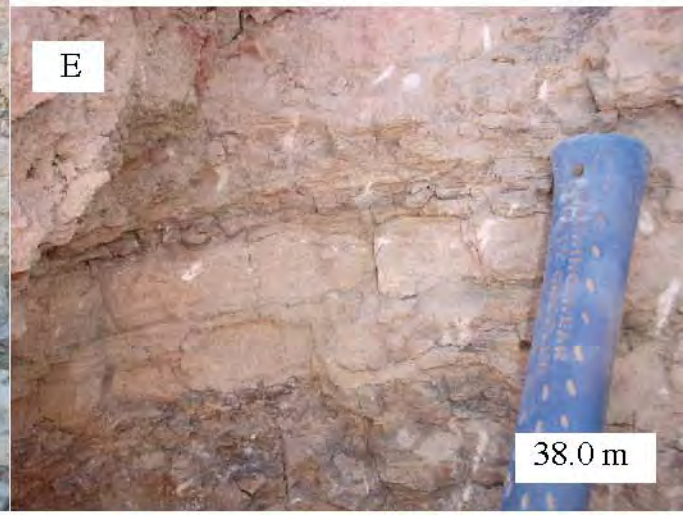
E
38.0 m

Figure 19. Thin section photomicrographs of sample 6.1 m with plane polarized light. A) 2.5x magnification shows a lense of organics and pyrite (arrow). B) 2.5x magnification shows a burrow, excessive polishing has thinned upper portion of the slide rendering it lighter in color. C) 10x magnification shows thin organic stringers (arrows) and silt (white shapes).

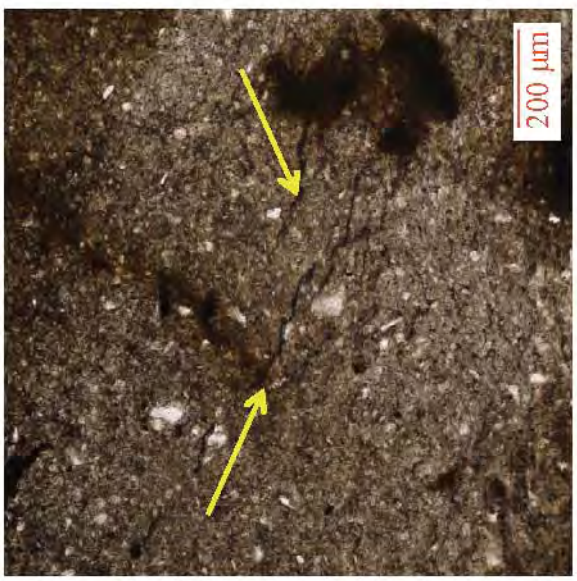

C

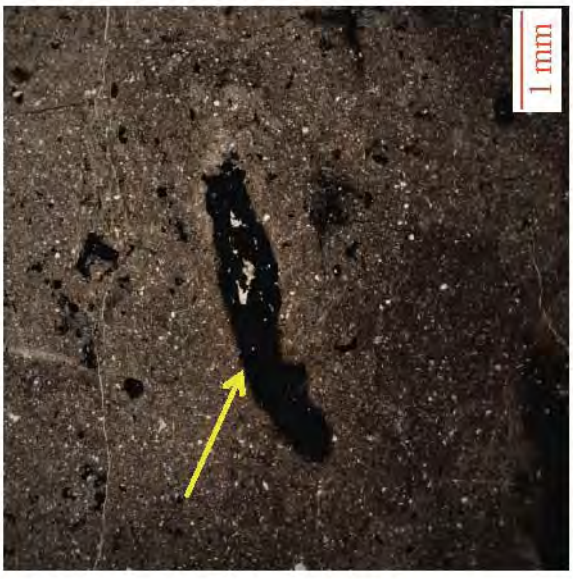

A

B

Figure 20. Interval 2 stratigraphic section and photos. A) Detailed stratigraphic section for Interval 2. B) A Bc horizon. C) A horizon with meniscate backfill burrows. D) An area with fine sand and silt with a Bz horizon infilling the uneven layer below. E) Highlights the mini-faults in the sandy layer. F) A succession of sandstone and conglomerates. G) A Bt horizon with ~3 mm reduction circles. See Figure 15 for legend.

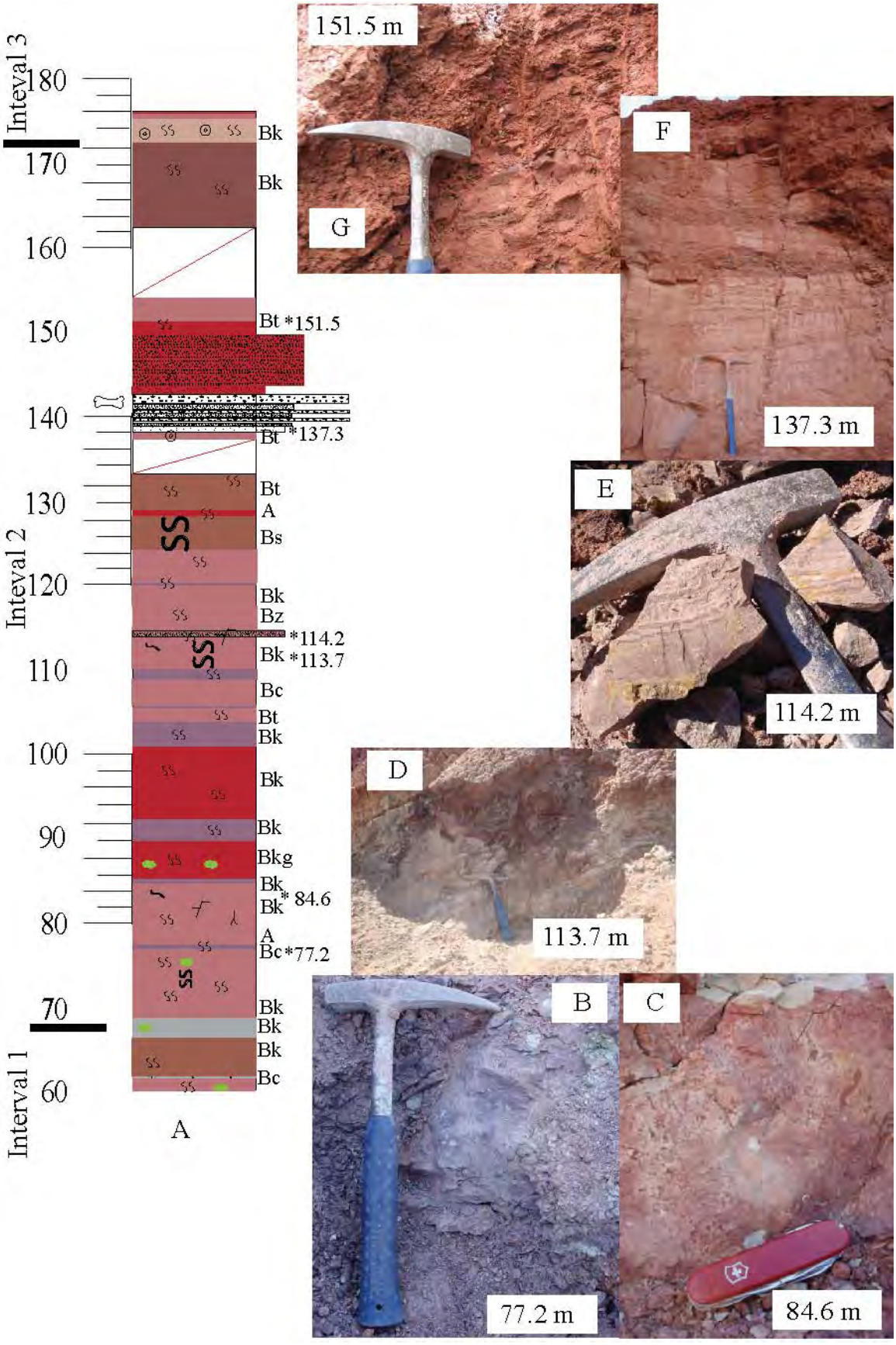
Inteval 3
180
170
160
150
140
130
120
110
100
90
80
70
Interval 1
60
Inteval 2
Bk
Bk
Bt *151.5
Bt *137.3
Bt
A
Bs
Bk
Bz
*114.2
Bk *113.7
Bc
Bt
Bk
Bk
Bkg
Bk
Bk* 84.6
A
Bc*77.2
Bk
Bk
Bk
Bc
A
151.5 m
G
F
137.3 m
E
114.2 m
D
113.7 m
B
77.2 m
C
84.6 m

Figure 21. Thin section photomicrographs of sample 84.6 m under plane polarized light. A) 2.5x magnification of a meniscate backfilled burrow. B) 10x magnification shows a concentrated illitic lense with silt grains within. C) 10x magnification shows the overall texture of the sample.

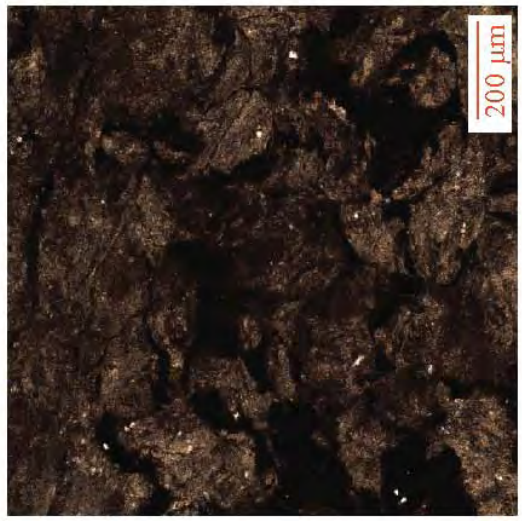

C

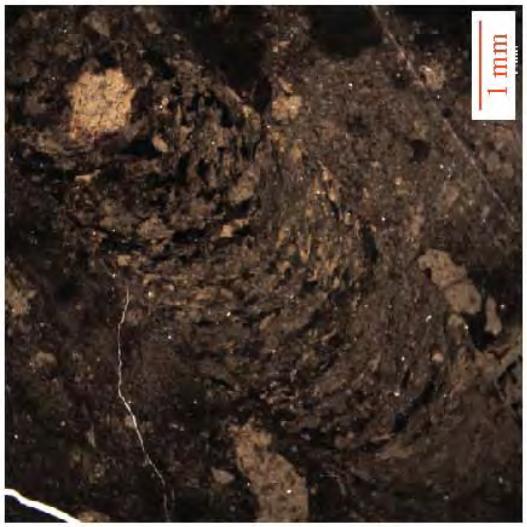

A

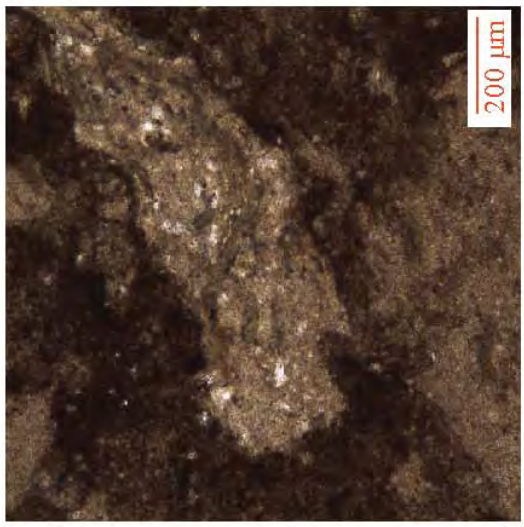

B

Figure 22. Interval 3 stratigraphic section and photos. A) detailed stratigraphic section for interval 3. B) 173.4 m, a Bk horizon. C) 185.5 m, a Bs horizon overlain by a sand layer. D) 191.6 m, a sandy interval with reduction along preferential bedding. E) 196.0 m is a Bs horizon showing an area of large slickensides. F) 216.3 m Bk horizon with a reduction feature in the center. G) 229.6 m is a silty sand interval with reduction areas along bedding. See Figure 15 for legend.

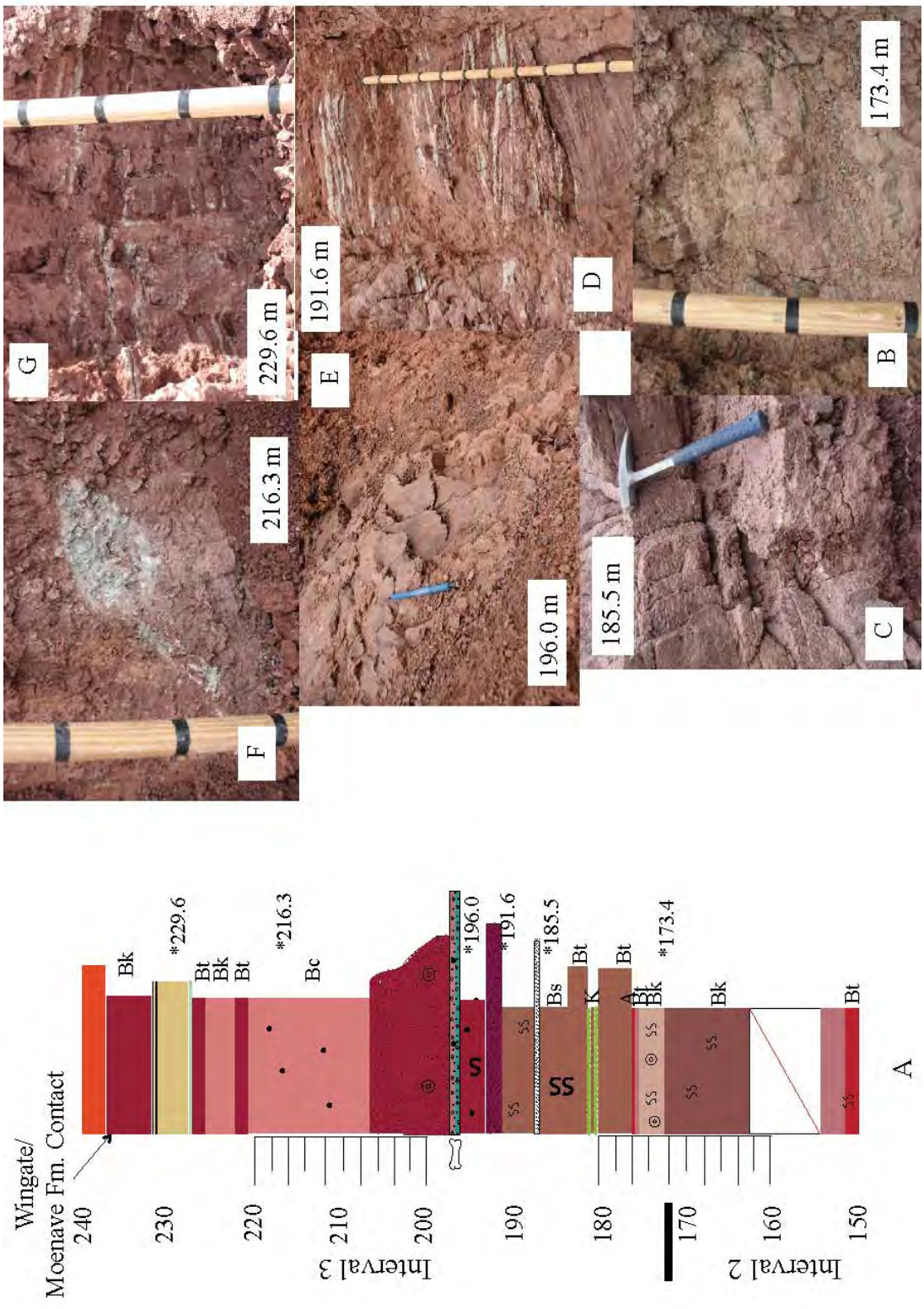
G
229.6 m
F
216.3 m
E
191.6 m
196.0 m
D
185.5 m
C
B
173.4 m
Wingate/
Moenave Fm. Contact
240
230
220
210
200
190
180
170
160
150
Interval 3
Interval 2
Bk
*229.6
Bt
Bk
Bt
*216.3
Bc
*196.0
*191.6
S
SS
*185.5
Bs
Bt
K
Bt
A
Bt
Bk
*173.4
Bk
Bt
A

Figure 23. Thin section photomicrographs of sample 190.9 m, C = Chert, Q = Quartz, S = Sedimentary rock fragment, F = feldspar. A) 2.5 x magnification shows the overall texture of the sample and S in the upper left image shows a laminated sedimentary rock fragment, B) 5x magnification shows a higher magnification image of the grains. C) is the same image as B but under cross-polarized light.

A

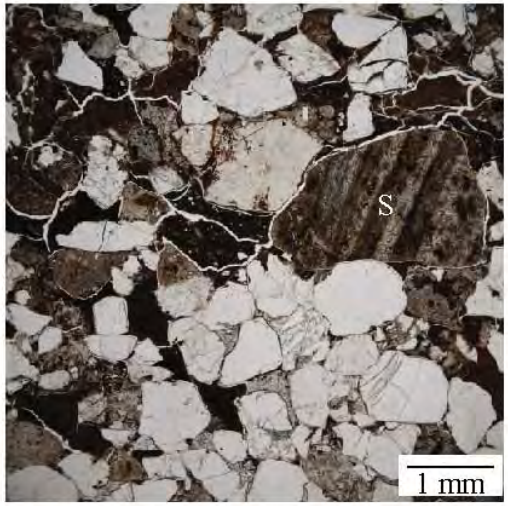

Plane-polarized light

B

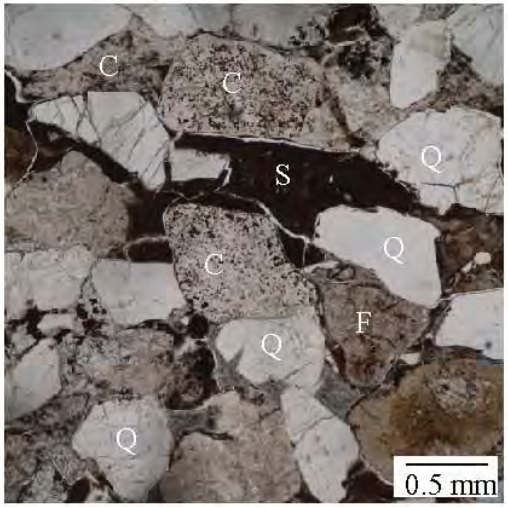

C

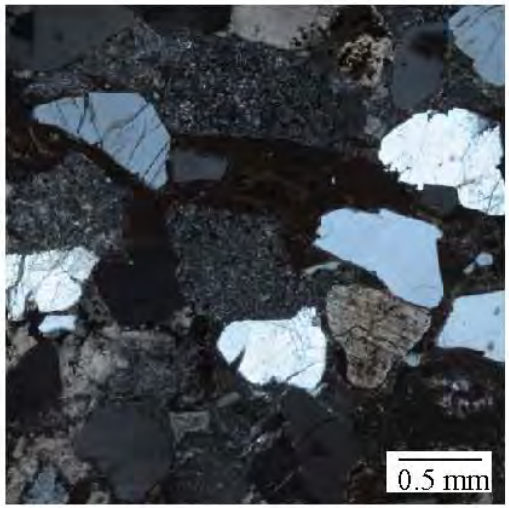

Cross-polarized light

Figure 24. Stratigraphic Section 2 diffractogram at sample 24.6 m, (d(angstroms), 2θ).

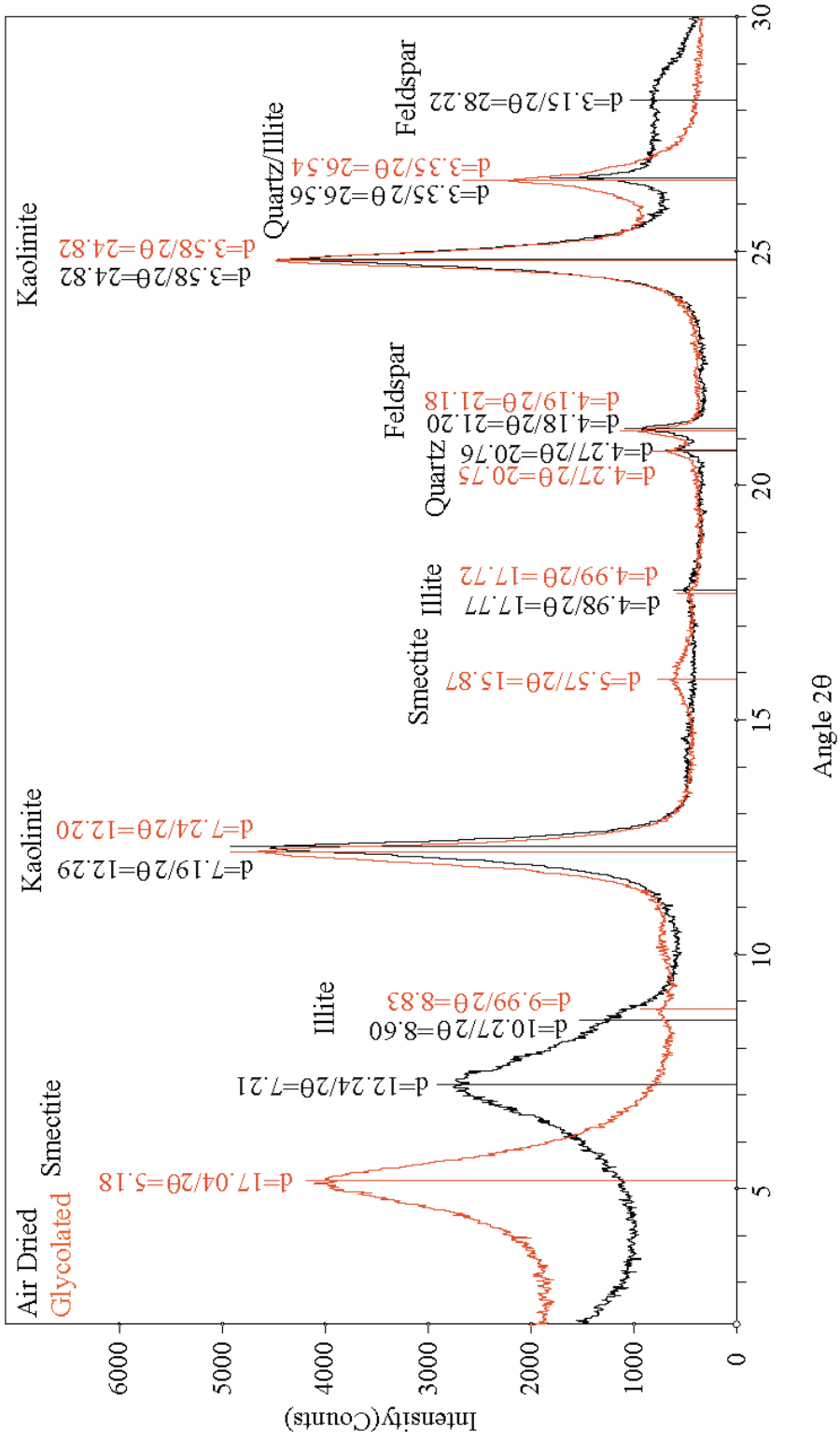
Air Dried
Glycolated
Smectite
Kaolinite
Illite
Kaolinite
Smectite
Illite
Quartz
Feldspar
Kaolinite
Quartz/Illite
Feldspar
d=17.04/2θ=5.18
d=12.24/2θ=7.21
d=10.27/2θ=8.60
d=9.99/2θ=8.83
d=7.19/2θ=12.29
d=7.24/2θ=12.20
d=5.57/2θ=15.87
d=4.98/2θ=17.77
d=4.99/2θ=17.72
d=4.27/2θ=20.75
d=4.27/2θ=20.76
d=4.18/2θ=21.20
d=4.19/2θ=21.18
d=3.58/2θ=24.82
d=3.58/2θ=24.82
d=3.35/2θ=26.56
d=3.35/2θ=26.54
d=3.15/2θ=28.22
Intensity(Counts)
Angle 2θ
0
1000
2000
3000
4000
5000
6000
5
10
15
20
25
30

Figure 25. X-ray diffraction patterns of clay throughout the section. The patterns are not to scale in the vertical. Note kaolinite decreases upsection while smectite becomes more evident at 22.4 m.

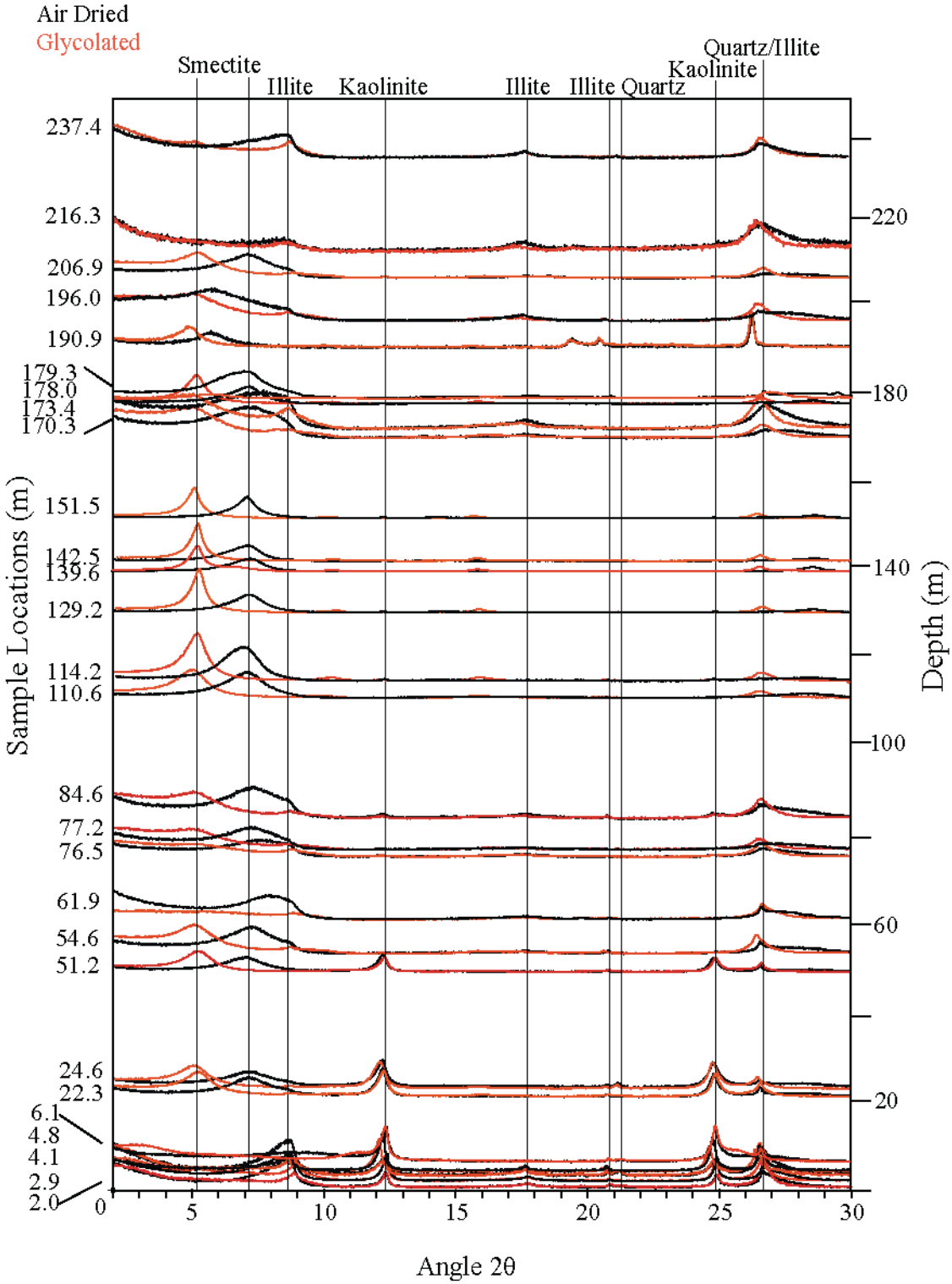
Air Dried
Glycolated
Smectite
Illite
Kaolinite
Illite
Illite
Quartz
Quartz/Illite
Kaolinite
237.4
216.3
206.9
196.0
190.9
179.3
178.0
173.4
170.3
151.5
142.5
139.6
129.2
114.2
110.6
84.6
77.2
76.5
61.9
54.6
51.2
24.6
22.3
6.1
4.8
4.1
2.9
2.0
Sample Locations (m)
220
180
140
100
60
20
Depth (m)
0
5
10
15
20
25
30
Angle 2θ

Figure 26. Relative clay % of samples that were analyzed by x-ray diffraction. I/S was identified in three samples (6.1, 61.9 and 216.3 m) but did not contain peaks to calculate relative % and are therefore omitted from this plot.

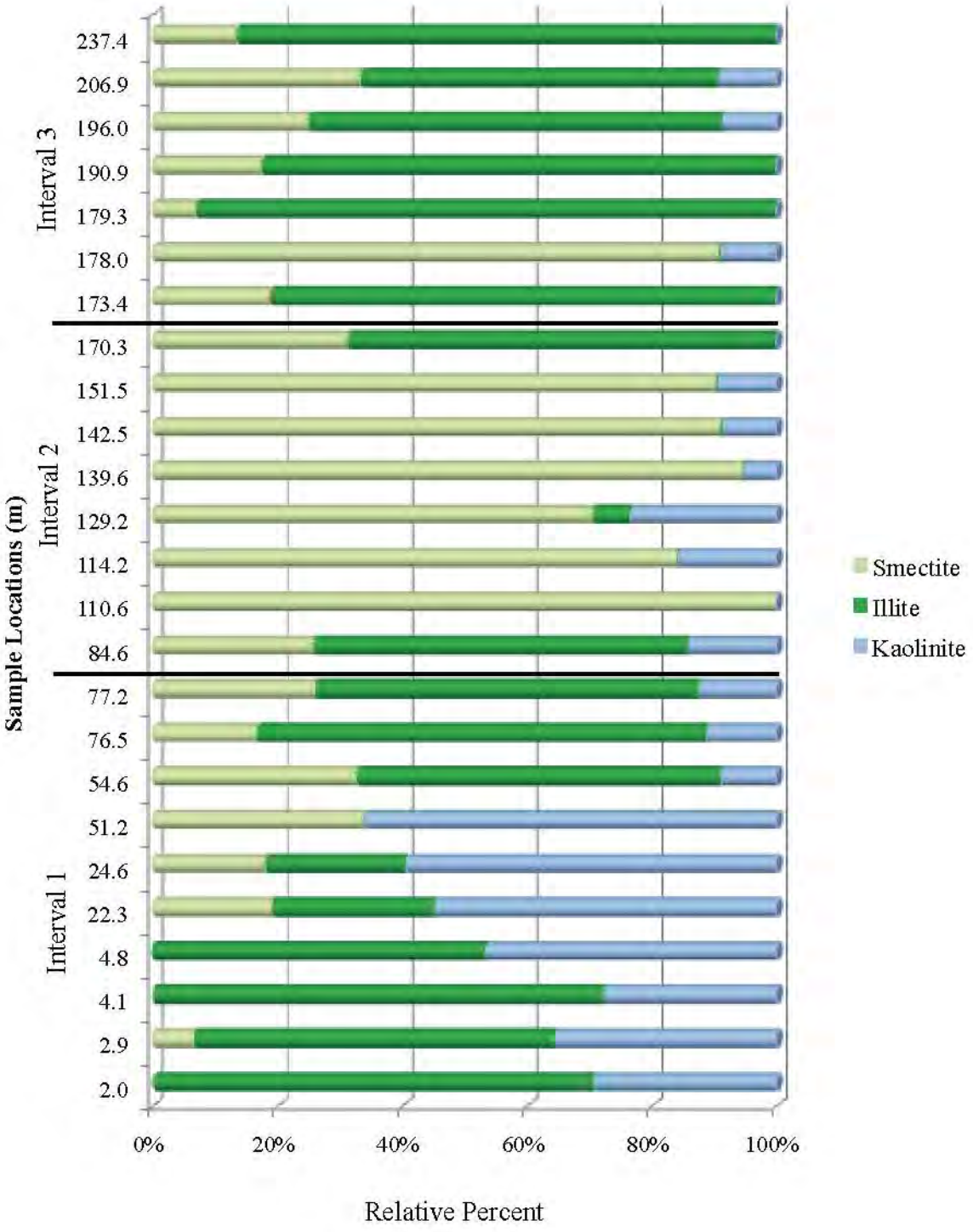
Sample Locations (m)
Interval 3
Interval 2
Interval 1
237.4
206.9
196.0
190.9
179.3
178.0
173.4
170.3
151.5
142.5
139.6
129.2
114.2
110.6
84.6
77.2
76.5
54.6
51.2
24.6
22.3
4.8
4.1
2.9
2.0
0%
20%
40%
60%
80%
100%
Relative Percent
Smectite
Illite
Kaolinite

Figure 27. QEMSCAN data for epoxy plug 6.1 m, 5 mm x 1 mm rectangle with 3 mm pixel spacing, a paleosol sample from interval 1. A) From left: Backscatter image, map of all minerals, each individual mineral in decreasing abundance excluding other silicates and siderite. B) Mineral abundances. C) 25 mm diameter, approximate location of measured area. D) Close up view.

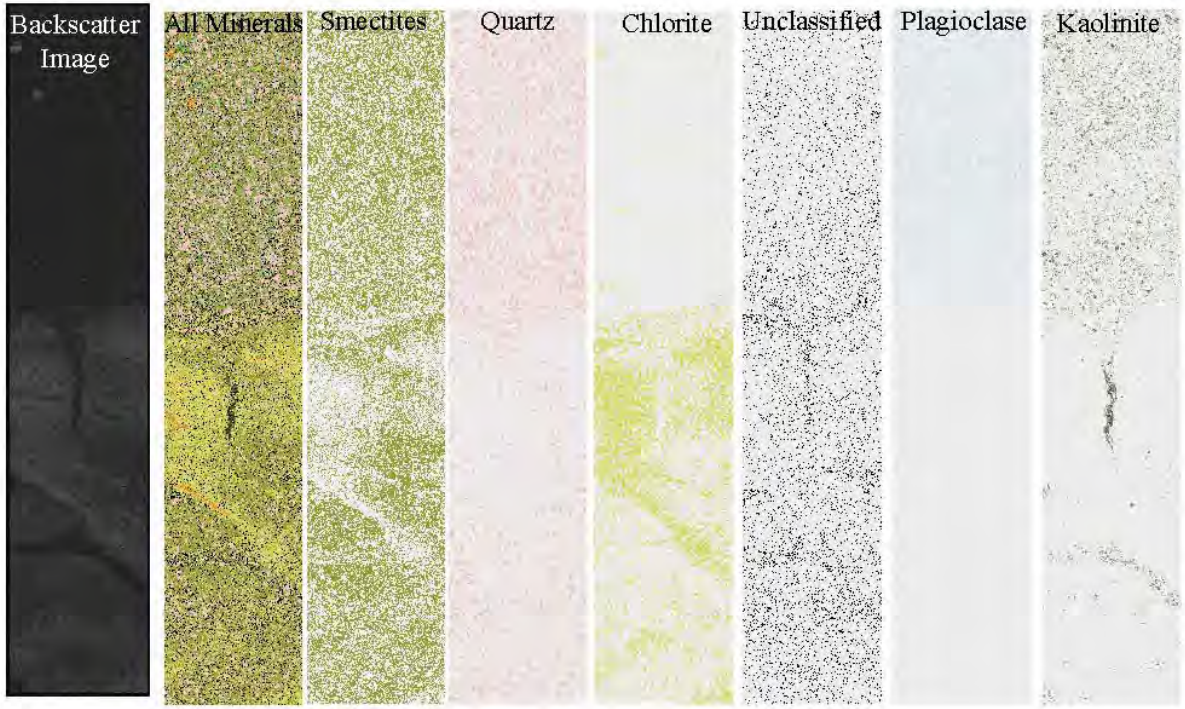

A

C

B

Mineral Name	Pixels	Area %
Smectites	263511	45.53
Quartz	115323	19.93
Chlorite	101422	17.52
Unclassified	44765	7.73
Plagioclase	19623	3.39
Kaolinite	18981	3.28
Other Silicates	10543	1.82
Siderite	4572	0.79

D

Figure 28. QEMSCAN analyses from fine to coarse sandstones.

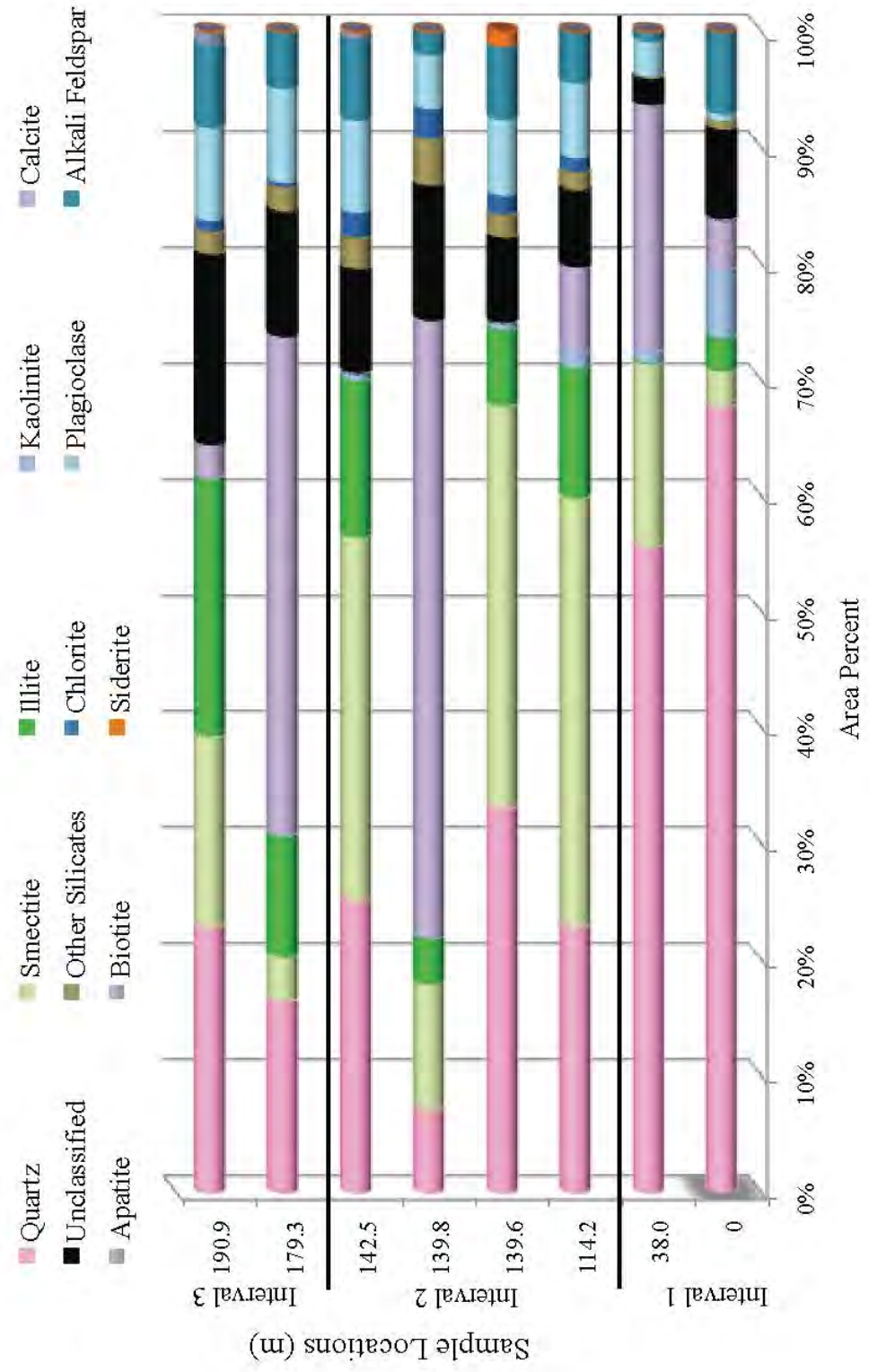
Quartz
Smectite
Illite
Kaolinite
Calcite
Unclassified
Other Silicates
Chlorite
Plagioclase
Alkali Feldspar
Apatite
Biotite
Siderite
Interval 3
190.9
179.3
Interval 2
142.5
139.8
139.6
114.2
Interval 1
38.0
0
Sample Locations (m)
0%
10%
20%
30%
40%
50%
60%
70%
80%
90%
100%
Area Percent

Figure 29. QEMSCAN data from paleosol samples.

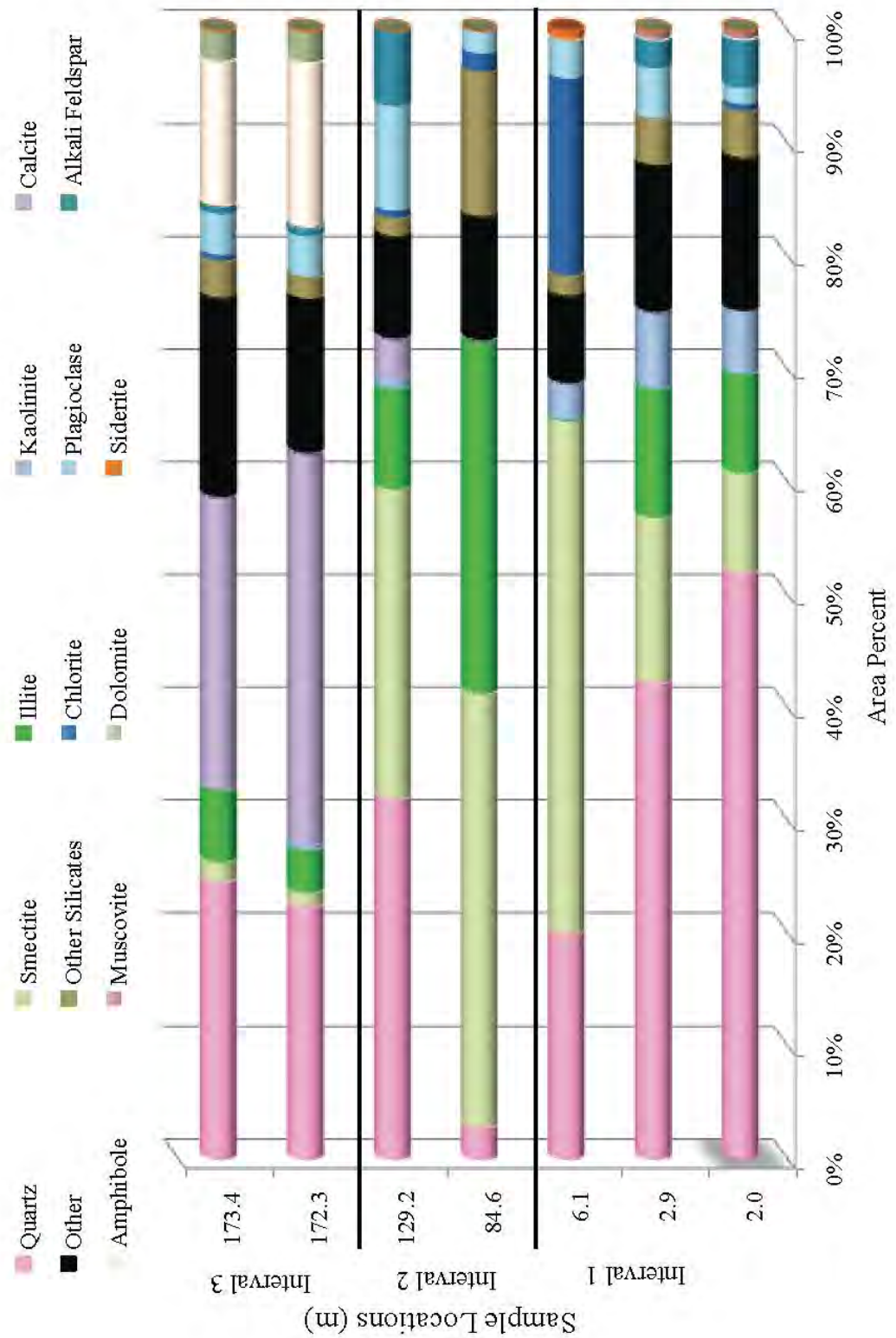
Quartz
Other
Amphibole
Smectite
Other Silicates
Muscovite
Illite
Chlorite
Dolomite
Kaolinite
Plagioclase
Siderite
Calcite
Alkali Feldspar
Sample Locations (m)
Interval 3
Interval 2
Interval 1
173.4
172.3
129.2
84.6
6.1
2.9
2.0
0%
10%
20%
30%
40%
50%
60%
70%
80%
90%
100%
Area Percent

Figure 30. All QEMSCAN data, values are in weight percent of sample.
* = Paleosol horizon

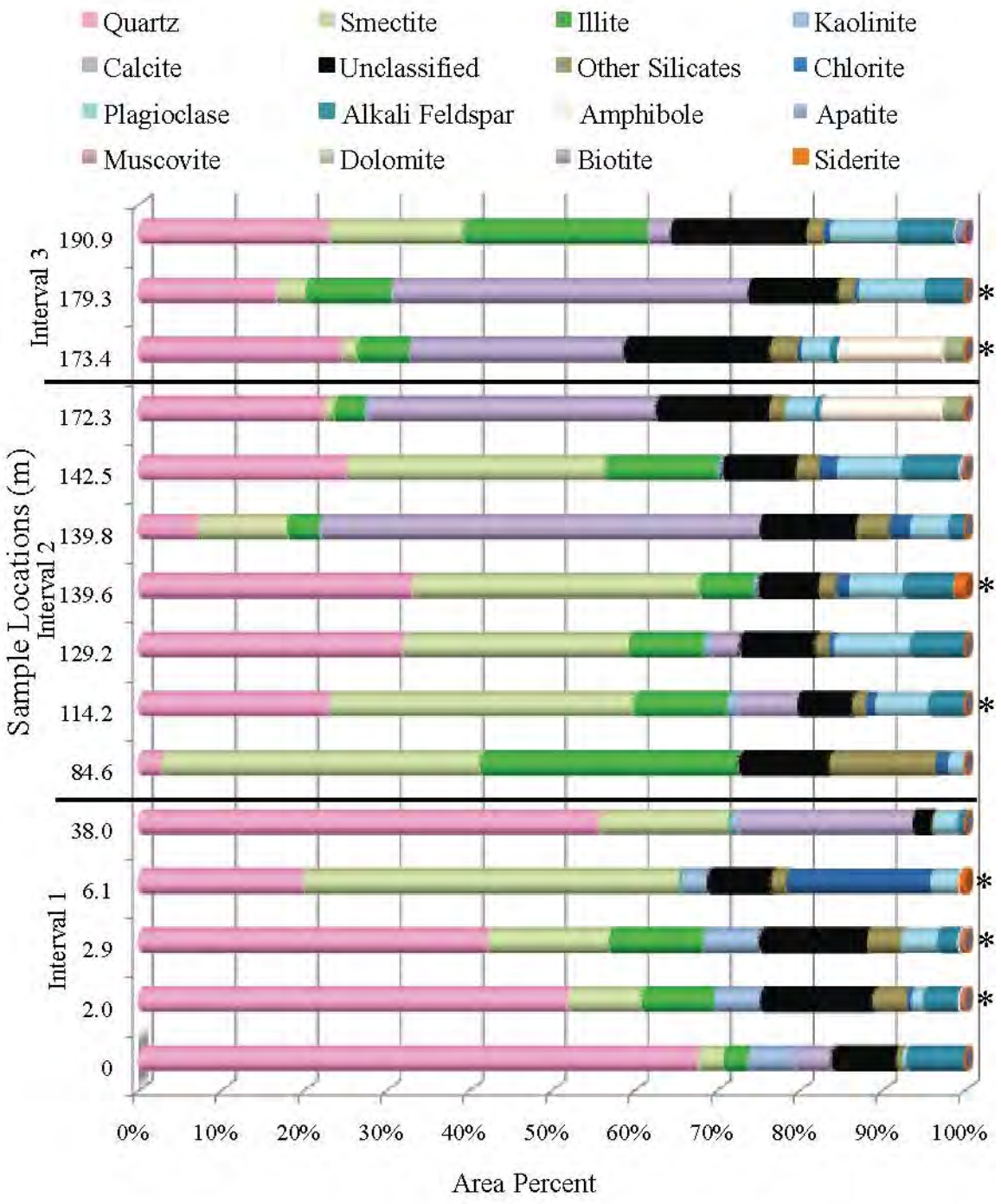
Quartz
Smectite
Illite
Kaolinite
Calcite
Unclassified
Other Silicates
Chlorite
Plagioclase
Alkali Feldspar
Amphibole
Apatite
Muscovite
Dolomite
Biotite
Siderite
Sample Locations (m)
Interval 3
190.9
179.3
173.4
Interval 2
172.3
142.5
139.8
139.6
129.2
114.2
84.6
Interval 1
38.0
6.1
2.9
2.0
0
*
0%
10%
20%
30%
40%
50%
60%
70%
80%
90%
100%
Area Percent

Figure 31. Paleosol textures for the first four paleosol samples analyzed using QEMSCAN. A) and B) show illite rimming alkali feldspar grains. C) Siderite (a minor portion of the sample), interspersed throughout an area dominated by chlorite. D) A carbonate nodule and the higher magnification image shows quartz grains dispersed throughout a matrix of illite, E) A lense of chlorite and smectite and a matrix of dominantly illite. F) shows the illite rimming alkali feldspar grains. G) and H) show calcite cementing grains together. Detailed mineral modal proportions of all samples are given in Appendix C. Each sample is 1000 microns in width unless otherwise noted.

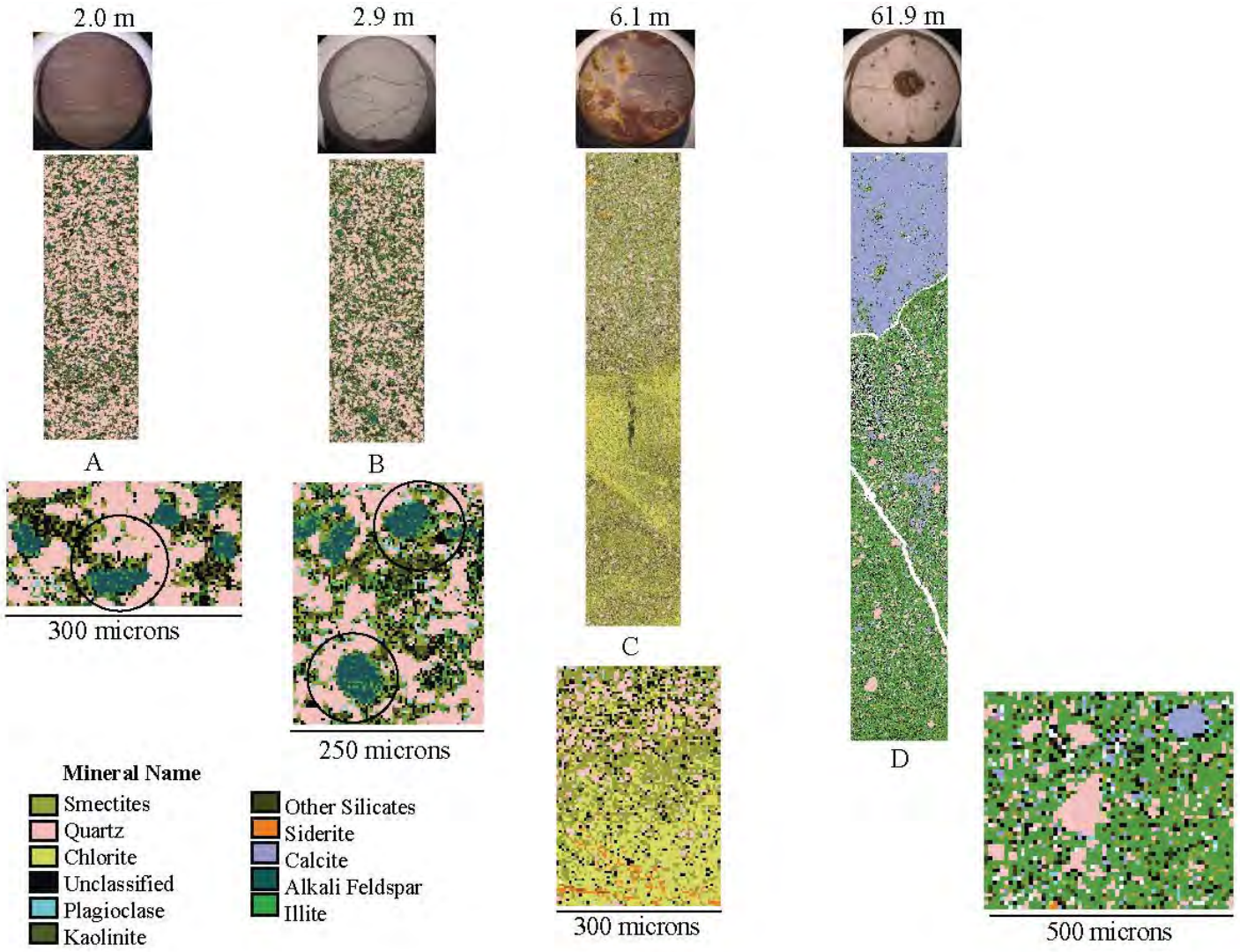
2.0 m
2.9 m
6.1 m
61.9 m
A
B
C
D
300 microns
250 microns
300 microns
500 microns
Mineral Name
Smectites
Quartz
Chlorite
Unclassified
Plagioclase
Kaolinite
Other Silicates
Siderite
Calcite
Alkali Feldspar
Illite

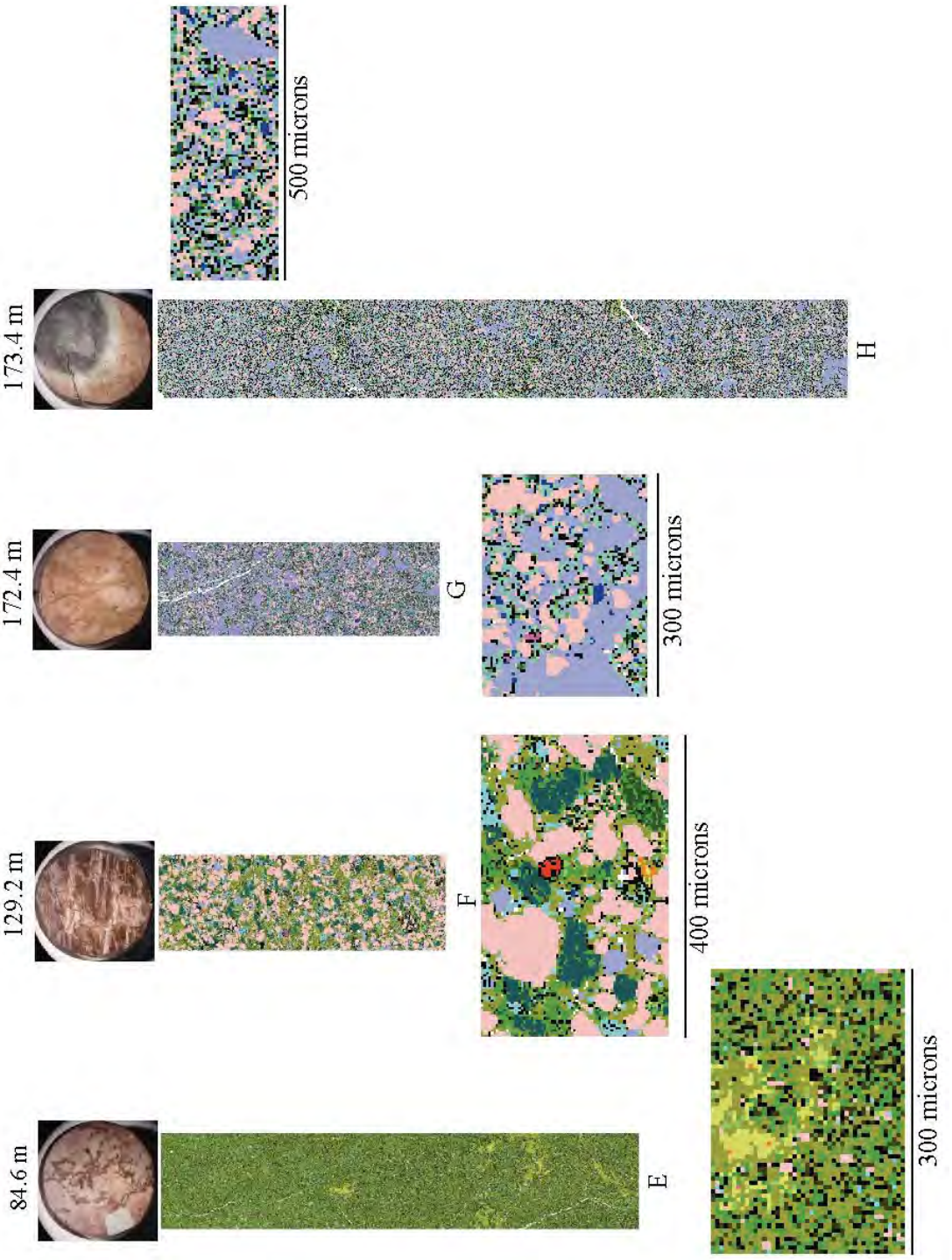
84.6 m
129.2 m
172.4 m
173.4 m
E
F
G
H
300 microns
400 microns
300 microns
500 microns

Figure 32. All QEMSCAN clay data normalized to 100%.
* = Paleosol sample

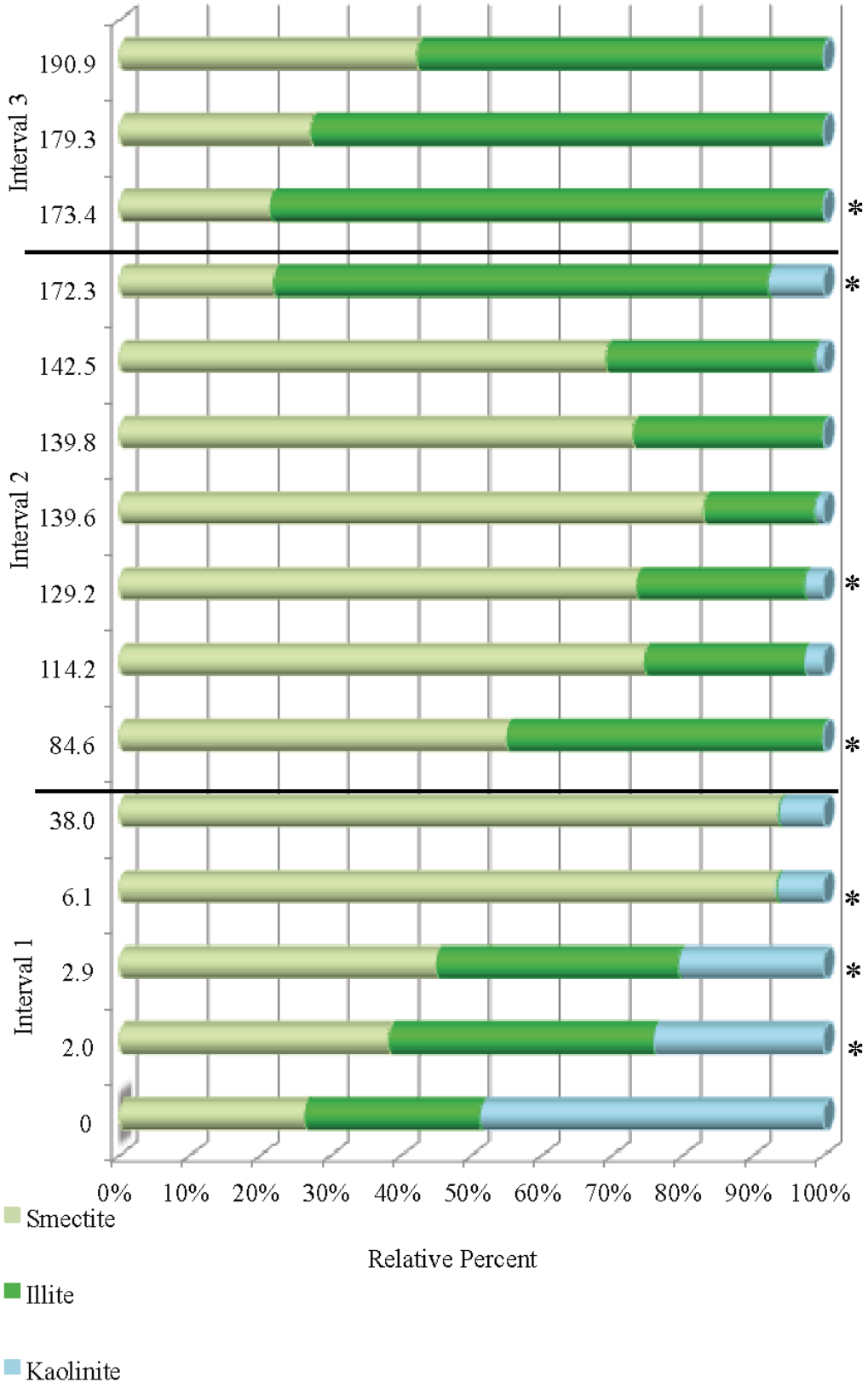
Interval 3
190.9
179.3
173.4
Interval 2
172.3
142.5
139.8
139.6
129.2
114.2
84.6
Interval 1
38.0
6.1
2.9
2.0
0
*
0%
10%
20%
30%
40%
50%
60%
70%
80%
90%
100%
Relative Percent
Smectite
Illite
Kaolinite

Figure 33. Graphs comparing XRD and QEMSCAN. A) 11 samples analyzed with XRD, Sample 6.1 m contains I/S but values could not be calculated, shown on the plot to highlight the difference between XRD and QEMSCAN. B) Same 11 samples analyzed with QEMSCAN showing clay data only. The data is not expected to be exactly the same but show similar trends such a decrease in kaolinite upsection and a predominance of smectite in interval 2.

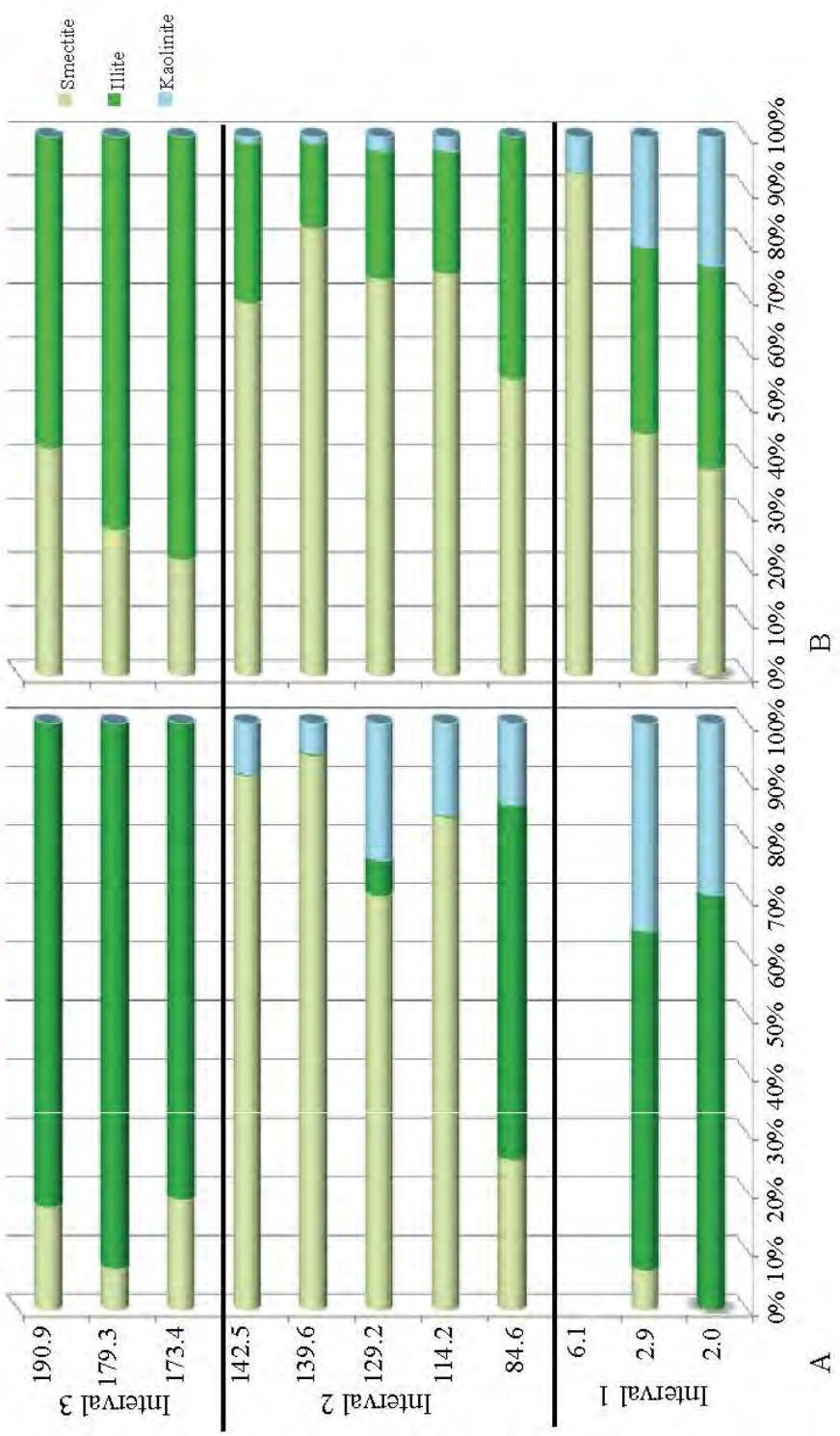
Smectite
Illite
Kaolinite
Interval 3
190.9
179.3
173.4
Interval 2
142.5
139.6
129.2
114.2
84.6
Interval 1
6.1
2.9
2.0
0% 10% 20% 30% 40% 50% 60% 70% 80% 90% 100%
A
B

Table 3. Clay Portion of the QEMSCAN Data

		Illite		Kaolinite		Smectite				
Interval	Depth (m)	Pixels	Area %	Pixels	Area %	Pixels	Area %	Total Clay Pixels	All Pixels	% Clay in Sample
1	0	7762	25	15189	49	8192	26	31143	265527	12
	2.0	43994	38	28089	24	44443	38	116526	498147	23
	2.9	56240	34	33849	21	73718	45	163807	498021	33
	6.1	0	0	18981	7	263511	93	282492	578740	49
	38.0	0	0	2060	6	30016	94	32076	190482	17
2	84.6	101094	45	0	0	124041	55	225135	323064	70
	114.2	31081	23	3722	3	102389	75	137192	276916	50
	129.2	16717	24	1965	3	51955	74	70637	189049	37
	139.6	9308	16	767	1	48961	83	59036	140987	42
	139.8	14415	27	0	0	38793	73	53208	360426	15
	142.5	63409	30	2627	1	147686	69	213722	469488	46
3	172.3	13121	70	1474	8	4099	22	18694	344645	5
	173.4	29102	79	0	0	7956	21	37058	453661	8
	179.3	20460	73	0	0	7607	27	28067	197673	14
	190.9	99150	58	0	0	72347	42	171497	442755	39

DISCUSSION

The Chinle Formation stratigraphy of the study area (Paria) comprises river and floodplain environments as evidenced by the abundant pedogenic features in the paleosols. The relatively thick Chinle Formation succession here is a good place to document a poorly-studied section and determine if any paleoclimate implications can be interpreted using stratigraphy, clay mineralogy, composition, and textures. On visual inspection and initial interpretations, the three distinct intervals of colors across the butte (Figure 12) are related to changes in depositional style during the Late Triassic, which I discuss in the following paragraphs.

Sedimentology and Stratigraphy:

Shinarump

The Chinle Formation units of the Paria region includes the basal Shinarump Member which infills paleovalleys in the Lower Triassic Moenkopi Formation (Figure 13). The Shinarump Member is a sandstone and conglomeratic sandstone unit that was deposited within braided streams. The abundance of trough cross beds and the fining upwards are partial evidence for braided stream deposition (Dubiel 1987). Additionally, the geometries and characteristics of these sandstones and their proximity to an abundance of paleosols are indicative of a fully terrestrial continental deposit. These streams predominantly flowed in a northwesterly direction, as indicated by paleocurrents

in the study area (Figure 14) and confirmed by other regional studies (Blakey and Gubitosa, 1983).

Interval 1 (Blue Mesa Member and Sonsela Member Equivalent)

Interval 1 consists predominantly of low chroma colors (Figure 15). In sample 6.1 m, burrows as well as root structures can be seen (Figure 18). The root structures are evidenced by the drab yellow halos, which form when anaerobic activity occurs in stagnant water around roots and chemically reduces the surfaces leaving the areas oxidized (Retallack, 1990). At 56.5 m, the upper portion of interval 1, pedogenic carbonate nodules are seen in increasing amounts associated with a K horizon (a resistant layer consisting of coalesced nodules) (Figure 18). The clay data below 6.1 m show that smectite is lacking and I/S is evident as in inflection at the beginning of the difractogram in sample 6.1 m (Figure 25). This inflection means that there are some swelling clays in the sample, but nothing identifiable and relative percent cannot be calculated. The lack of smectite and the evidence of illite could mean that smectite was converted to I/S during burial. However, studies have shown that the change from smectite to I/S to illite is a very gradual change that can be seen over hundreds of meters (Moore and Reynolds, 1989). The change in the Paria samples is found over a very short range, around 20 m. Alternatively, the lack of smectite in this interval could also mean the source area of the sediment only had illite and I/S available therefore no smectite could be deposited. The mineral composition and textures of QEMSCAN samples that are paleosols can be seen in Figure 31. Samples 2.0 and 2.9 m are similar in composition except that 2.0 is a bit siltier, but both show illite rimming the alkali feldspar grains which indicate that the illite

formed *in situ.* The clays in samples 6.1 and 61.9 m do not rim any of the grains and seem to be randomly dispersed throughout the samples.

Interval 1 represents vertisols and calcisols (the K-horizons) and indicates a moderately wet climate. Soils were periodically waterlogged and abundant gleying and mottling occurred. Pedogenic carbonate nodules are found near the top of interval one, indicating seasonal wetting and drying (monsoonal conditions) became a more pronounced part of the climate. Pedogenic carbonates form in climates where distinctive seasonal variations in precipitation minus evaporation occur (Breecker, 2010). The presence of pedogenic calcite, especially in nodular layers, is important because it has paleoclimatic implications. Calcite precipitates out when the soil goes through wet/dry cycles with evaporation. The wetting causes calcite to infiltrate to a certain extent within the soil horizon (dependent on grain size, amount of moisture available, etc), and after drying, the calcite precipitates out. Eventually very resistant layers (K-horizons) can form after enough accumulation. The presence of pedogenic carbonate nodules from 56.5 until 68.8 m (interval 1), and in overlying intervals at 84.6 to 100.8, 110.6, 178.2 m indicate that seasonal dryness is present (Figure 16; Breecker, 2010).

Interval 1 is interpreted to include the Blue Mesa Member and Sonsela Members. In the literature, the Blue Mesa is described as a grayish-purple and light greenish-gray bentonitic mudstone with minor red-bed mudstones. In addition, color mottling, pedogenic bioturbation, reduction spots, calcrete nodules and horizons are characteristic of the Blue Mesa at Petrified Forest National Park (Heckert and Lucas, 2002) and the same features are seen at Paria. The Sonsela Member located in the Petrified Forest National park consists of interbedded sandstones and mudstones (Martz and Parker,

2010). The mudstone units of the Sonsela Member, in comparison to the Blue Mesa Member, contain a greater variety of colors, and less blue-greys and exhibits a greater maturity of calcretes and nodules that form coalesced horizons (Tanner and Lucas, 2006). The mudstones found in Martha's Butte beds of the Sonsela Member contain the red and gray "candy stripping" and well-developed pedogenic carbonates nodules are most similar to the rock units found at Paria.

Interval 2 (Petrified Forest Member Equivalent)

Interval 2 contains few low chroma colors and is predominantly red in color (Figure 15). Burrows are present sparsely within the section (Figure 23). There are carbonate nodular layers sporadically seen throughout interval 2 (Figure 20). The texture of samples 84.6 m (Figure 32) implies that the smectite is found in masses in a matrix of illite. This could indicate that the smectite formed from the alteration of ash because it is localized in the sample. QEMSCAN sample 129.2 m shows the alkali feldspar grains are being rimmed by illite indicating formation *in situ* (Figure 31). An increase in sand is evident in the latter portion of the section and from 139 to 149 m, a 10 m thick channel sandstone with interbedded conglomerate at the base is present. The presence of this channel may indicate it was avulsing or migrating across the floodplain at this time because this is the first evidence of a channel in this section (Figure 16).

Interval 2 represents vertisols and calcisols as well as small braided streams in comparison to the Shinarump Member braided streams. Interval 2 shows an increase in monsoonal conditions due to the abundance of pedogenic carbonates throughout the section as compared to interval 1. It also contains an abundance of red-colored rocks that may be related to seasonal wetting and drying (Parrish, 1992). Red soils can result from

the presence of hematite, which form under well-drained conditions. This can be attributed to paleoclimate but can also be the result of channel avulsion causing better-drained conditions (Fallin et al., 2004). The red colors in Paria are rarely associated with channel sandstones so are unlikely to be caused by channel avulsion. However, ferric oxides arguably can form in early to late diagenetic oxidizing Eh-pH conditions, potentially indicating red beds have no significance to paleoclimate (Dubiel, 1993a). The paleosol colors of Paria could be affected by paleoclimate or diagenetic alteration but cannot be fully resolved with the methods in this study.

The Petrified Forest Member is characteristically bright and variegated in color and contain some structureless, nonresistant claystone and clayey siltstone; cross-stratified non-resistant clay sandstone; and fewer cross-stratified ledge forming sandstones (Stewart et al., 1972). The Petrified Forest Member of Paria exhibits the same general characteristic rock types and is represented by interval 2.

Interval 3 (Owl Rock Member Equivalent)

The most distinguishing feature of interval 3 is the higher proportion of sand than either interval 1 or 2 and more abundant larger slickensides (Figure 16). Carbonate nodules are lacking in the last 22 m of section potentially indicating more persistent aridity. The textures of samples 172.4 and 173.4 m both show that calcite is in the matrix and comprises 20-30% of the sample (Figure 32). This means that it probably formed from the wetting and re-drying of the paleosols and the calcite leached into the soil, filling in pores.

Interval 3 represents the same types of soils as the first two intervals, vertisols and calcisols. The absence of calcisols from the end of the section may indicate the end of the

monsoonal climate but it also could indicate that there wasn't enough calcium carbonate in the system to precipitate out.

The average grain size changes throughout all three intervals. Interval 3 has the coarsest grain sizes. The finer grain sizes, silts and clays are found most abundantly at the base of the section in interval 1. These fine grain sizes impede drainage and causes water logged soils. Up-section in the upper portion of interval 2 and throughout interval 3, sand (Figure 16) is a more major part of the rocks therefore the ability of soils to drain increases. The increase in grain size is likely due to the fact that the river systems are avulsing in intervals 2 and the bottom portion of interval 3 or that ephemeral stream deposits are forming from the more intense seasonal rains.

Interval 3 is most likely the equivalent of the Owl Rock Member. As noted from the literature this member contains pale red to light-greenish-gray carbonate ledges with various brown colored mudstone, siltstone, and fine sandstones (Dubiel, 1993).

Paleoclimate

One of the goals of this project is to determine if the Chinle Formation paleosols of Paria give any indications of the changing climate of the Late Triassic in Utah. Regarding clay mineralogy, kaolinite seems to be the only clay that formed from specific paleoclimatic conditions within the study area. Kaolinite is most abundant (30-65% of the clay portion of the samples) in the lower portion of interval 1 (Figures 27). It generally forms in warm humid climates (Curtis, 1990). If the kaolinite in the section is detrital, it indicates that the source area (likely to the south since streams in general flow in a northwesterly direction) was found in a humid climate. If it is authigenic, then it could be a weathering product of feldspars (Schultz, 1963). Kaolinite is found sporadically in

minor amounts (0-25%) of the clay portion of samples in intervals 2 and 3, which indicates fluctuating climatic conditions of aridity and humidity. It seems likely that the kaolinite formed elsewhere in the basin to the southeast where the climate was similar and then deposited in Paria because the kaolinite is found randomly dispersed throughout the QEMSCAN samples (Figure 32) not as grain coatings or the alteration of other grains. This means that the kaolinite was likely transported, and although there would be a time lag from formation to re-deposition, it indicates that somewhere nearby the environmental conditions were appropriate (humid) for formation. Therefore it can be inferred that the source area climate as well as Paria were both humid to an extent during kaolinite formation and re-deposition.

The smectite clays found in Paria could be the result of chemical weathering from warm temperatures and greater rainfall (Robert and Kennett, 1994). However, abundant volcanic input was likely during the Late Triassic, from the active Cordilleran arc as well as possibly the Mogollon slope (Figure 2). Volcanic ash alters to smectite clay (Tribble, 1994). Therefore it is likely that most of the smectite clay found in the rocks at Paria is derived from volcanic ash and not from climate induced weathering reactions.

Illite is found sporadically throughout the section but most abundantly within the first and third intervals. If illite was authigenic or formed in the soil, a clay rim may be seen around the deteriorating grain or delicate intergrowths. Illite is found to be rimming grains, mostly alkali feldspar grains in the QEMSCAN samples (Figure 32). The alteration of feldspar to illite is a common occurrence (Nesbitt and Young, 1989) and does not have major paleoclimate indications.

Diagenetic minerals can be difficult to distinguish but are formed after burial and are affected by increasing pressure and temperature. Interstratified illite/smectite (I/S) is a diagenetic or detrital mineral. The Chinle Formation did not reach the appropriate burial depth and temperature for illite to form from smectite (Zuber and Parnell, 1989), but experimental work has show shown that the repeated wetting and dying of smectites in highly alkaline solutions can cause illitization to occur (Sroden and Eberl, 1984). Such conditions are not evident at Paria, and therefore it is likely that the I/S is detrital, forming elsewhere at an earlier time and then re-deposited in the Paria strata.

The increase in calcite and pedogenic carbonate in the rocks also point to increased seasonality, pedogenic carbonates form in climates where distinctive seasonal variations occur (Breecker, 2010). The increased sand in the upper portions of the section came mostly from channel avulsion and/or the increase in ephemeral streams. These ephemeral streams form from the more intense seasonal rains that caused increased erosion of intrabasinal material.

In summary, the clay kaolinite is a paleoclimate indicator of humid conditions whereas smectite probably formed from the volcanic ash that was being brought in by the Cordilleran Arc and/or a more southerly source (Figure 2). Illite is probably for the most part detrital except for samples where it rims alkali feldspar grains, indicating *in situ* formation. The increase in calcite and sand in the section also suggests increased dryness. It is important to note that this is just one section in one field area. Some of these paleoclimate indicators maybe localized but without further study in different areas, the degree of how localized these factors are cannot be determined. In addition, the changes upsection may be due to the changes in paleoclimate coupled with the northward

movement of Pangea. Trying to disentangle climate from the northward movement of Pangea or basin-scale tectonic change would be an ideal further study for this region.

QEMSCAN vs Clay Mineralogy XRD

One important difference between x-ray diffraction and QEMSCAN analysis that should be noted is that XRD clay samples are from crushed whole rock samples, unbiased to any grains or color change, whereas there were very specific goals for the QEMSCAN analyses; to better understand the differences and textures within the sample. Therefore they should be similar in composition but there is no expectation that they should be exactly the same.

XRD analysis is the standard when identifying clay minerals in a sample. In order to determine if QEMSCAN is a viable method for identifying clays, 11 samples analyzed with QEMSCAN were also analyzed with XRD (Figure 31), and they showed very similar trends. Although XRD is a relatively simple and quick way to identify clay minerals, it does not give information regarding textures. QEMSCAN allows for compositional and textural data and the association of particles. If a sample is layered or laminated for example, QEMSCAN is able to identify the mineral make up of each layer, which can give clues to how it formed.

QEMSCAN is a newer technology that has the potential to better identify fine-grained sedimentary rocks, whereas clay XRD work is a better constrained technology. By comparing each method in regards to clay minerals in each sample, the rigorousness of the QEMSCAN method was tested.

One of the main issues with QEMSCAN is that the interchangeable cations in smectite clays allows for many substitutions that the QEMSCAN Oil & Gas SIP

produced by FEI does not account for. For each clay mineral a specific amount of each element is allowed in a particle. If the amount exceeds or falls short of these values, or if an element such as titanium is found in the sample but not in the SIP, the particle is marked as "other." This explains why there is a range in "other" from 2 to ~18% of samples. QEMSCAN identifies the larger sedimentary grains more accurately than clays. One of the main reasons for this is that a 20 μm quartz grain with a 2 μm pixel spacing will be analyzed 10 times, whereas a 2 μm clay will only be analyzed once. On an elemental map of the sample minor discrepancies in the quartz grain can be resolved using the surrounding data but there is no way of resolving a 2 μm grain with surrounding particles because they are discrete particles. There is also the issue of edge effects, if the beam analyzes between a quartz grain and a clay particle, a mixture of the two compositions will be acquired and more than likely neither particle will be identified correctly.

Another reason for the difficulty in differentiating clays such as smectite and illite is due to their complex and interchangeable chemical formulas. One of the most common smectites, montmorillonite, has the chemical formula: $(Al_{1.67}Mg_{0.33})Si_4O_{10}(OH)_2$. Illite has the general chemical formula of $K_{0.65}Al_2(Al_{0.65,}Si_{3.35,})O_{10}(OH)_{2,}$ and kaolinite has the chemical formula of $Al_2Si_2O_5(OH)_{4.}$ The distinguishing feature of illite compared to smectite and kaolinite is that it contains potassium (K) but it shares the same basic elements of Al, Si, O, and H. The chemical formulas above are the idealized general formulas; once substitutions occur the mineral composition can change dramatically therefore the SIP for identifying minerals may have difficulties distinguishing the substituted versions. Table 4 shows the similarities of the compositions regarding their

elemental weight percent. Some of the elements are also on the border of the detection limit, which is about 5%. When elements are below the detection limit for a mineral phase, the identification program will depend on other factors in order to accurately identify a mineral, such as the ratio of the other minerals.

An obvious issue that can be seen when comparing data is that XRD does not identify any chlorite within the samples whereas QEMSCAN does identify this mineral. The main issue with chlorite is that it can be a clay-sized mineral or form in larger aggregates. This could explain why the clay work did not identify chlorite but QEMSCAN did. The grain size of the chlorite was larger than 2 micrometers and never made it to the glass slide for x-ray analysis. On the other hand, the SIP program could be misidentifying an iron-rich muscovite as chlorite.

The results outlined in the previous sections indicate some key differences between XRD and QEMSCAN analytical methods. XRD analysis uses the spacing between the clay structures to identify the minerals whereas QEMSCAN identifies the elements (Fe, Al, Si) and puts them together to give a chemical formula. The pitfalls of XRD work include overlapping peaks for specific minerals so individual peak can be masked; therefore the exact identification may not be able to be determined. QEMSCAN on the other hand does not use dangerous chemicals, is non-destructive, and can use whole rock, thin sections or epoxy plugs compared to powdered samples on a slide. QEMSCAN does have the capability to analyze powdered samples and this is what should be used for quantitative analysis.

Even with some of the limitations, QEMSCAN is a good general indicator of the minerals, specifically clay minerals in a sample. The three thin sections that were

described petrographically are a minor portion of this study but were made to ground-truth the data from QEMSCAN and XRD. The advantage of thin section work is that a trained eye can visually identify the grains, some of the clays, and view the grain interactions. What thin section petrography of fine-grained samples doesn't give is a quantitative account of the sample, and point counting a sample is only useful when studying sandstones and siltstones, not claystones. Using all three methods, QEMSCAN, XRD, and thin sections is ideal, but if a quick quantitative and qualitative account of a sample is needed, QEMSCAN would be ideal.

Figure 34. Summary of the data in the study relating the stratigraphic and clay analyses to paleoclimate.

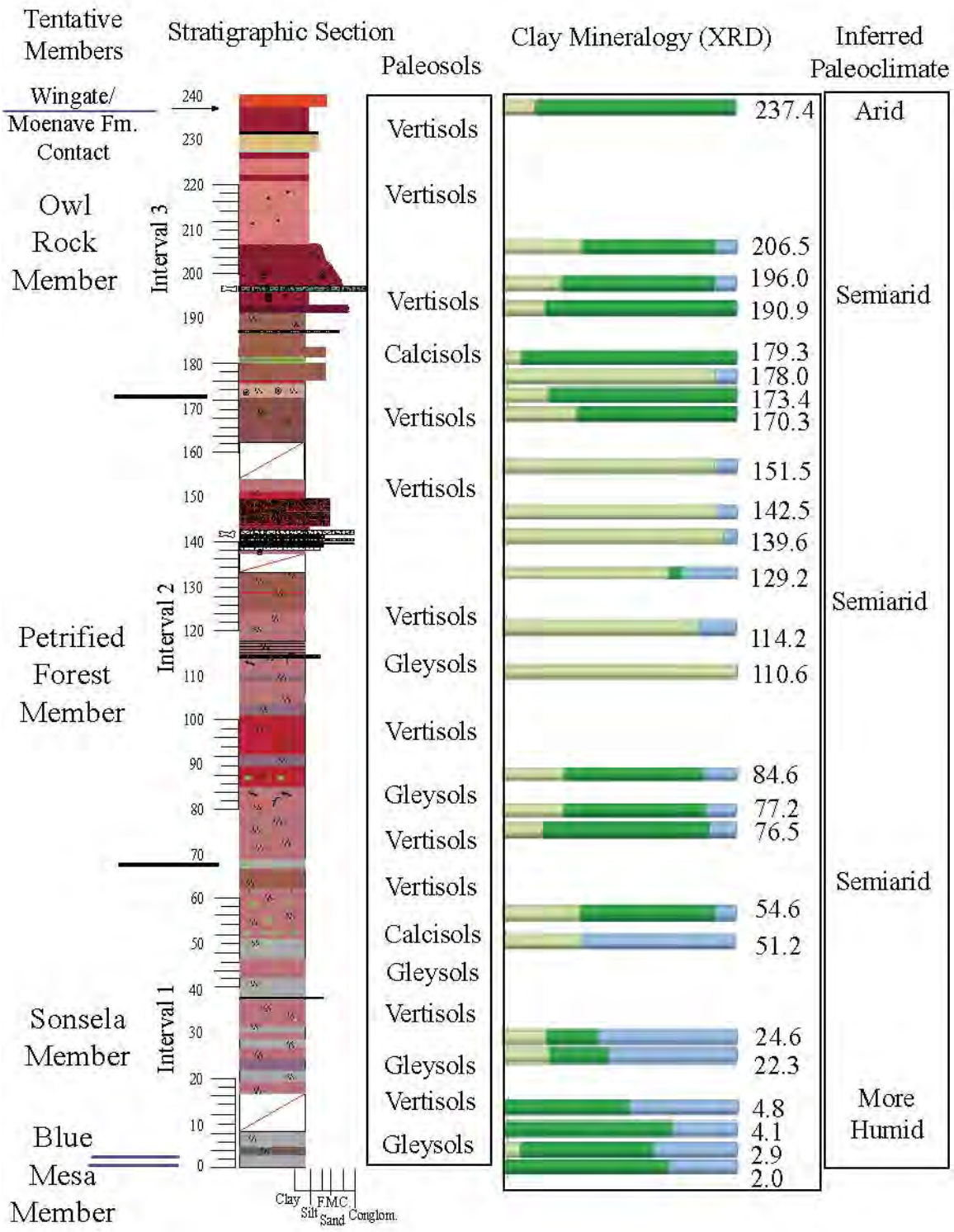
Tentative Members
Stratigraphic Section
Paleosols
Clay Mineralogy (XRD)
Inferred Paleoclimate
Wingate/ Moenave Fm. Contact
Owl Rock Member
Petrified Forest Member
Sonsela Member
Blue Mesa Member
Interval 3
Interval 2
Interval 1
240
230
220
210
200
190
180
170
160
150
140
130
120
110
100
90
80
70
60
50
40
30
20
10
0
Vertisols
Vertisols
Vertisols
Calcisols
Vertisols
Vertisols
Vertisols
Gleysols
Vertisols
Gleysols
Vertisols
Vertisols
Calcisols
Gleysols
Vertisols
Gleysols
Vertisols
Gleysols
237.4
206.5
196.0
190.9
179.3
178.0
173.4
170.3
151.5
142.5
139.6
129.2
114.2
110.6
84.6
77.2
76.5
54.6
51.2
24.6
22.3
4.8
4.1
2.9
2.0
Arid
Semiarid
Semiarid
Semiarid
More Humid
Clay
Silt
F.M.C.
Sand
Conglom.

Table 4. Elemental Weight % (El. Wt%) of Select Minerals

	Illite	Kaolinite	Na-Montmorillonite (Smectite)	Chlorite	Muscovite
Elements	El. Wt %	El. Wt %	El. Wt %	El. Wt %	El. Wt %
K	6.60	0.00	0.00	0.00	9.82
Na	0.00	0.00	2.09	0.00	0.00
Mg	0.00	0.00	2.20	11.78	0.00
Al	18.57	20.90	12.25	8.72	20.32
Fe2	0.00	0.00	0.00	18.05	0.00
Fe3	0.00	0.00	0.00	0.00	0.00
Si	24.44	21.76	30.60	13.61	21.15
O	41.56	30.99	43.59	25.85	40.17
H, OH	0.52	1.56	0.55	1.30	0.51
O	8.31	24.79	8.72	20.68	8.03
Total	100	100	100	100	100

CONCLUSIONS

1) Clay mineralogy of paleosols alone implies but does not prove that there were major climatic shifts during Chinle Formation deposition in the Paria study area. The clay mineral kaolinite found within the section in addition to other features found indicate that the base of the section was likely more humid than the rest of the section. Smectite on the other hand does not seem to have any paleoclimatic indications and is likely the result of alteration of volcanic ash. Although it has been hypothesized that mainly the lower half of the Chinle Formation was affected by volcanic activity (Stewart et al., 1972), clay minerals and volcanic fragments indicate that volcanism was a significant portion of the upper half of the Chinle Formation as well.
2) Combining clay mineralogy with sedimentologic observations and regional stratigraphy does support an overall shift from seasonally wet to much drier conditions as evidenced by the change in paleosol types from gleysols to more vertisols and calcisols during the Late Triassic in the study area. Pedogenic carbonates found in the second and third intervals indicate that the climate became increasingly arid and seasonal overall but was punctuated by times of humidity. By the end of the Late Triassic and into the Jurassic, eolian sand was a dominating force of sedimentation.

3) QEMSCAN vs XRD: QEMSCAN is a non-destructive method that is used to identify the composition and texture of a sample. After analysis of a range of Chinle Formation rocks of different grain sizes and composition, the details of the strengths and weaknesses of QEMSCAN for this project has been revealed. QEMSCAN is an excellent tool to identify minerals in larger grained samples but it is not as good for clay-sized particles in a sample due to cation substitutions in clays and the inability to identify mixed layer clays such as illite/smectite (I/S). Although QEMSCAN may not be able to identify all clay minerals, it is still an excellent compositional tool that can give detailed information about a sample. QEMSCAN is a tool to put into a geoscientists toolbox and combined with other types of data such as x-ray diffraction, can further information gathered in a project.
    a. One of the main advantages that QEMSCAN can offer that x-ray diffraction cannot is compositional and textural information of a sample. For example in the elemental maps produced by QEMSCAN, it is easy to see illite rimming alkali feldspar grains but if XRD alone was performed, illite and feldspar would be identified but the grain interactions would not be.
4) It is important that continued work with paleosols in the Chinle Formation of Utah is performed so the effects of paleoclimate on soil formation can be better understood across Late Triassic outcrops.

APPENDIX A

STRATIGRAPHIC SECTION DESCRIPTION

Table A1. Stratigraphic Section Descriptions

Horizon Type	Thickness (cm)	**Cum Thick (m)**	Grain size	Color	Rock Color Values	Description	Mottles	Nodules	Burrows	Root traces	Lower contact	React to acid?
Interval 1												
C	150	**150**	silt/clay	Brownish Gray	5 YR 4/1	drab silt colored silt and clay	No	No	No	No	Indistinct	No
C	50	**200**	silt/clay	Brownish Gray	5 YR 4/1	yellow mottles	Yellow 2cm	No	No	No	Indistinct	No
C	75	**275**	silt/clay	Brownish Gray	5 YR 4/1	fewer mottles	Yellow	No	No	No	Indistinct	No
Bt	15	**290**	silt/clay	Light Olive Gray	5Y 6/1	more resistant layer, more homogenous, structureless, better cemented than previous	1/2 cm yellow blebs (Light olive brown)	No	No	No	Indistinct	No
Bt	60	**350**	silt/clay	Grayish Red	5R 4/2	more friable, slickenslides, (potential dendrites)	No	No	No	No	Indistinct	No
Bt	60	**410**	silt/clay	Grayish Red	5R 4/2	oval concentric olive mottles	Yes	No	No	No	Indistinct	No
Bt	40	**450**	silt/clay	Grayish Red	5R 4/2	more homogenous than above but fewer olive mottles	Yes	No	No	No	Indistinct	No

Table A1. Continued

Bt	30	**480**	silt/clay	Grayish Red	5R 4/2	mainly red with odd colorings, biotite flakes	Light Olive brown 5 Y 5/6 and Pale yellowish Green 10 GY 7/2	No	No	No	Indistinct	No
Bt	5	**485**	silt/clay	Grayish Red Purple	5 RP 4/2	friable, more clay, breaks apart more easily	Lt Olive blebs 1/2 cm	No	No	No	Interfinge ring	No
Bt	10	**495**	silt/clay	Grayish Red Purple AND Grayish Yellow Green	5 RP 4/2 AND 5 GY 7/2	more consolidated	Green yellow mottles	No	No	No	Indistinct	No
A	115	**610**	silt/clay	Grayish Red Purple	5 RP 4/2	slickensides, more interfingering of friable and less friable silt	Olive green	No	Yes	No	Indistinct	No
Bt	100	**710**	silt/clay	Grayish blue	5 PB 5/2	mostly massive, slightly friable with clay, many colored mottles, yellow mottles are 1/2 cm blebs	Dark Yellowish Orange 10 YR 6/6 AND Grayish Red Purple 5 RP 4/2	No	No	No	Indistinct	No

Table A1. Continued

Bt	140	**850**	silt/clay	Grayish Red Purple	5 RP 4/2	mottles, slickensides, not well consolidated	same 2 colors as above	No	No	No	Indistinct	No
N/A	790	**1640**	N/A	N/A	N/A	N/A (Cover)	N/A	N/A	N/A	N/A	N/A	N/A
A	35	**1675**	silt/clay	Light Olive Gray	5 Y 6/1	calcite precipitated out between peds, more consolidated and cemented	Lt Olive Brown 5 Y 5/6 blebs AND Grayish Red Purple 5 RP 4/2	No	No	No	Indistinct	Calcite along peds
Bt	100	**1775**	silt/clay	Grayish Red	10 R 4/2	more friable, mostly purple but some lt olive gray, more yellow mottles in big chunks ~ 2cm oval, abundant slickensides, lines of yellow (root traces?)	dark yellowish orange, 10 YR 6/6 AND grayish yellow green 5 GY 7/2	No	No	No	Indistinct	No

Table A1. Continued

Bt	140	**1915**	silt/clay	Pale Red	5 R 6/2	similar to previous meter but slightly more red, somewhat sparlier, slicks abundant, yellow blebs still throughout, less calcite blebs	Green mottles more abundant upsection, gets veiny, same grayish yellow green color as above	No	No	No	Indistinct	Blebs do
Bt	320	**2235**	silt/clay		5 Y 5/2	varies from light olive gray and often transitions to grayish red purple (5 RP 4/2)		No	Yes	No	Indistinct	No
A	230	**2465**	silt/clay	Grayish Red Purple	5 RP 4/2	some areas of yellow ~5 cm in size, irregular shapes	Mottling with lt olive brown (5Y 5/6) with pale olive haloes (10Y 6/2) around lt olive	No	Yes	No	Indistinct	No
Bt	220	**2685**	silt/clay	Grayish Red & Lt Olive Grey	5 R 4/2 & 5Y 6/1	same as previous, slickensides, mottling, not a predominant color, calcite blebs on faces	Purple and yellow (olive brown) mottles	No	No	No	Indistinct	Blebs do

Table A1. Continued

A	200	**2885**	silt/clay	Med Lt Gray	N5	gray with yellow blebs, little to no purple, slickennsides are fewer, well cemented	Lt olive br (5Y 5/6)	No	No	No	Indistinct	No
Bt	140	**3025**	silt/clay	Grayish Red	10 R 4/2	small slickensides	Some mottles pale olive (10Y 6/2)	No	No	No	Indistinct	No
Bt	170	**3195**	silt/clay	Lt Olive Gray	5Y 6/1	gray with yellow mottly veins, some slickensides	Lt olive br (5Y 5/6)	No	No	No	Indistinct	No
Bt	150	**3345**	silt/clay	Grayish Red	10 R 4/2	mottling abundant	Lt olive gray (5Y 6/1) Moderate yellow (5Y 7/6)	No	No	No	Indistinct	No
Bt	170	**3515**	silt/clay	Grayish Red	10 R 4/2	lenses of yellow gray	Yellowish gray (5Y 8/1)	No	No	No	Indistinct	No
Bt	230	**3745**	silt/clay	Grayish Red	10 R 4/2	slickensides, few yellow blebs	Pale Olive (10Y 6/2)	No	No	No	Indistinct	No
A	30	**3775**	silt/clay	Olive Gray	5 Y 4/1	gray with red mottles	Few grayish red	No	No	No	Indistinct	No
N/A	25	**3800**	fine & medium sand	Lt Olive Gray	5 Y 6/1	subrounded to subangular grains, laminae with darker gray color	No	No	No	No	Planar	Carb Cement
A	380	**4180**	silt/clay	Olive Gray	5 Y 4/1	massive gray, somewhat friable, few to no mottles	Few	No	No	No	Indistinct	No

Table A1. Continued

A	80	**4260**	silt/clay	Olive Gray	6 Y 4/1	same as above but with more mottles (purple and yellow)	Purple and yellow	No	No	No	Indistinct	No
Bt	260	**4520**	silt/clay	Grayish Red	10 R 4/2	red with green mottles	Lt Olive Gray 5 Y 5/2	No	No	No	Indistinct	No
Bt	140	**4660**	silt/clay	Red	5 R 5/4	homogenous red horizon	No	No	No	No	Indistinct	No
A	460	**5120**	silt/clay	Lt Olive Gray	5 Y 6/1	gradual gradation to gray	No	No	No	No	Indistinct	No
Bt	340	**5460**	silt/clay	Grayish Red	5 R 4/2	few pale yellowish green mottles	Dark Yellowish orange (10 YR 6/6)	No	No	No	Gradual	No
K	190	**5650**	silt/clay	Grayish Red	5 R 4/2	red with green mottled carbonate nodules, some calcite crystals are well formed, basically all nodular layer	Pale Greenish yellow (10Y 8/2)	Yes	No	No	Uneven due to carb nodules	Nods
Bk	520	**6170**	silt/clay	Grayish Red	5 R 4/2	red with green mottles sporadic, few nodules, non rounded shapes, don't fizz, slowly lightens in color to lt brownish gray (5 YR 6/1)	Red and Green	Yes	No	No	Grades into fewer carb nodules, Gradual	Nods
Bc	20	**6190**	silt/clay	Lt Olive Gray	5 Y 6/1	gray friable w/black nodules, slight tones of red	No	Yes-2mm	No	No	Gradual	Nods

Table A1. Continued

Bk	460	**6650**	silt/clay	Pale Reddish Brown, grades into dark reddish brown, grayish red and grayish red purple	10 R 5/4 AND 10R 3/4 AND 5 R 4/2 AND 5 RP 4/2	veiny mottles, increased carbonate nodules as you go up, more green and purple zones, some yellow areas of mottling, matrix does not fizz	Yes Greenish gray (5GY 6/1) AND Pale olive 10Y 6/2 and green zones	up to ~20 cm	no	no	Indistinct	Nods
Bk	230	**6880**	silt/clay	Greenish Gray	5 GY 6/1	very friable, some grayish red purple (5 RP 4/2)	No	1-2 cm carb nod	no	no	Transitio nal into red	Nods
Interval 2												
Bk	775	**7655**	silt/clay	Grayish red	10 R 4/2	red w/green mottles and small 1-2 cm carb nodules, abundant slicks in lower portion, yellow mottles, grades into a purple color	Dark yellowish orange AND Greenish gray 5 GY 6/1	Yes	No	No	Gradation al from previous	Nods

Table A1. Continued

Bc	70	**7725**	silt/clay	Grayish red purple	5 RP 4/2	small regions of dusky red in matrix slickensides	Veiny, some mottles grayish yellow green 5GY 7/2 AND Lt olive brown blebs (5 Y 5/6) very few	No	No	No	Grades from Red to purple	No
A	55	**7780**	silt/clay	Grayish Red	10 R 4/2	very friable, green mottled zones, pale greenish yellow, mottles circular, black and reddish blebs	Yes	No	Yes	No	Indistinct	No
Bk	680	**8460**	silt/clay	Grayish red purple	5 RP 4/2	purple unit that looks faulted	No	Yes	Yes	No	Indistinct	Nods
Bk	65	**8525**	silt/clay	Grayish red purple	5 RP 4/2	abundant carb nodules	Olive gray blebs (5 Y 3/2) and dark greenish yellow, 10 Y 6/6	Yes	No	No	Gradual	Nods
Bkg	485	**9010**	silt/clay	Dusky red	5R 3/4	red matrix w/some carbonate nodules, pyritized nodules, black blebs	Grayish yellow green (5 GY 7/2)	Yes	No	No	Gradual	Nods

Table A1. Continued

Bk	260	**9270**	silt/clay	Grayish Red Purple AND Grayish Red	5 RP 4/2 AND 5 R 5/4	some green mottles that fizz with acid	Pale Olive (10Y 6/2)	Yes (pale olive)	No	No	Gradual	Yes
Bk	810	**10080**	silt/clay	Moderate red	5 R 4/6	red matrix w/green mottles in thin ~1 cm lensy areas, black nodules	Pale Olive 10Y 6/2	Yes	No	No	Gradual	Nods
Bk	305	**10385**	silt/clay	Grayish red purple	5 RP 4/2	purple with green mottles, ~2 mm black round blebs, green mottles react with acid	Pale Olive 10Y 6/3	No	No	No	Grades from red to purple	yes, the green mottles do
Bt	140	**10525**	silt/clay	Grayish red	10 R 4/2	as you continue up the green mottles get larger up to couple cm	Small green ones which are flattened along horizons (greenish gray 5 GY 6/1)		No	No	Gradual	No
Bt	30	**10555**	silt/clay	Grayish red purple	5RP 4/2	thin layers of purple w/green blebs, greenish gray, 4 mm wide	No	No	No	No	Indistinct	No
Bc	370	**10925**	silt/clay	Grayish red	10 R 4/2	greenish gray blebs small and very few	No	No	No	No	Indistinct	No
Bc	140	**11065**	silt/clay	Grayish Red Purple	5 RP 4/2	carbonate nodules	Green	Yes	No	No	Indistinct	Nods

Table A1. Continued

Bk	240	**11305**	silt/clay	Grayish red	10 R 4/2	flat shaped zones of dark yellowish orange (10 YR 6/6), small white blebs of carbonate found throughout sample	Small Greenish Gray 5GY 6/1	No	No	No	Indistinct	Nods
N/A	120	**11425**	fine sand and silt	Grayish Red Purple	5 RP 4/2	irregularly bedded ss/silt not bedded like the regional dip, small rip up clasts thoughout, some areas have more than others, looks like slump structures, area of dark reddish brown (10 R 3/4) area w/dark yellowish orage (10YR 6/6) found in some areas, not predominant	Greenish gray (mottles and layers) 5G G/1	No	No	No	Wavy	No
Bz	120	**11545**	silt/clay	Grayish Red	10R 4/2	Red w/very irregular green mottles throughout, white salt crystals on facies	Greenish Gray 5 GY 6/1	No	No	No	No	No

Table A1. Continued

Bk	290	**11835**	silt/clay	Indistinct colors, some Pale Red Purple and Pale Olive and Moderate Olive Brown	5RP 6/2 AND 10 Y 6/2 and 5Y 4/4	somewhat laminated and increasing upsection, wavy in some places, moderate olive brown in pockets	Yes	No	No	No	Gradual	Yes
	205	**12040**	silt/clay	Grayish Red Purple	5 RP 4/2	potential localized layer, not very continuous	Pale Olive 10 Y 6/2 lightly fizzes	No	No	No	purple grades into red	Yes
Bs	410	**12450**	silt/clay	Grayish red	10 R 4/2	abundant large slickensides	Greenish Gray 5 GY/1	No	No	No	purple grades into red here	select few places fizz
Bk	400	**12850**	silt/clay	Dark Reddish Brown and Light Olive Gray	10 R 3/4 AND 5 Y 6/1	No predominant color, a mix of the two colors	Yes	No	No	No	Gradual	Yes
A	70	**12920**	silt/clay	Dusky red	5 R 3/4	black areas with lighter red halos,	Pale Olive 10 Y 6/2	No	No	No	Gradual	No

Table A1. Continued

Bt	140	**13060**	silt/clay	Pale Reddish Brown	10 R 5/2	looks like the red above w/lots more veiny mottling	Might Greenish Gray (5 GY 8/1)	No	No	No	Gradual	No
Bt	280	**13340**	silt/clay	Pale Reddish Brown	10 R 5/4	grades into the pale reddish brown	Some light greenish gray but more abundant	No	No	No	Gradational	Yes
N/A	390	**13730**	N/A	N/A	N/A	covered slump area near ss	N/A	N/A	N/A	N/A	N/A	N/A
Bt	90	**13820**	silt/clay	Grayish Red	5R 4/2	red silt interfingers with ss, reduction circles	Green	No	No	No	Interfingers	No
N/A	80	**13900**	med sand with	Hints of pale red	5 RP 6/2	non laminated ss with reduction circles and mud clasts	No	No	No	No	Interfingers	No
N/A	60	**13960**	fine to med sand	Hints of pale red	5 RP 6/2	laminated ss w/ reduction circles	No	No	No	No	Gradual	Light fizz
N/A	20	**13980**	conglo merate	Hints of pale red	5 RP 6/2	black tooth found, 3x5 mm red rip up clast, coarse sand increases	No	No	No	No	Flat lam w/congom on top	Yes more so
N/A	30	**14010**	lam ss	Hints of pale red	5 RP 6/2	same as previous laminated ss	No	No	No	No	Conglom has an uneven surface	No
N/A	20	**14030**	conglom	Hints of pale red	5 RP 6/2	same as previous conglomerate	No	No	No	No	Distinct	No
N/A	80	**14110**	lam ss	Hints of pale red	5 RP 6/2	same previous laminated ss	No	No	No	No	Distinct	No

Table A1. Continued

N/A	140	**14250**	conglom	Grayish red	10 R 4/2 clasts	rip up clast conglomerate w/med sand, black organic matter, w/ laminated ss w/dark black organic rich layer, becomes finer upsection	No	No	No	No	Indistinct	No
N/A	120	**14370**	medium sand and silt	Mod red	5 R 4/6	subangular to subrounded grains	Yes Yellowish Gray 5 Y 8/1	No	No	No	Indistinct	No
N/A	600	**14970**	medium sand and silt	Mod Red	5 R 4/6	laminated material from above, some dark organic horizons	No	No	No	No	Planar from laminae	No
Bt	180	**15150**	silt/clay	Mod Red	5 R 4/6	similar to previous but with pale olive reduction spots	Yes	No	No	No	Wavy	No
Bt	230	**15380**	silt/clay	Grayish Red	10 R 4/2	much more friable, flaky	No	No	No	No	Gradual	No
N/A	800	**16180**	silt/clay	N/A	N/A	cover	N/A	N/A	N/A	N/A	N/A	N/A
Interval 3												
Bk	850	**17030**	silt/clay	Mod Red	5 R 4/6	mainly red silt w/green blebs and some green veining on a fine scale, less veiny upsection, black blebs, fizzes less than lower	Yellowish gray 5 Y 8/1 1 inch diameter	No	No	No	Not seen	Yes, green regions
Bk	200	**17230**	silt/clay	Mod Orange Pink	10 R 7/4	black veiny regions	Dusky yellow	No	No	No	Gradual	Yes

Table A1. Continued

Bk	110	**17340**	silt/clay	Grayish orange pink	5 YR 7/2	reduction circles, very pale green (10 G 8/2) dark greenish gray (5 GY 4/1), lt greenish gray (5 GY 8/1) outer	No	No	No	No	gradual, less red/pink	Yes
Bt	40	**17380**	silt/clay	Pale Red	10 R 6/2	similar to previous unit but slightly darker red	No	No	No	No	gradual	No
A	25	**17405**	silt/clay	Mod Red	5 R 4/6	discontinuous layers of light greenish gray, powdery above, green mottles up to 1 inch	Yes	No	No	No	Gradual	No
Bt	400	**17805**	med sand and silt	Pale Reddish Brown	10 R 5/4	sand with biotite flecks	No	No	No	No	Gradual	No
K	20	**17825**	carb nod layer	Lt Greenish Gray	5 G 8/1	carbonate conglomerate	No	Yes	No	No	Uneven	Yes
Bt	45	**17870**	silt/clay	Pale Reddish Br	10 R 5/2	red with mottles of green well consolidated material	Lt greenish gray	No	No	No	Uneven	No
K	60	**17930**	carb nod layer	Lt Greenish Gray	5 G 8/1	interfingers the carbonate layer and silt	No	No	No	No	Uneven	Yes
Bt	320	**18250**	silt w/ fs layers	Pale Reddish Brown	10 R 5/2	some lt greenish gray sand layers, some more red layers	Yes	No	No	No	Gradual	No

Table A1. Continued

Bs	260	**18510**	silt/clay	Dark Reddish Br	10 R 3/4	black blebs, slickensides	No	lt greenish gray to black carbs	No	No	Gradual	No
N/A	40	**18550**	vfs to c sand	Gray		x-bedded w/lt greenish gray carb cement	No	No	No	No	Distinct	yes
N/A	540	**19090**	silt to vc sand	Dark Reddish Br and Lt greenish gray	10 R 3/4 AND 5 G 8/1	laminated sand as you go up, less green, green reduction layers	Yes	No	No	No	Distinct	Green spots do
N/A	70	**19160**	med-coarse sand	Blackish Red and Lt Greenish Gray	5 R 2/2 AND	medium sand with green layers within bedding, mud rip up clasts throughout	No	No	No	No	Flat against SS	No
N/A	135	**19295**	med-coarse sand	Blackish Red and Lt Greenish Gray	5 R 2/2	layers of very coarse sand w/muddy layers in troughs, green layers in troughs	No	No	No	No	Rel Flat against trough x-beds	No
Bs	345	**19600**	silt/clay	Pale Reddish Brown AND Grayish Red	10 R 5/4 and 10R 4/2	abundant slickensides which are grayish red, non-descript, veiny, mottling, black areas that fizz	No	Made up of calcite	Yes	No	Distinct	Yes

Table A1. Continued

N/A	25	**19625**	Conglom 3mm	Lt Greenish Gray	5 G 8/1	lt greenish gray conglomerate, predominantly calcite conglomerate, mud clasts, black hues-likely organic	No	No	No	No	Distinct	Yes
N/A	35	**19660**	med sand/silt /conglom	Lt Greenish Gray and Grayish Red	5 G 8/1 AND 5 R 4/2	mud/sand above transitional not flat, big mud balls, pinkish(fizzes) sandy w/ mud balls and nodules within matrix supported, dinosaur bone fragments	Yes	Yes	No	No	Slightly erosional mostly flat	Nods Do
N/A	505	**20165**	med sand and silt	Mod Reddish Brown and Pale Greenish Yellow	10 R 4/6 AND 10 Y 8/2	sand not well consolidated, reduction layers, 5 cm thick layers decrease in size and shape more reduction circles, troughy green reduction layers	No	No	No	No	Indistinct, grades into troughy layers	No
N/A	130	**20295**	fine sand	Mod Red Brown	10 R 4/6	Red sand abundant spheroidal weathering reduction circles, dark green center, near top green is in laminations as it transitions to darker red	No	No	No	No	Distinct	No
N/A	210	**20505**	fine sand and silt	Mod Red Brown	10 R 4/6	sand interfingers with mud w/2 cm bleb carb nodules	No	2 cm and smaller	No	No	Lam turn into red, rel flat	Nodules do

Table A1. Continued

N/A	190	**20695**	vfs and silt	Mod Red Brown	10 R 4/6	indistinct mud unit comes apart in angular chunks does not spheroidal weather, ~90 cm up, 15 cm grayish yellow green layer 5 GY 7/2, select ~4 cm green lenses throughout	No	No	No	No	Relatively Flat	No
Bk	1380	**22075**	Silt w/some sand infill peds or cracks	Pale Reddish Brown	10 R 5/2	some veiny areas, green reduction circles 2.5cm diameter, last 100 cm carb layer, small lenses of sparry calcite	Lt olive brown blebs	Yes	No	No	Indistinct	Yes potentially the matrix
Bt	140	**22215**	silt/clay	Mod Reddish Brown	10 R 4/6	more muddy, few veins slightly splotchy w/dots green reduction circles (lt greenish gray) unconsolidated	No	No	No	No	Relatively Flat	No
Bk	390	**22605**	silt/clay	Pale Reddish Brown	10 R 5/4	more veins becomes more friable in small 3 cm aggregates, more consolidated as you go up and less fizz	No	No	No	No	Indistinct	Yes
	130	**22735**	silt/clay	Mod Red Brown	10 R 4/6	much moister, very similar w/green reducation areas	No	No	No	No	Indistinct	No
N/A	35	**22770**	vfs	Pale Olive	10 Y 6/2	black flecks/feldspars, trough x-bedded, lots of carbonate nodules	No	Yes	No	No	Planar w/SS	Only Nodules

Table A1. Continued

N/A	190	**22960**	vfs-silt	Yellowish gray and Dark Reddish Brown	5 Y 7/2 AND 10 R 3/4	somewhat laminated w/green lt greenish gray layers along bedding, 2 mm to 2 cm layers	No	No	No	No	Rel Planar	Lt Fizz
N/A	50	**23010**	vfs	Yellowish gray and Pale Reddish Brown	5 Y 7/2 AND 10 R 5/2	laminated sand, very micaceous, green along reduction surfaces	No	No	No	No	Gradual	Yes
Bk	730	**23740**	silt and clay	Mod Red Brown	10 R 4/6	mud w/lt green circles baseball sized, yellow green mottles spheroidal weather	Yes	No	No	No	Wavy	Lt Fizz
N/A	200	**23940**	vfs	Mod Reddish Orange	10 R 6/6	Wingate/Moenave Formations	No	No	No	No	No	No

VFS = very fine sand
med = medium
conglom = conglomerate
lam = laminated
ss = sandstone
nods = nodules

APPENDIX B

CLAY MINERALOGY

The following are 27 x-ray diffraction patterns with specific clays as well as quartz and feldspar identified on the plots. Peaks that do not pertain to clays are not labeled. Table 6 is the subsequent data with the three samples that contain illite/smectite (I/S) omitted.

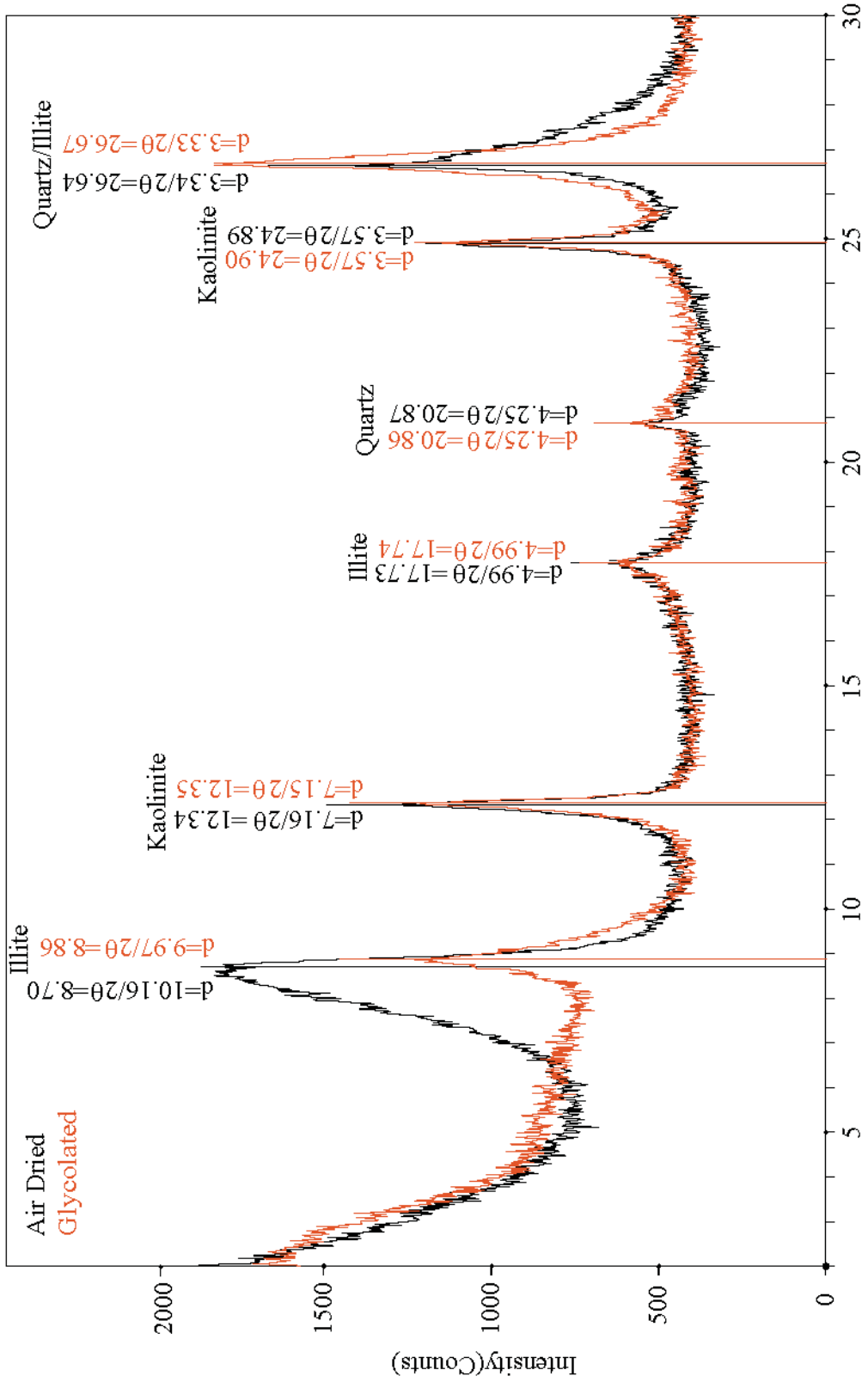

Figure B1. Stratigraphic Section 2: 2.0 m.

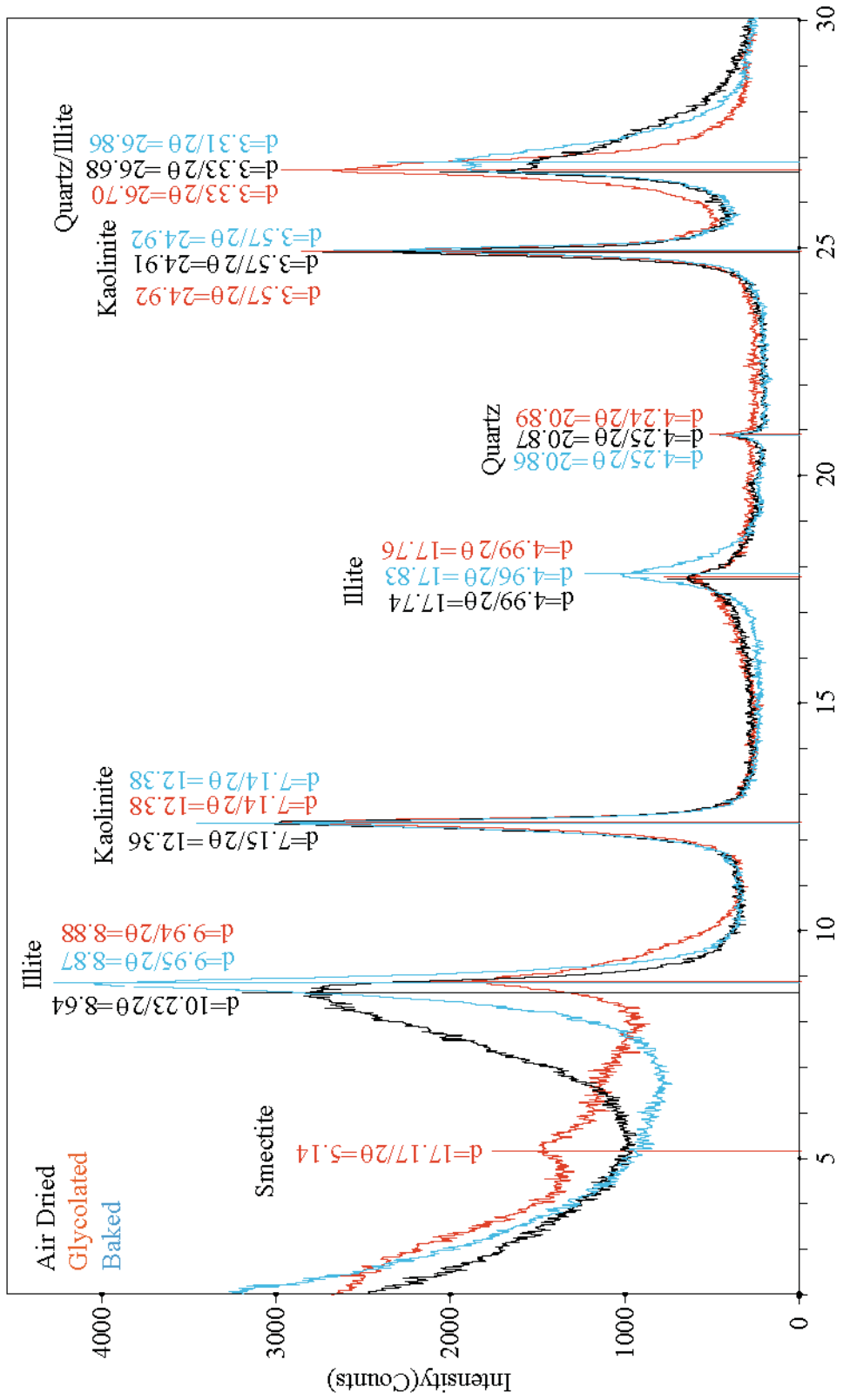

Figure B2. Stratigraphic Section 2: 2.9 m.

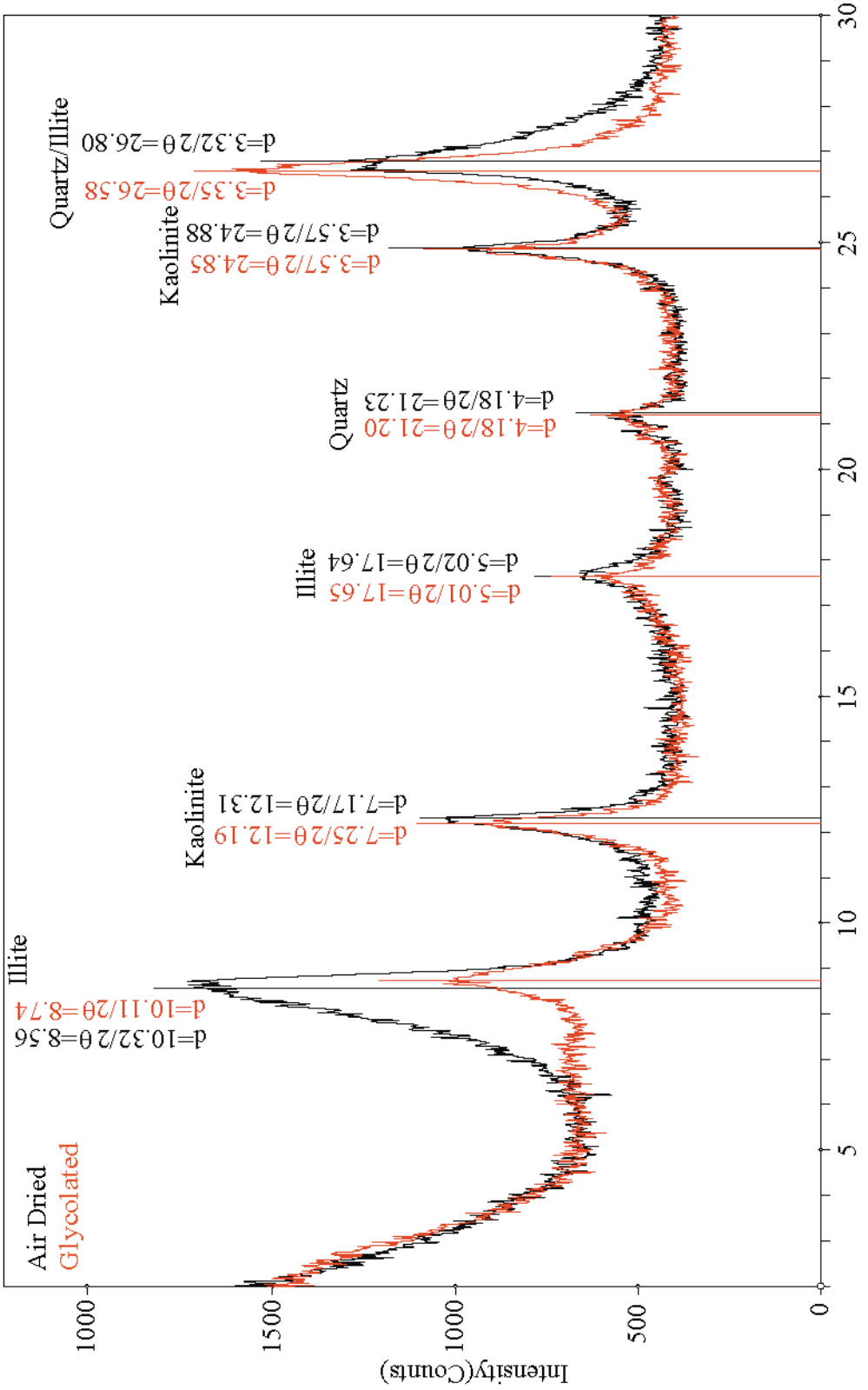

Figure B3. Stratigraphic Section 2: 4.1 m.

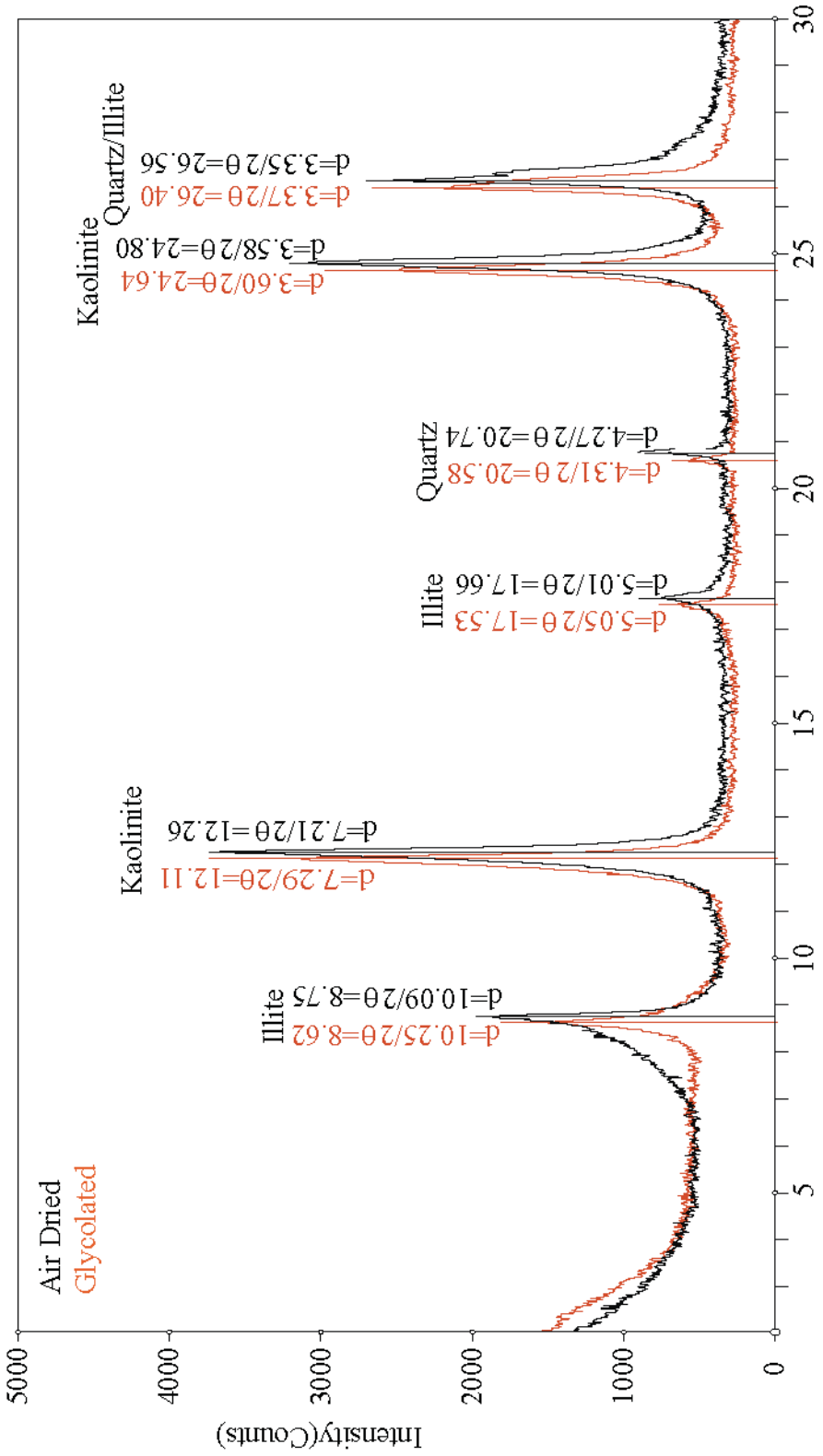

Figure B4. Stratigraphic Section 2: 4.8 m.

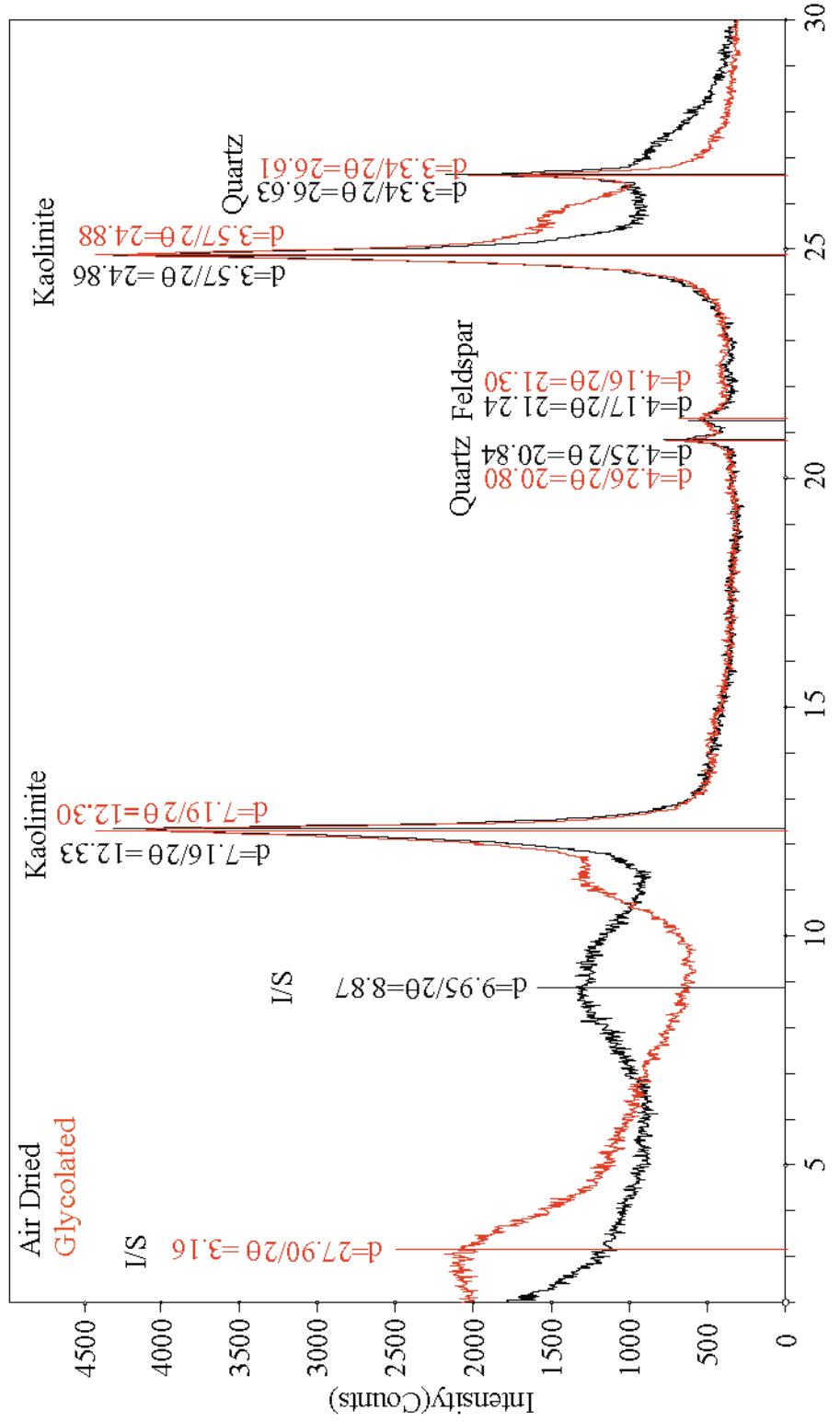

Figure B5. Stratigraphic Section 2: 6.1 m.

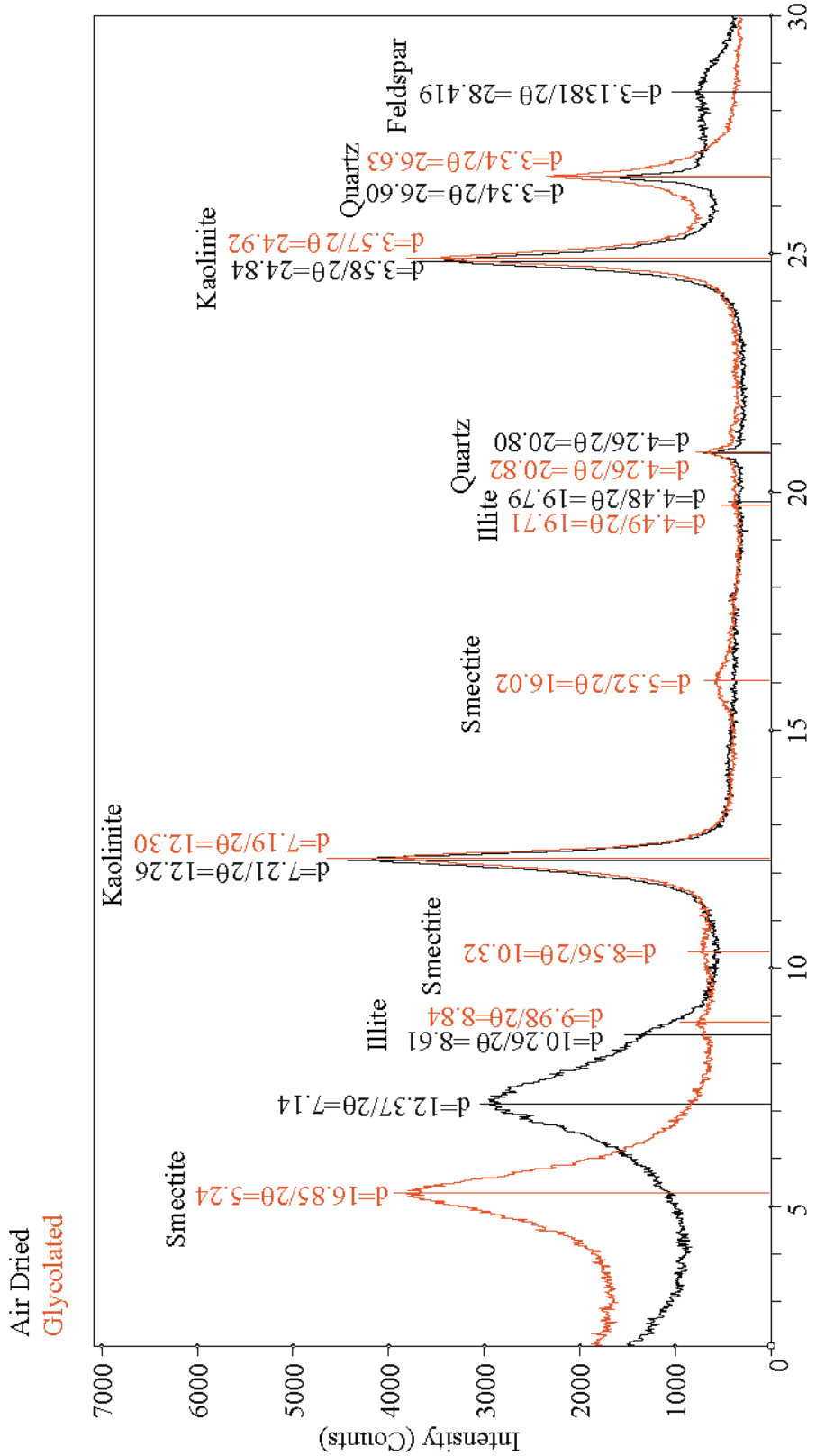

Figure B6. Stratigraphic Section 2: 22.3 m.

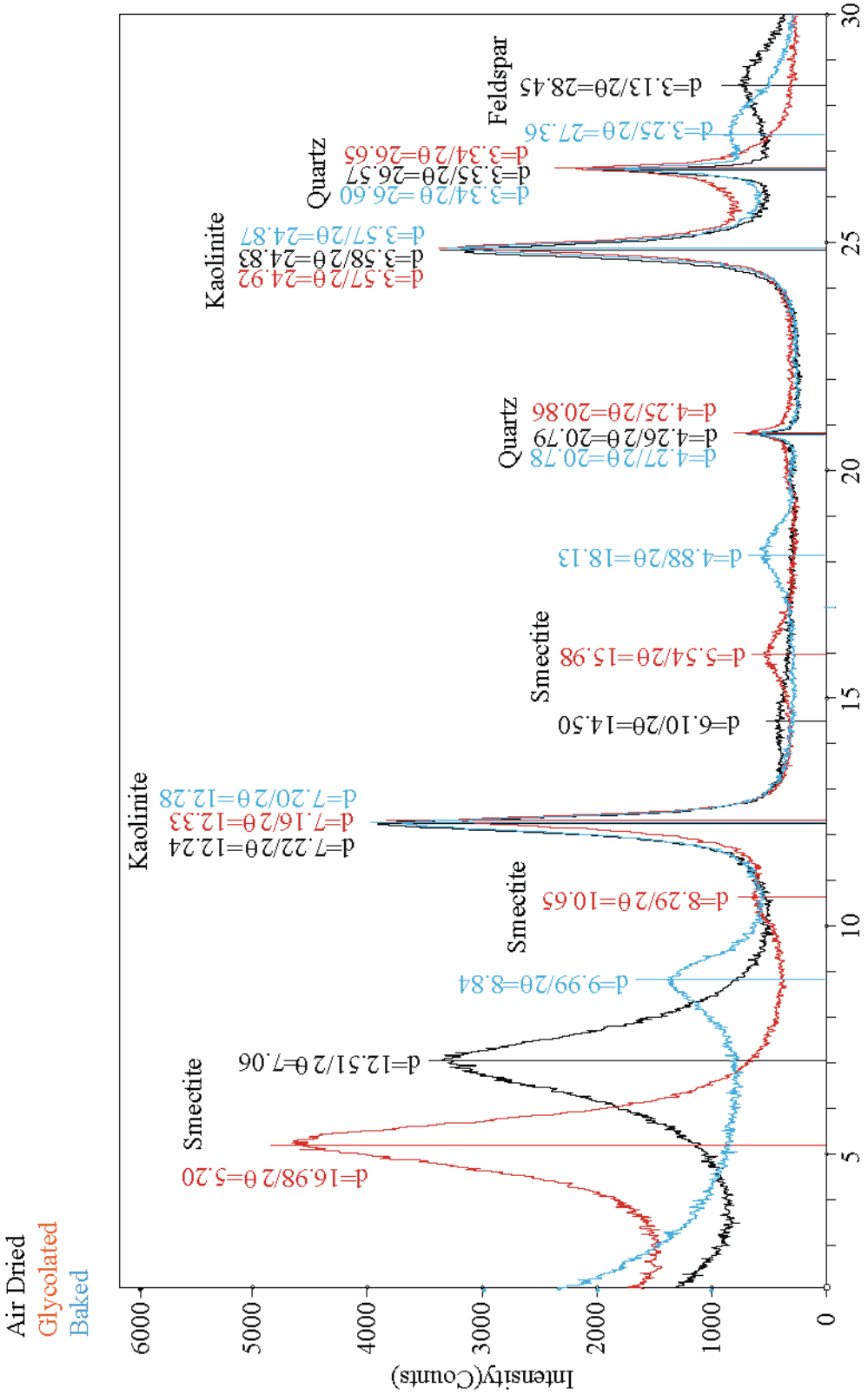

Figure B7. Stratigraphic Section 2: 51.2 m.

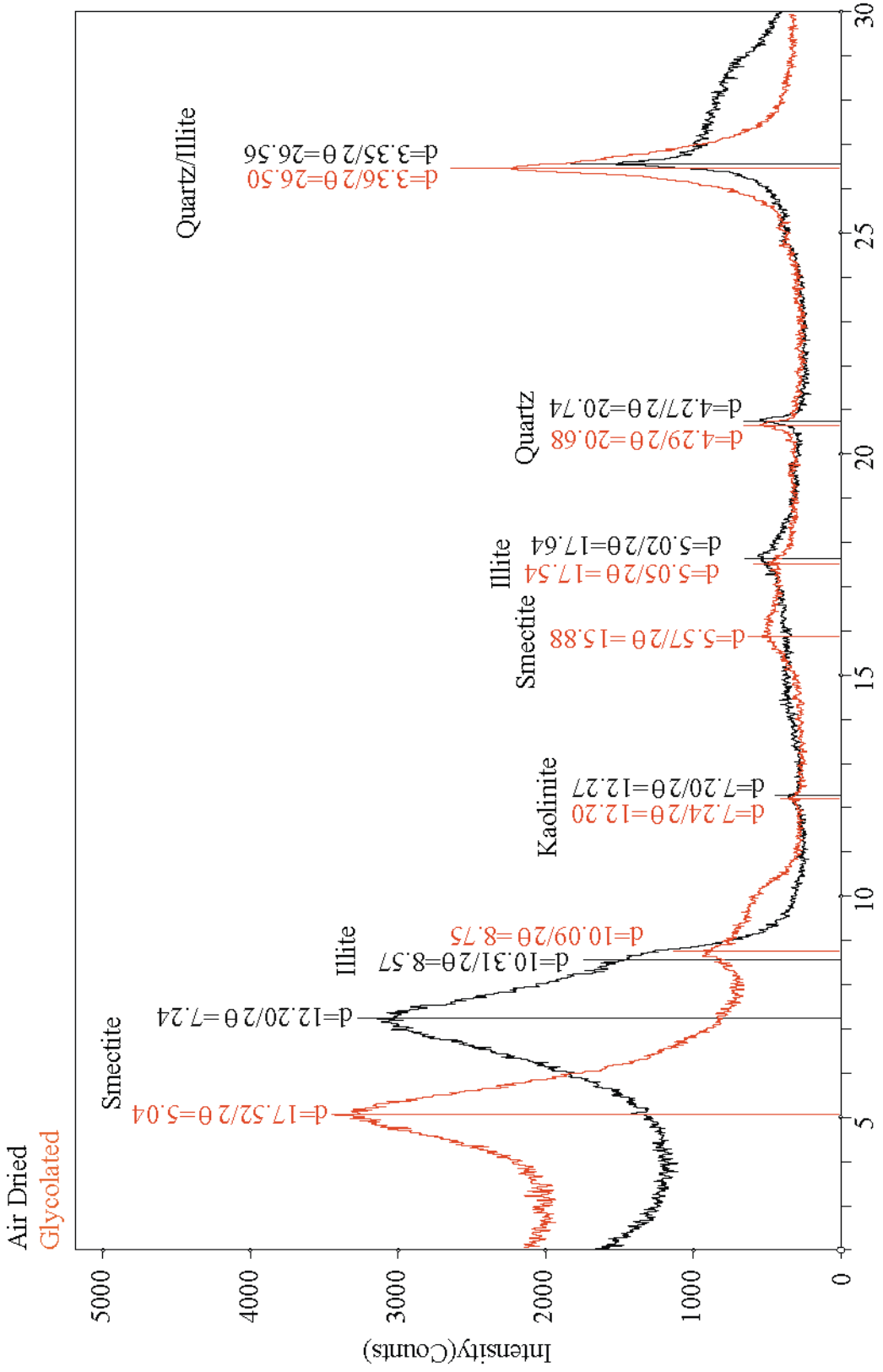

Figure B8. Stratigraphic Section 2: 54.0 m.

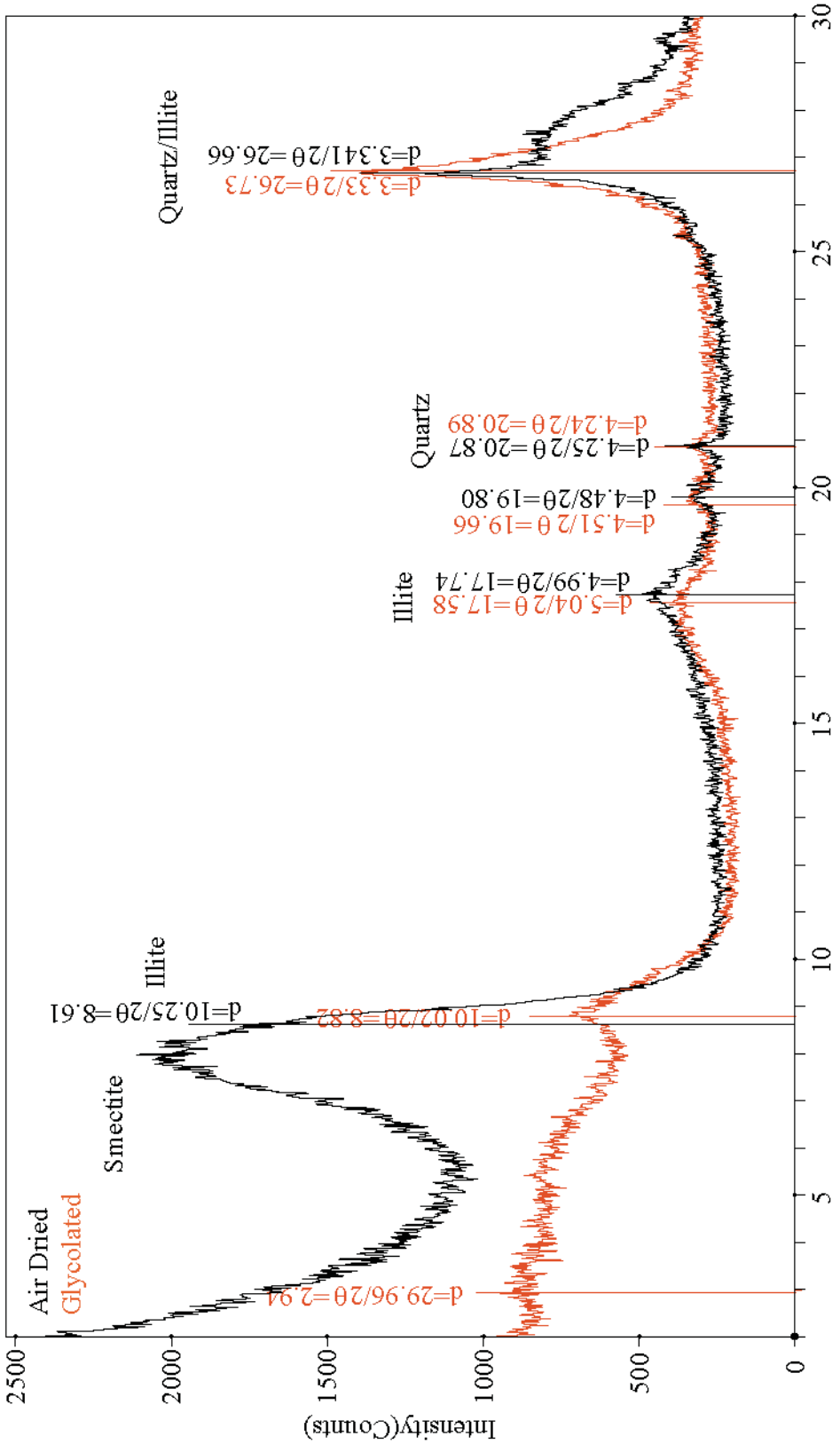

Figure B9. Stratigraphic Section 2: 61.9 m.

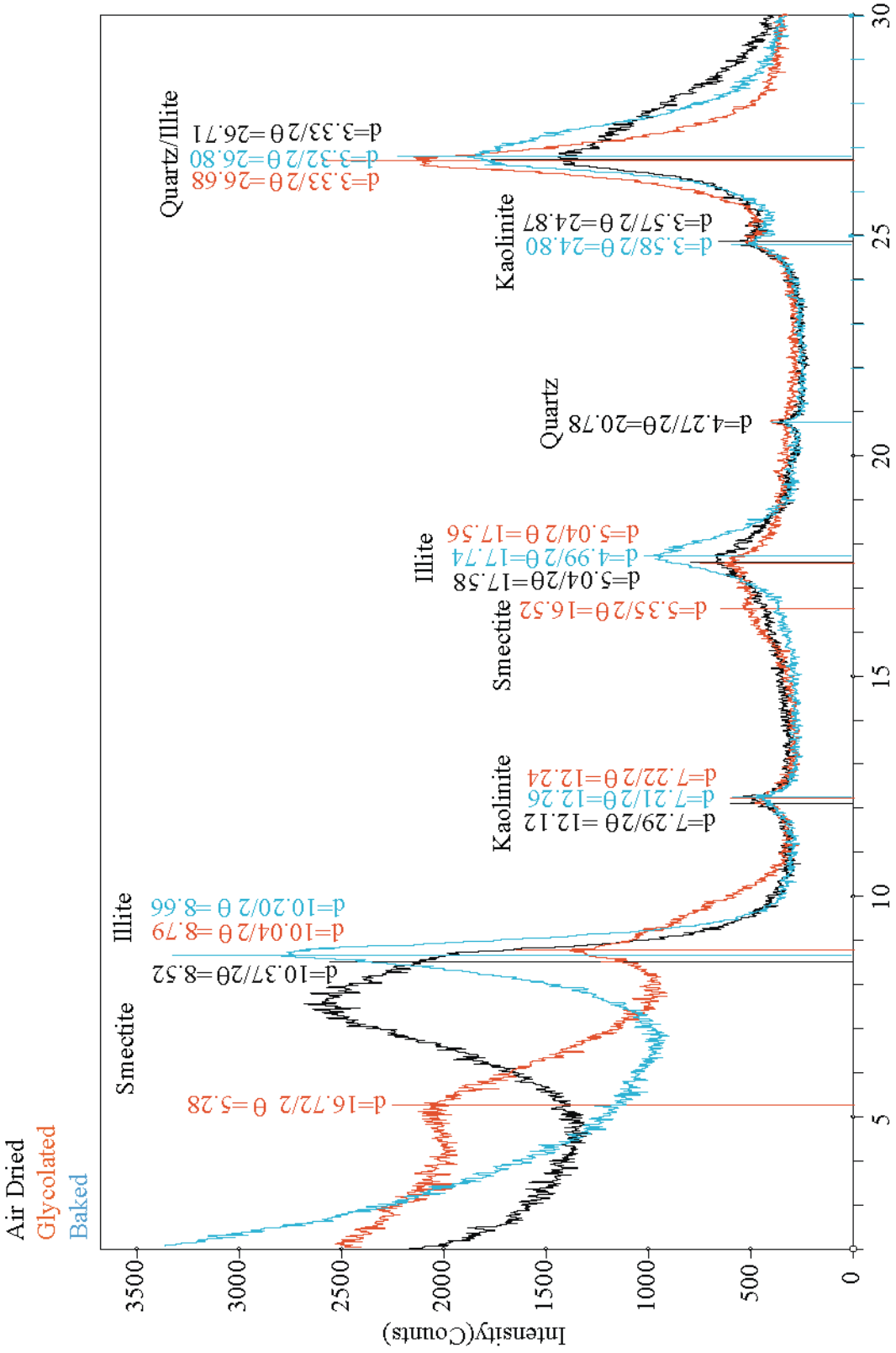

Figure B10. Stratigraphic Section 2: 76.5 m.

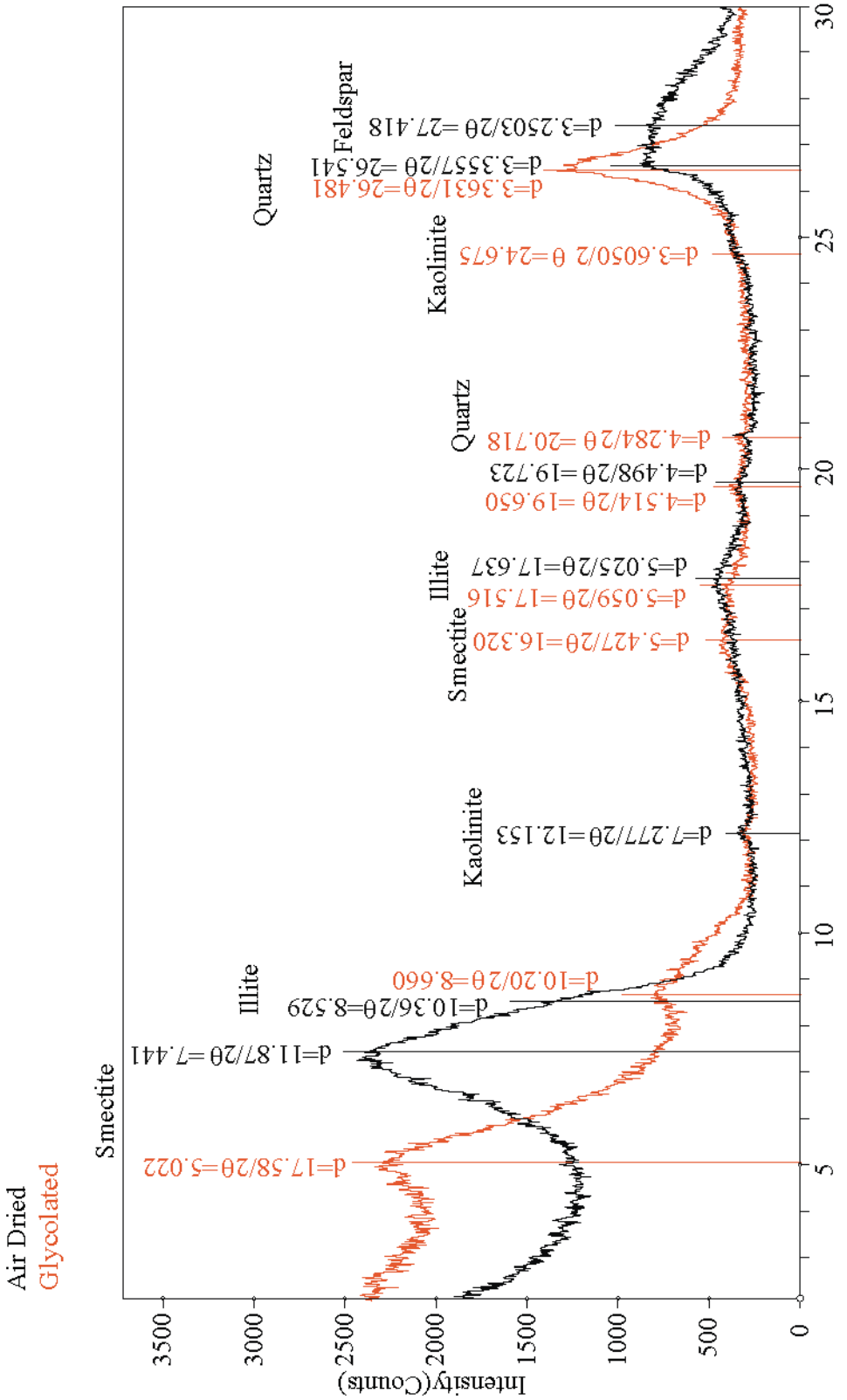

Figure B11. Stratigraphic Section 2: 77.2 m.

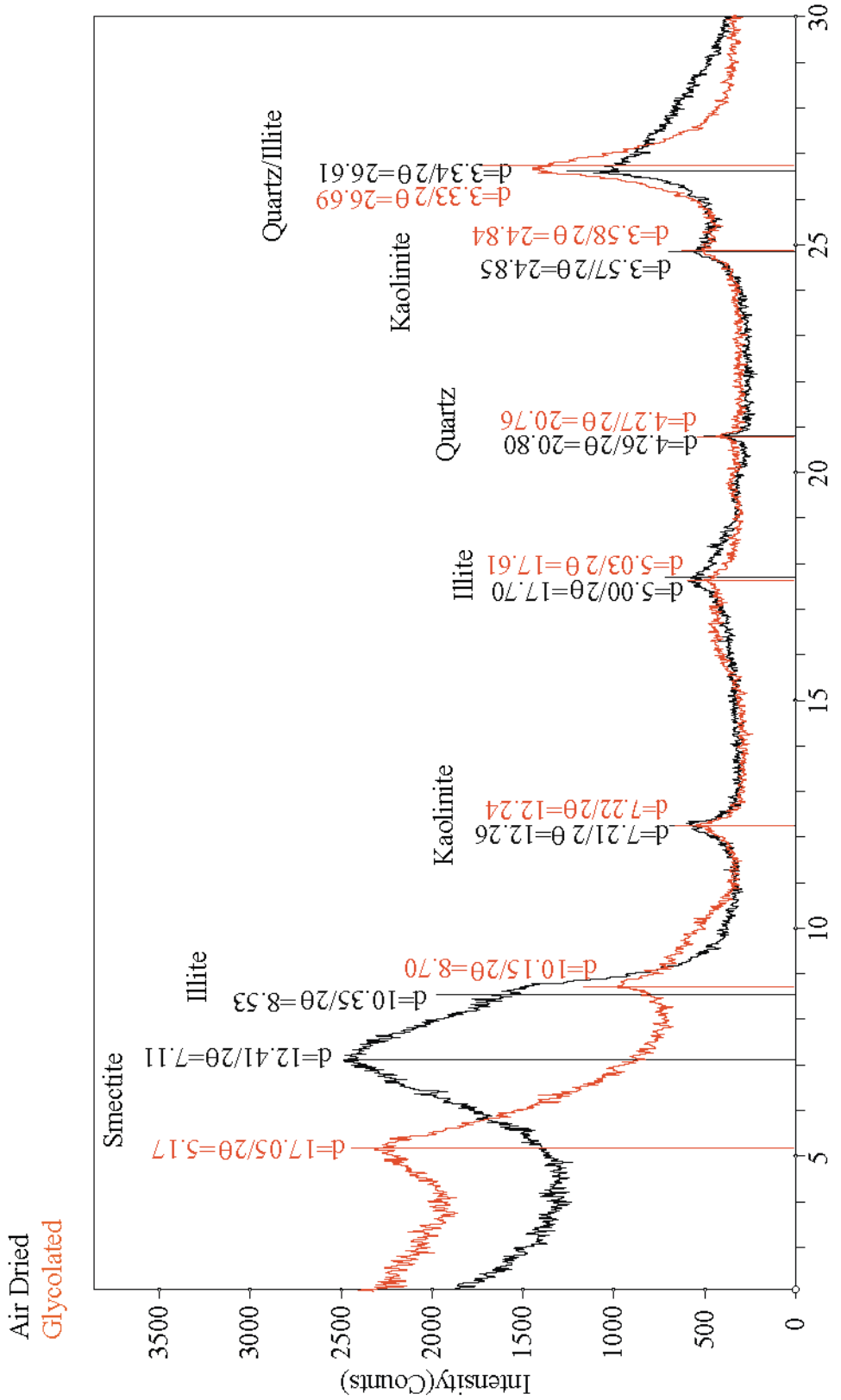

Figure B12. Stratigraphic Section 2: 84.6 m.

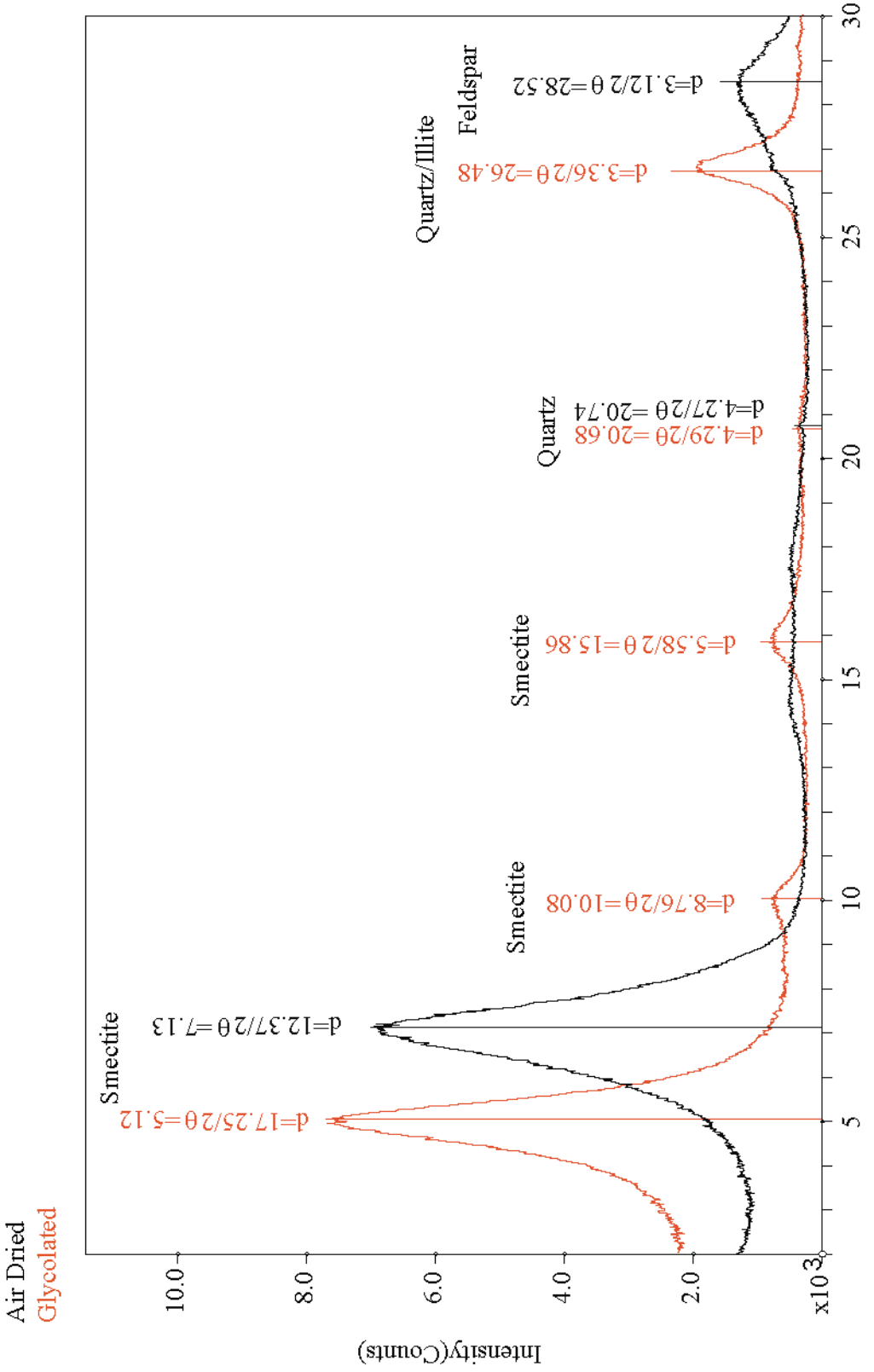

Figure B13. Stratigraphic Section 2: 110.6 m.

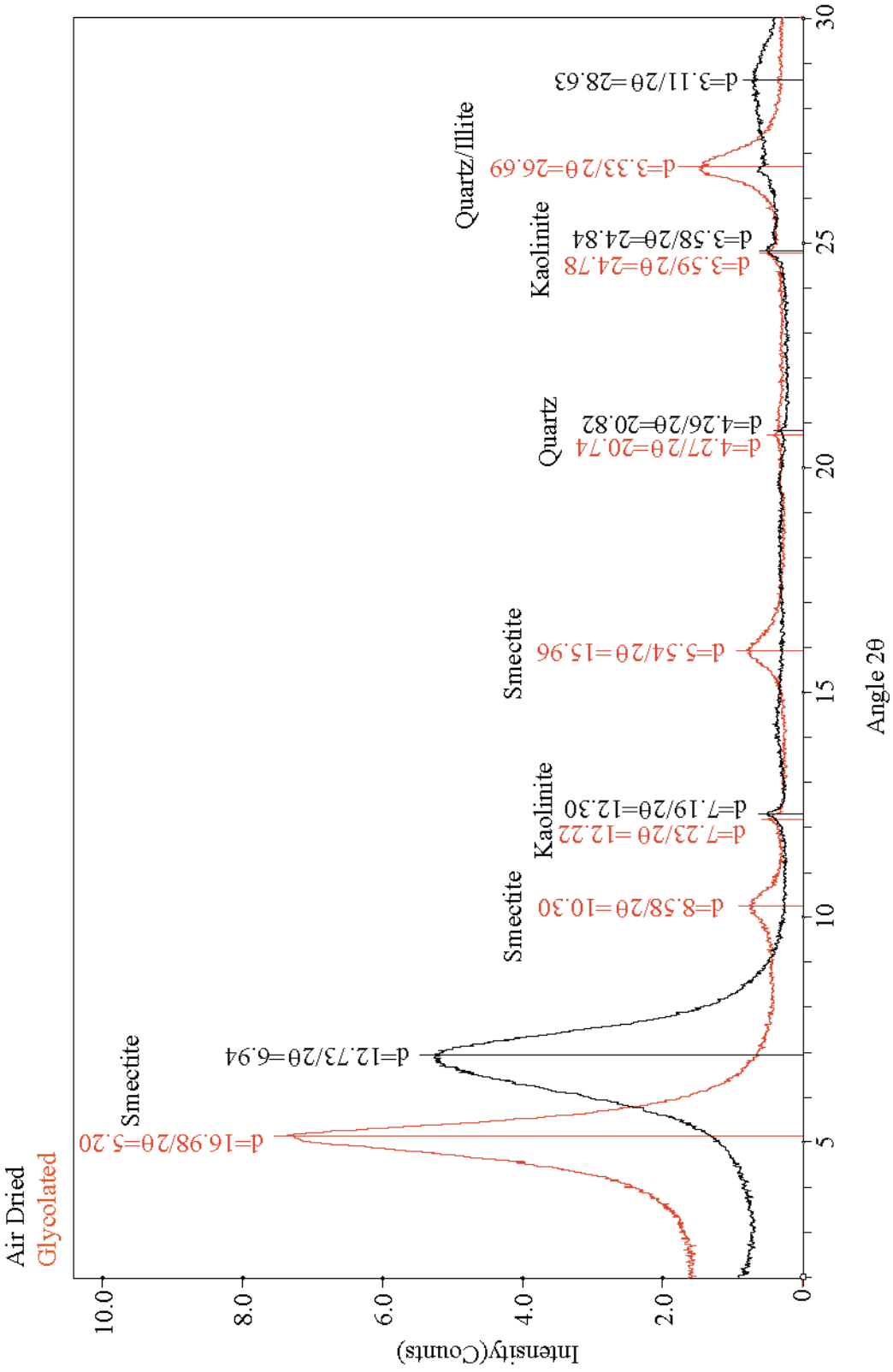

Figure B14. Stratigraphic Section 2: 114.2 m.

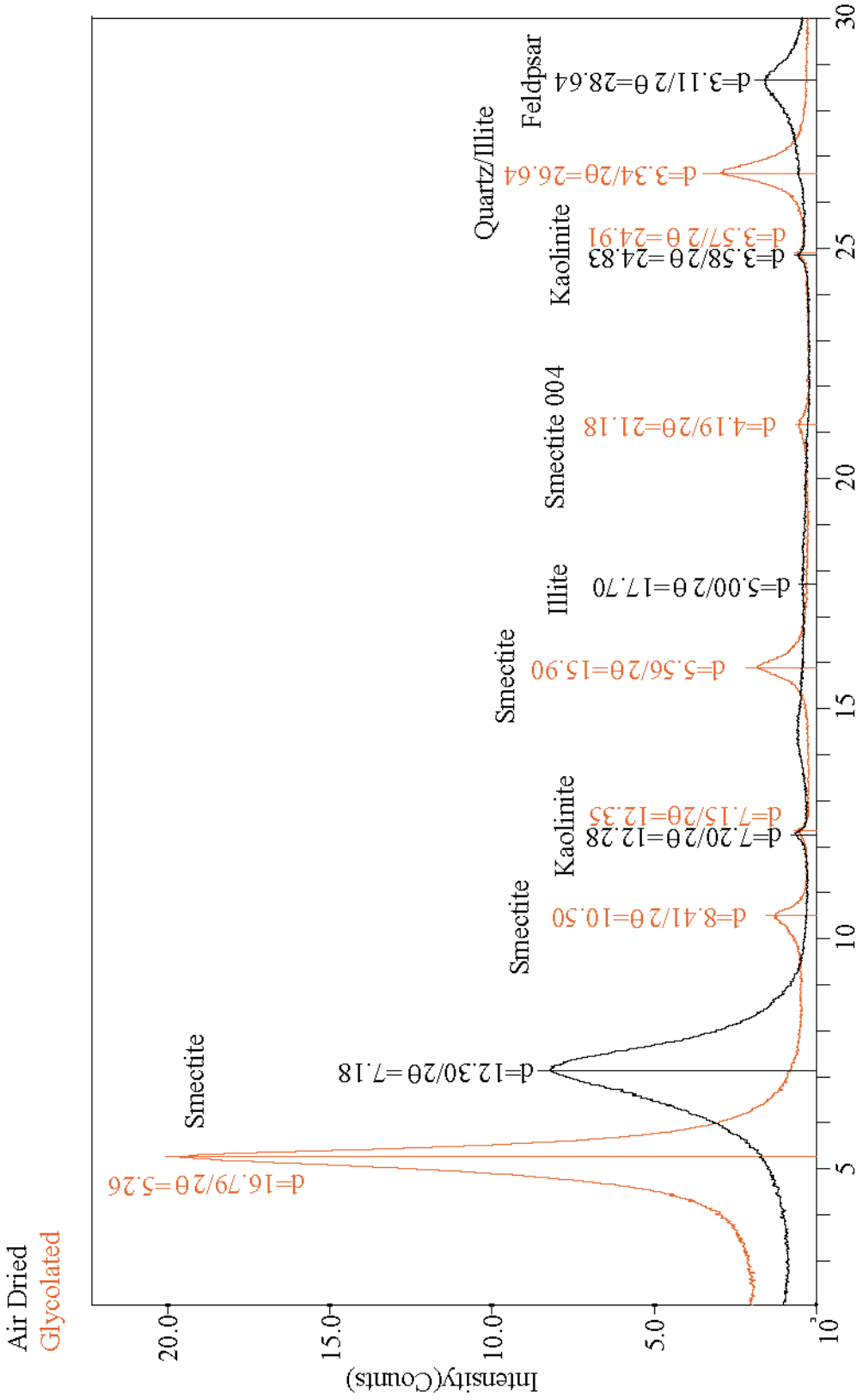

Figure B15. Stratigraphic Section 2: 129.2 m.

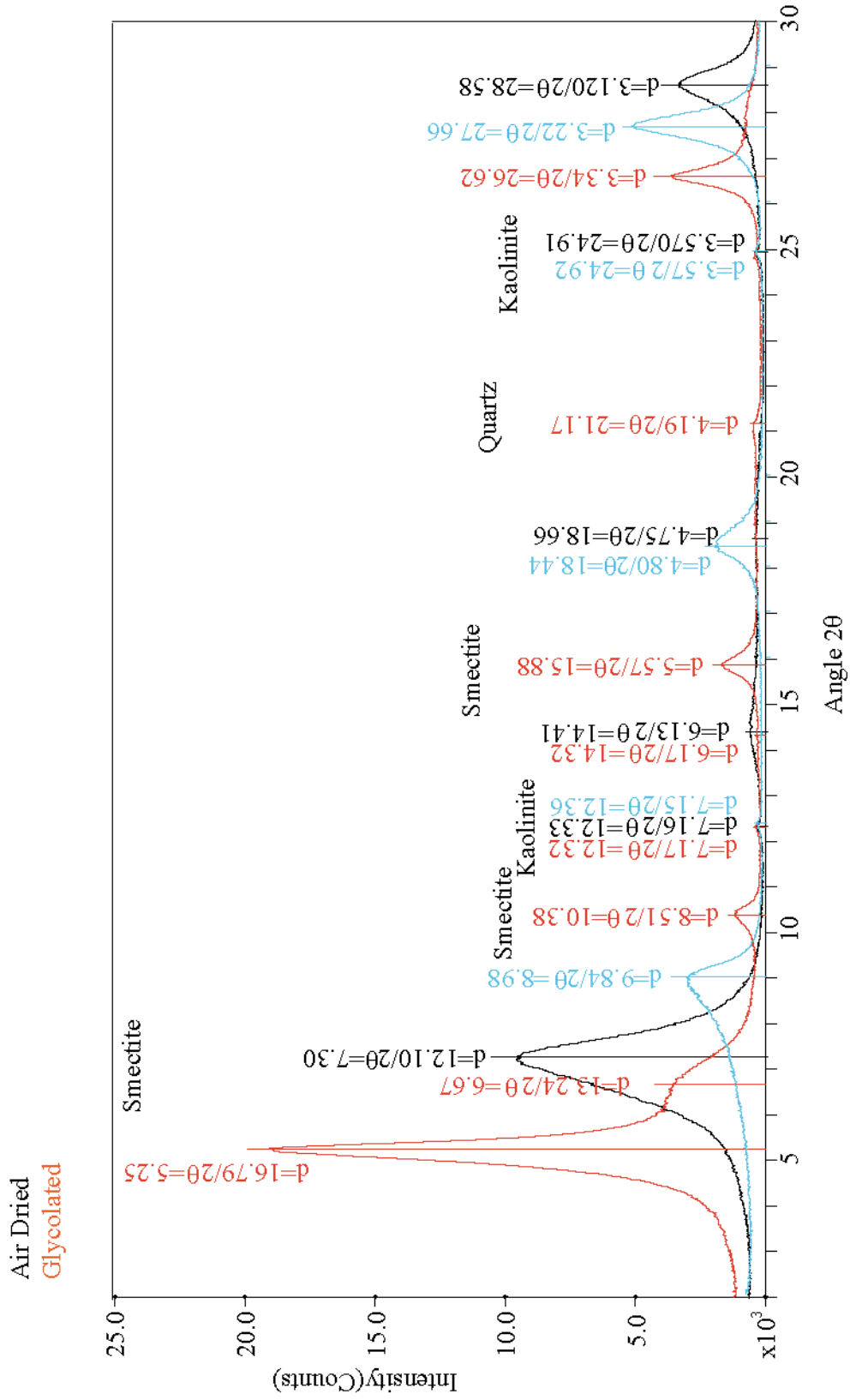

Figure B16. Stratigraphic Section 2: 139.6 m.

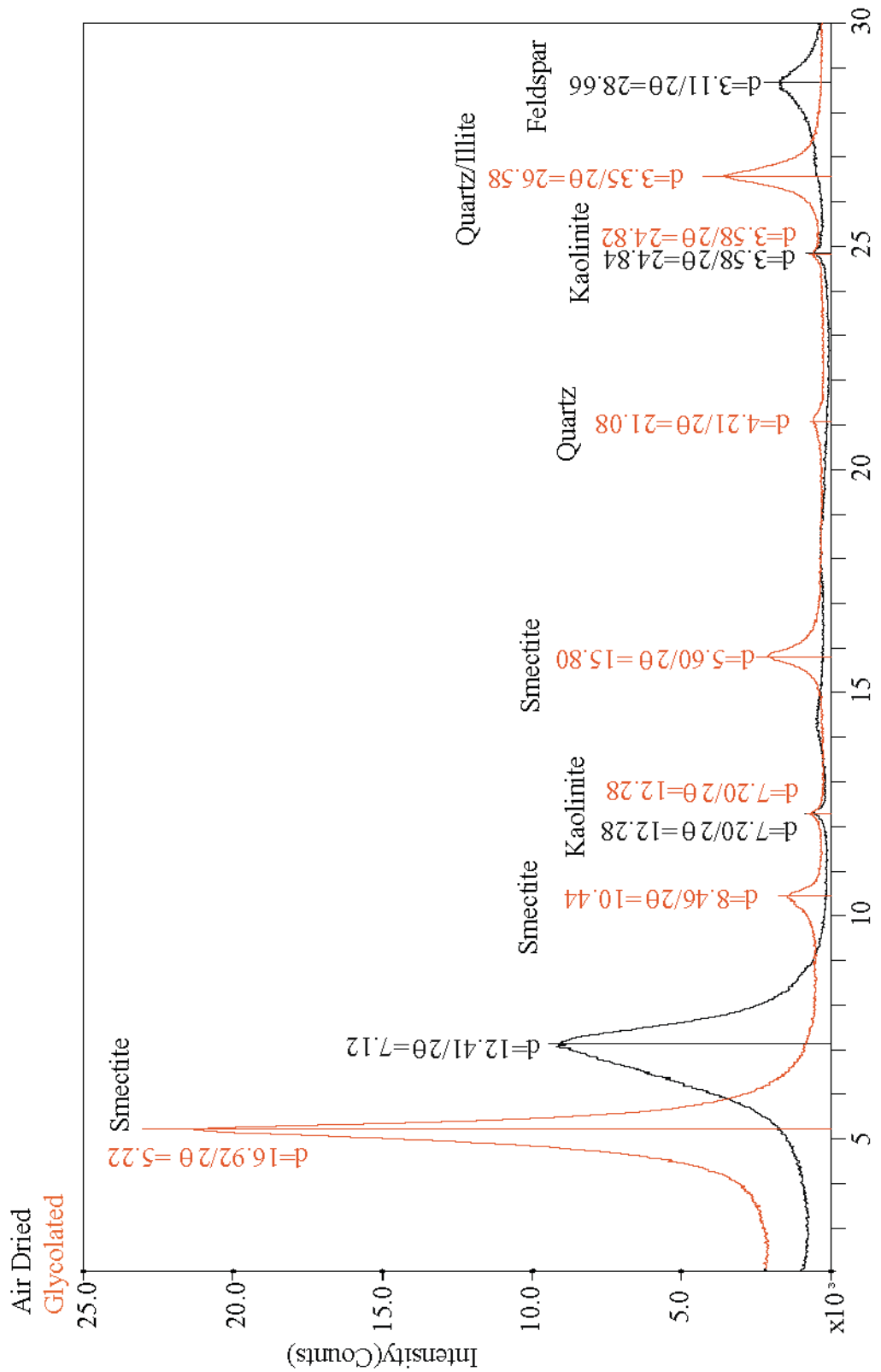

Figure B17. Stratigraphic Section 2: 142.5 m.

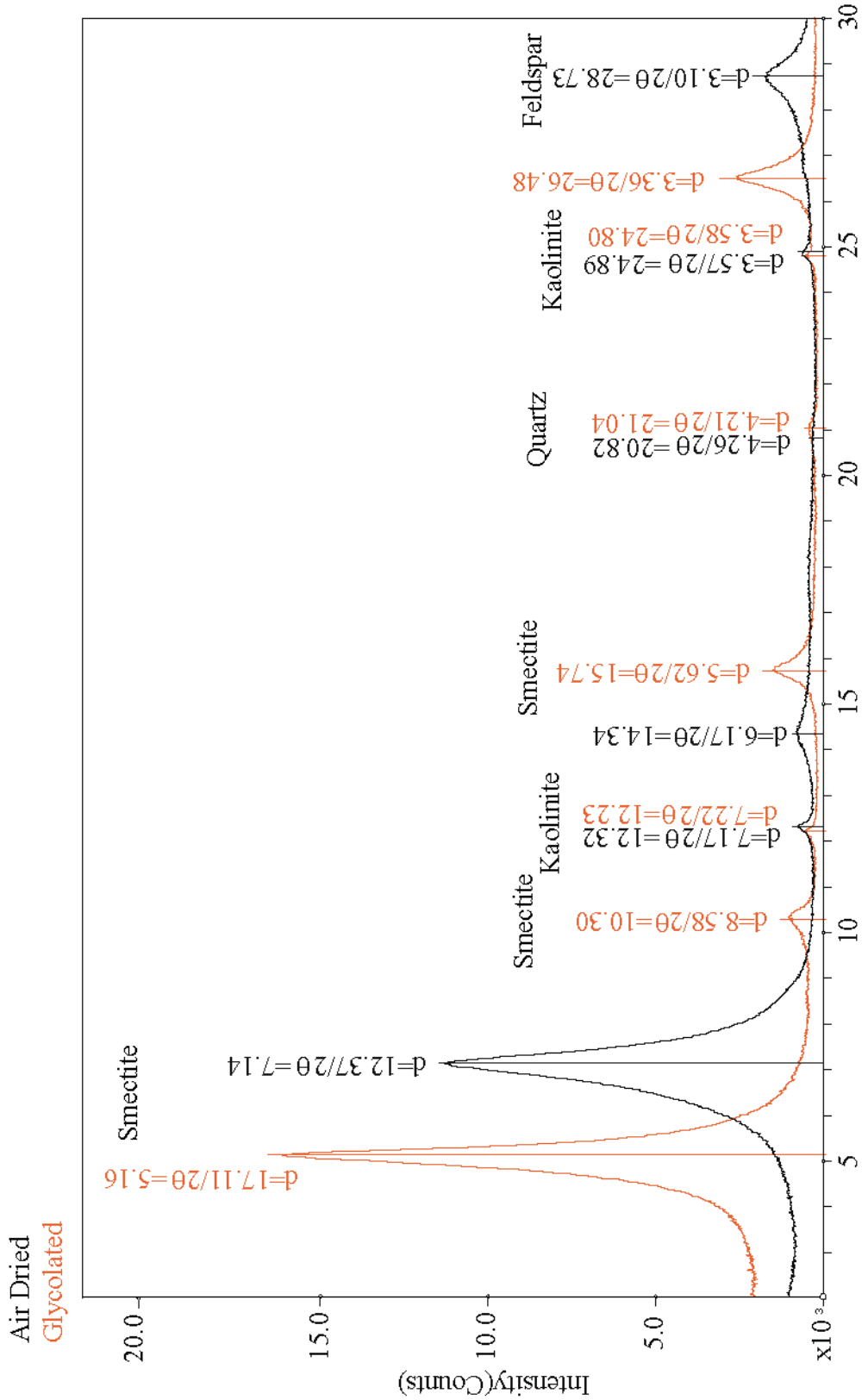

Figure B18. Stratigraphic Section 2: 151.5 m.

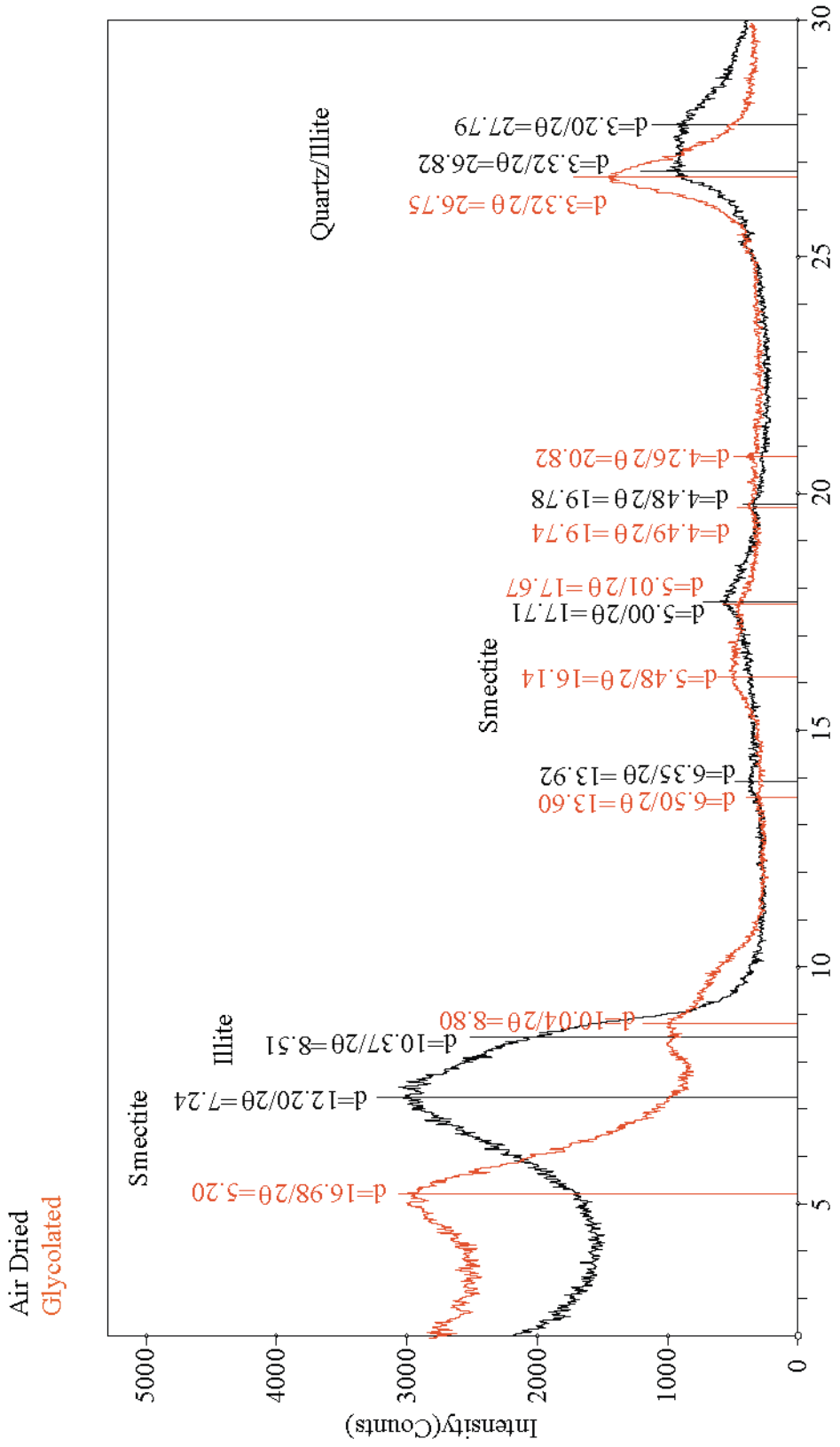

Figure B19. Stratigraphic Section 2: 170.3 m.

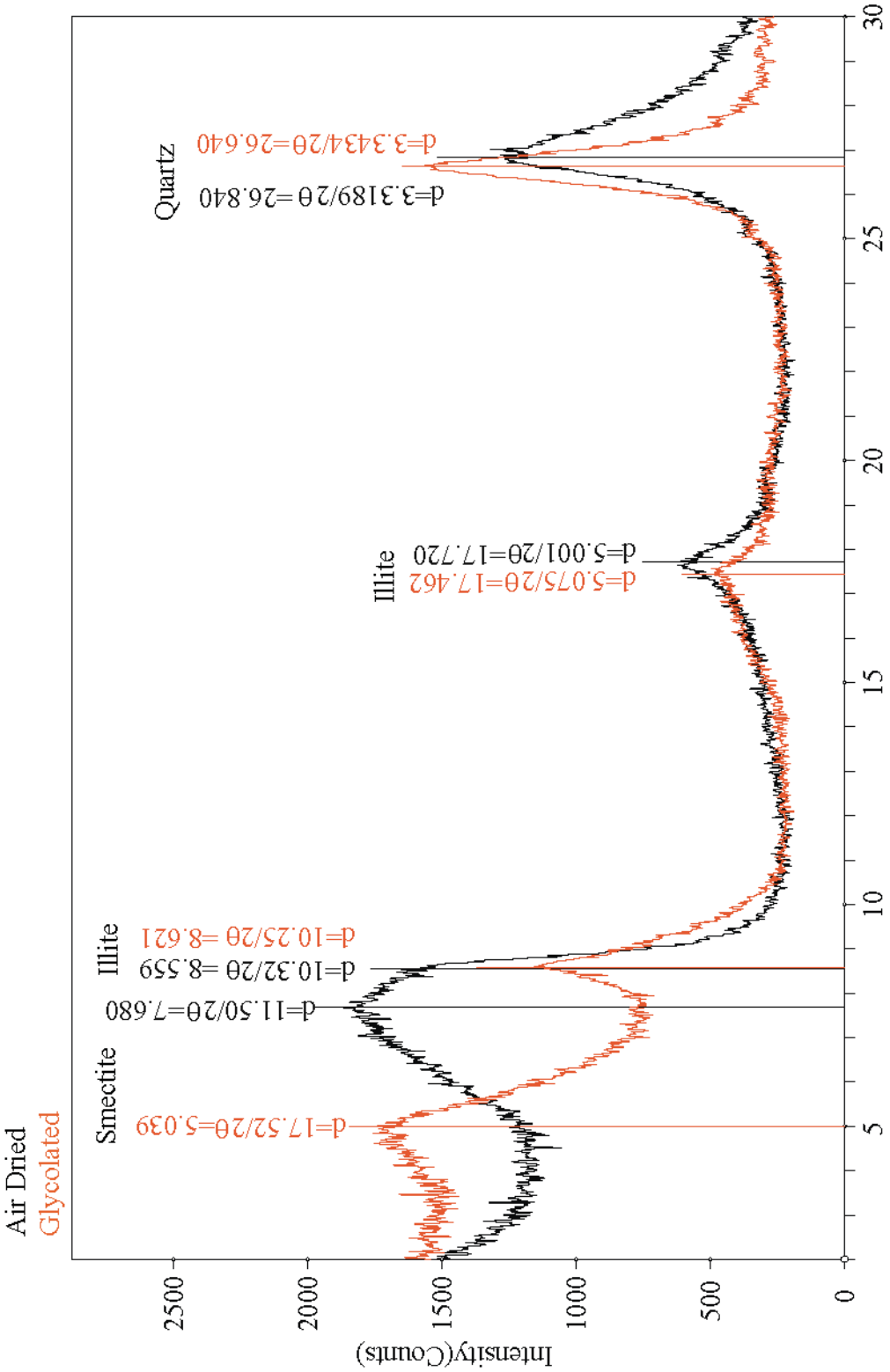

Figure B20. Stratigraphic Section 2: 173.4 m.

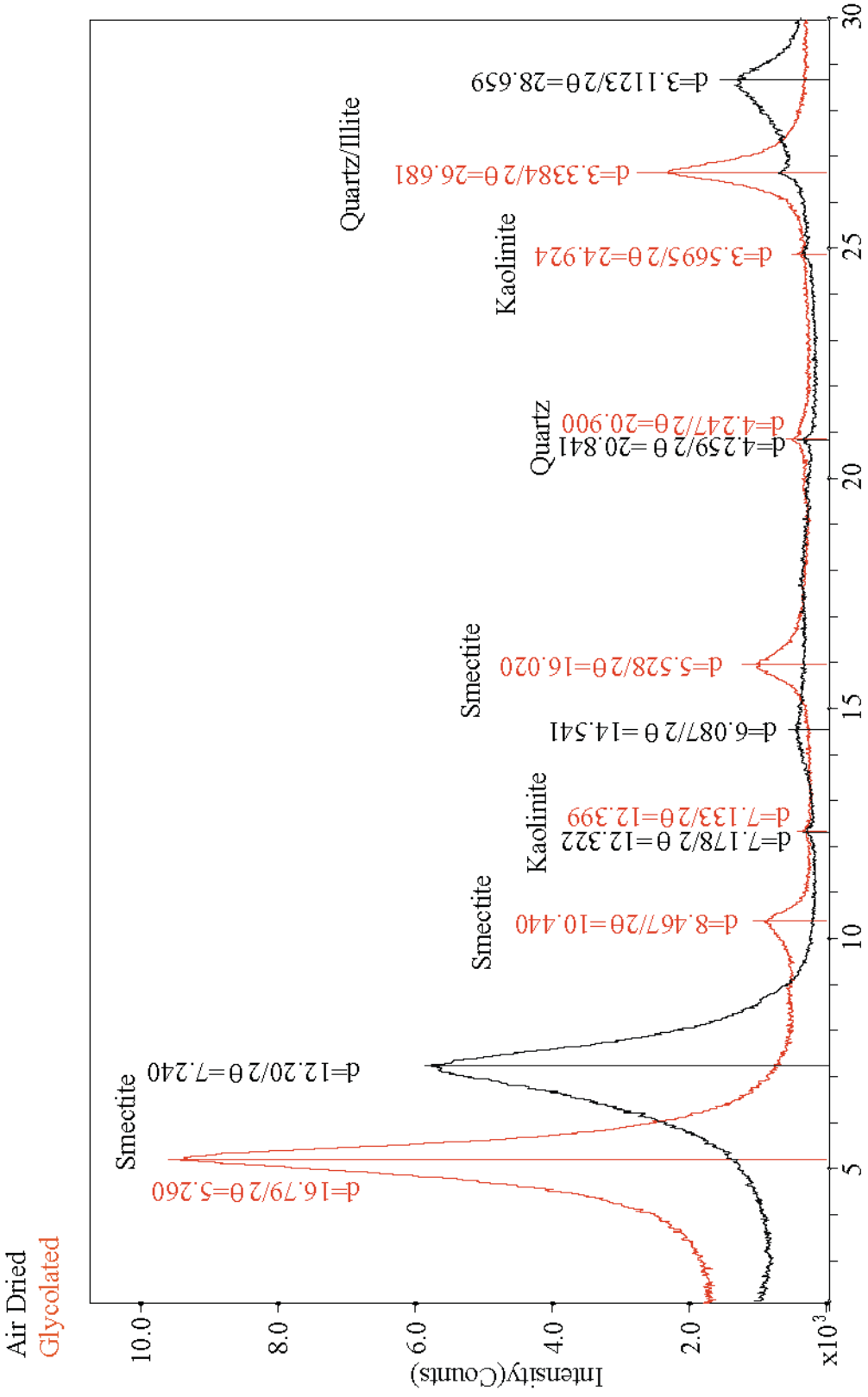

Figure B21. Stratigraphic Section 2: 178.0 m.

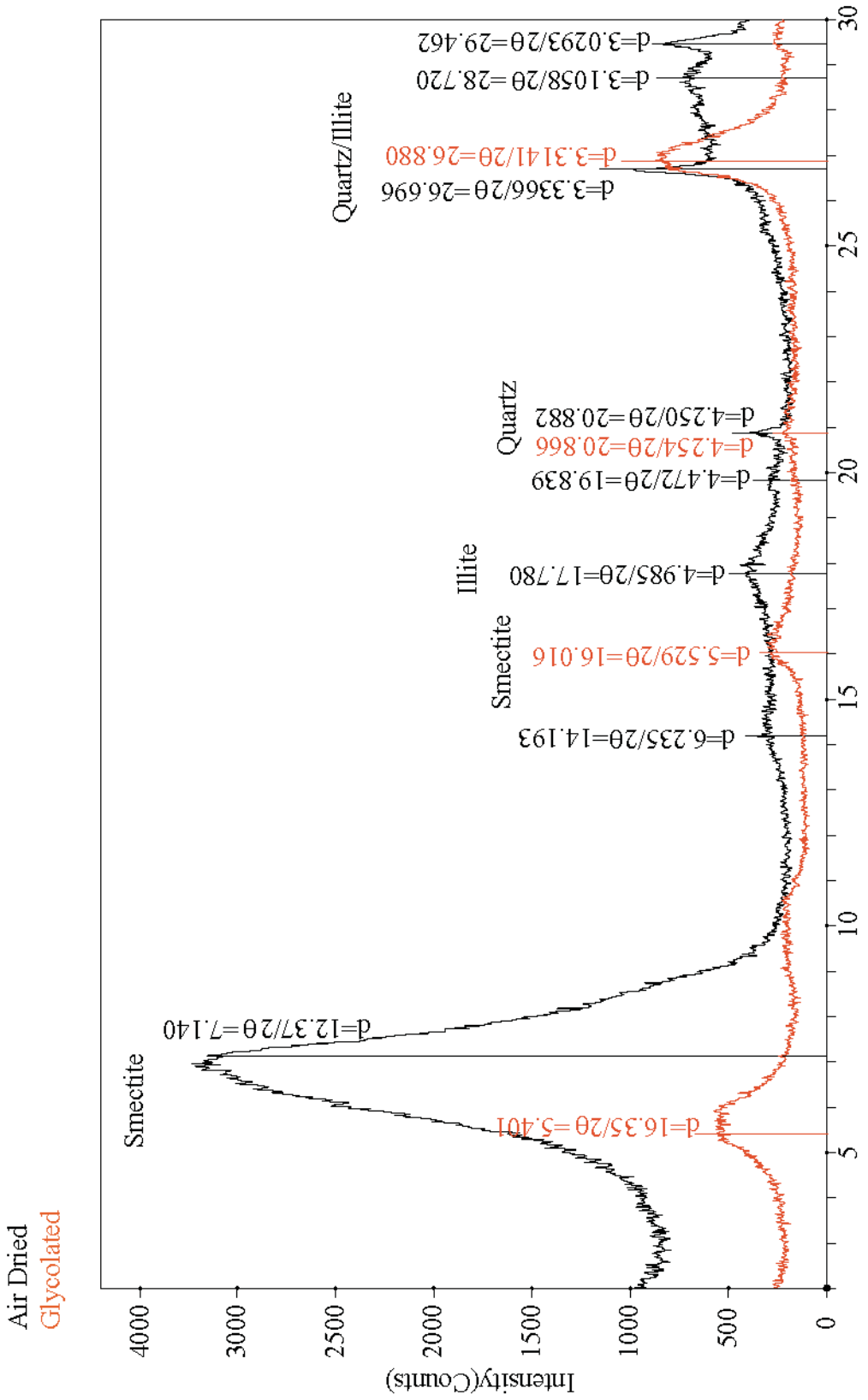

Figure B22. Stratigraphic Section 2: 179.3 m.

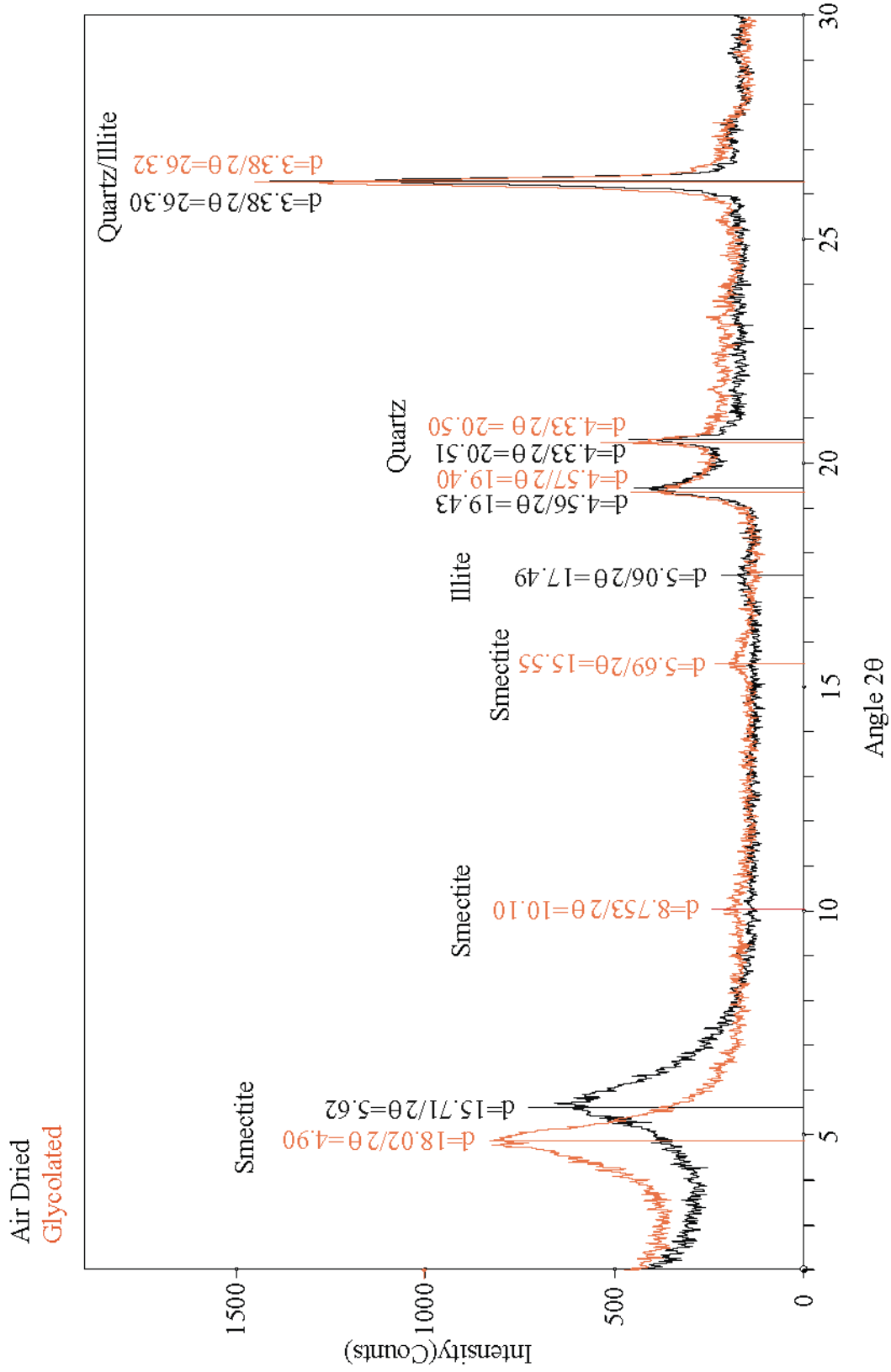

Figure B23. Stratigraphic Section 2: 190.9 m.

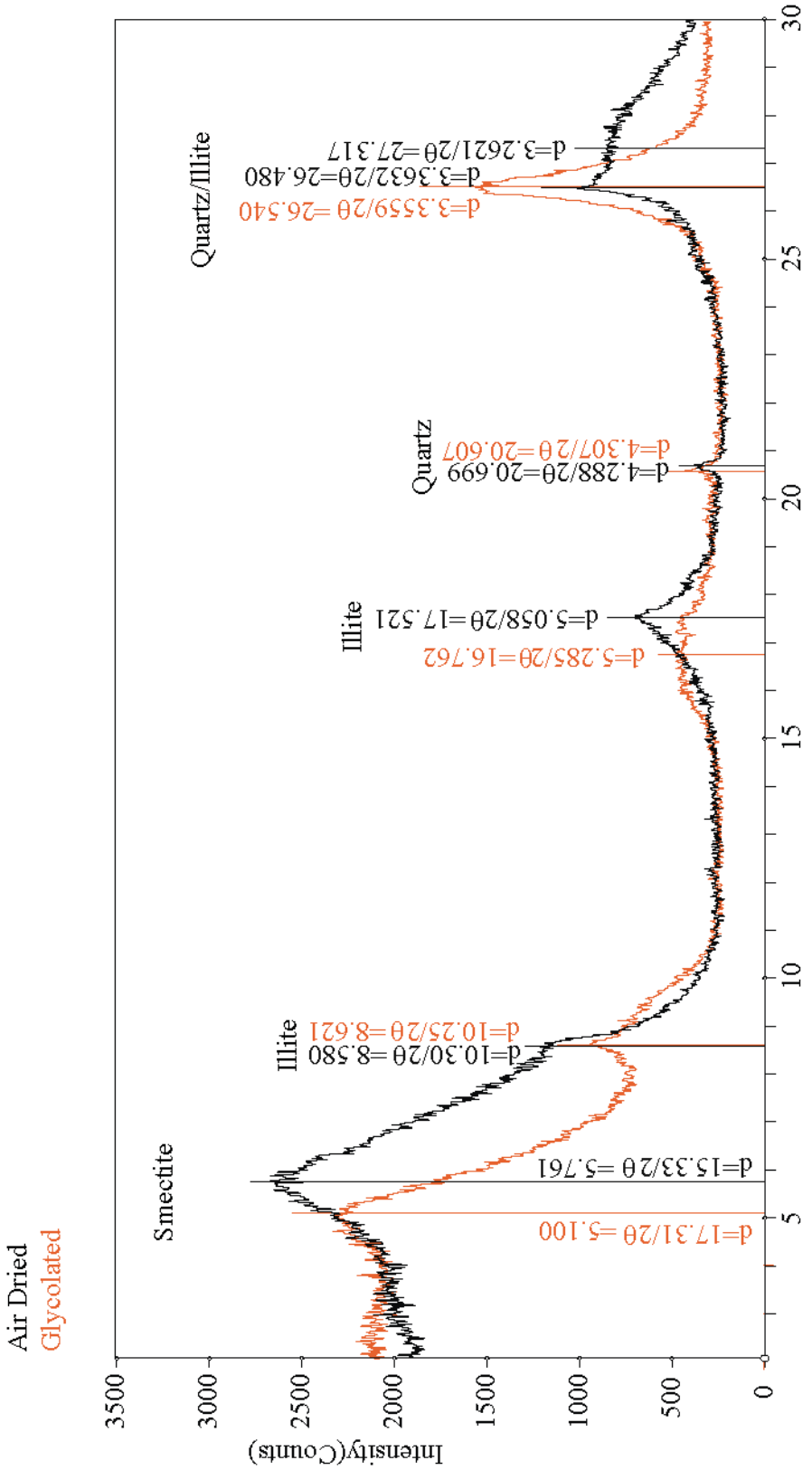

Figure B24. Stratigraphic Section 2: 196.0 m.

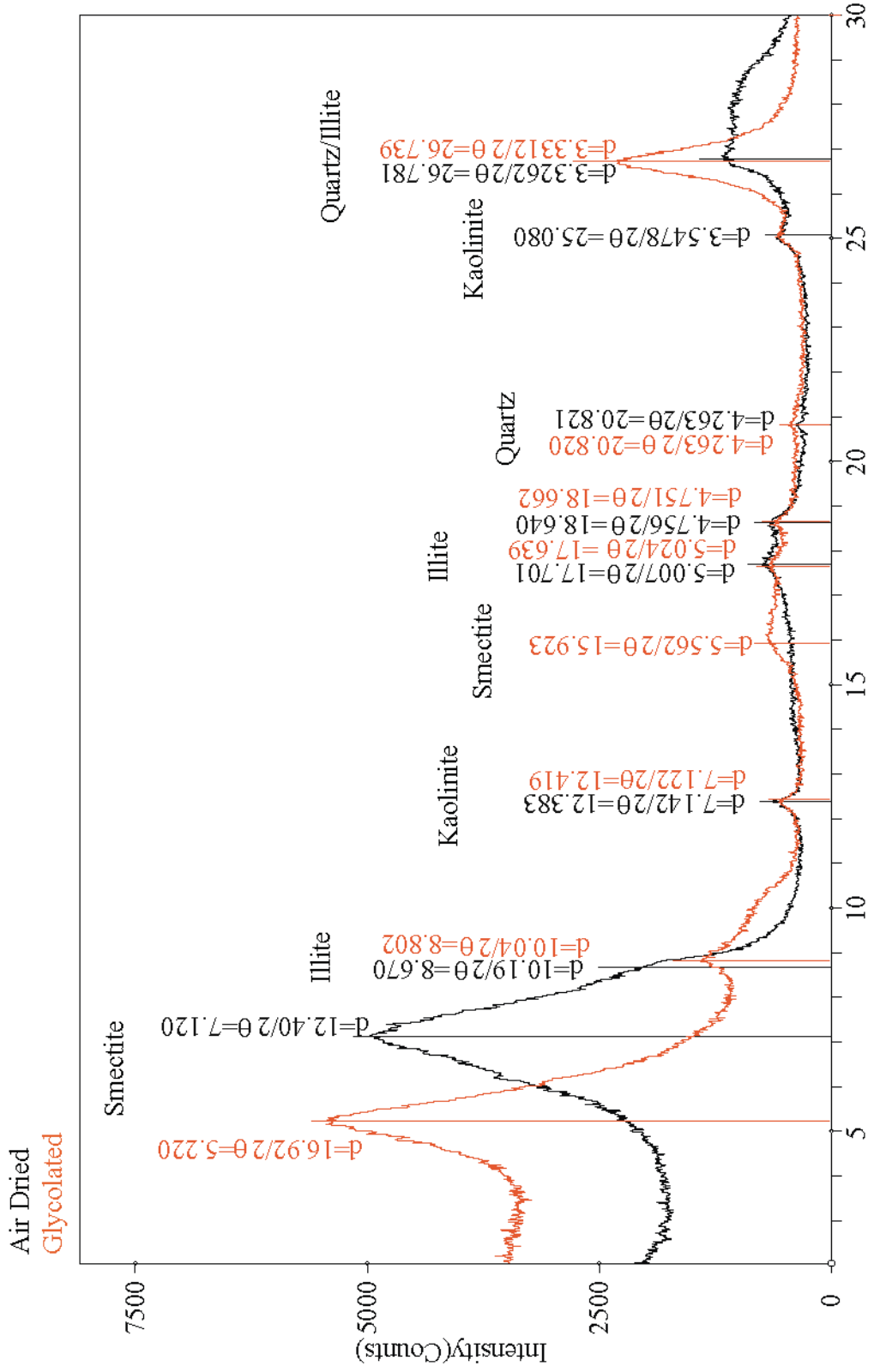

Figure B25. Stratigraphic Section 2: 206.9 m.

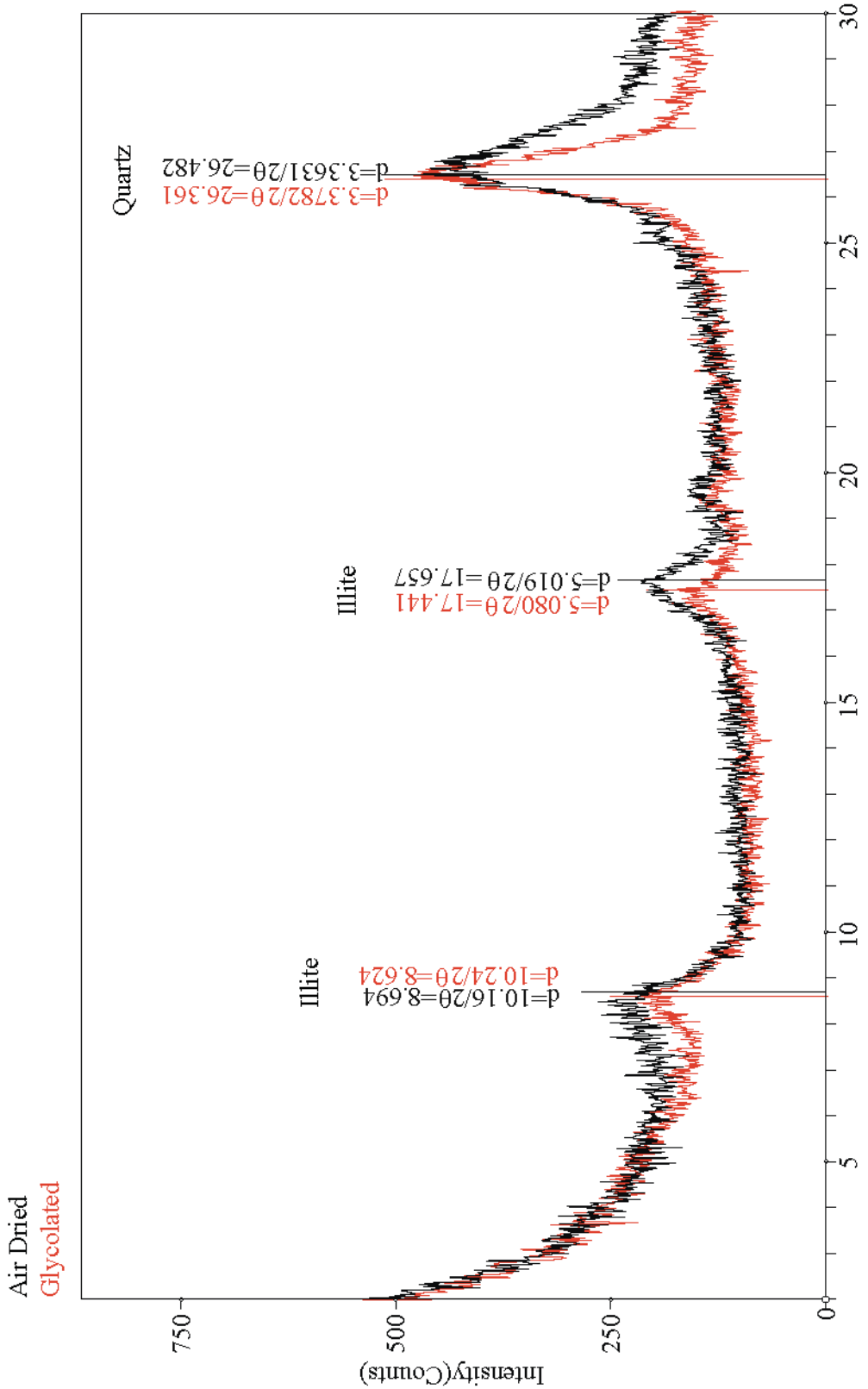

Figure B26. Stratigraphic Section 2: 216.3 m.

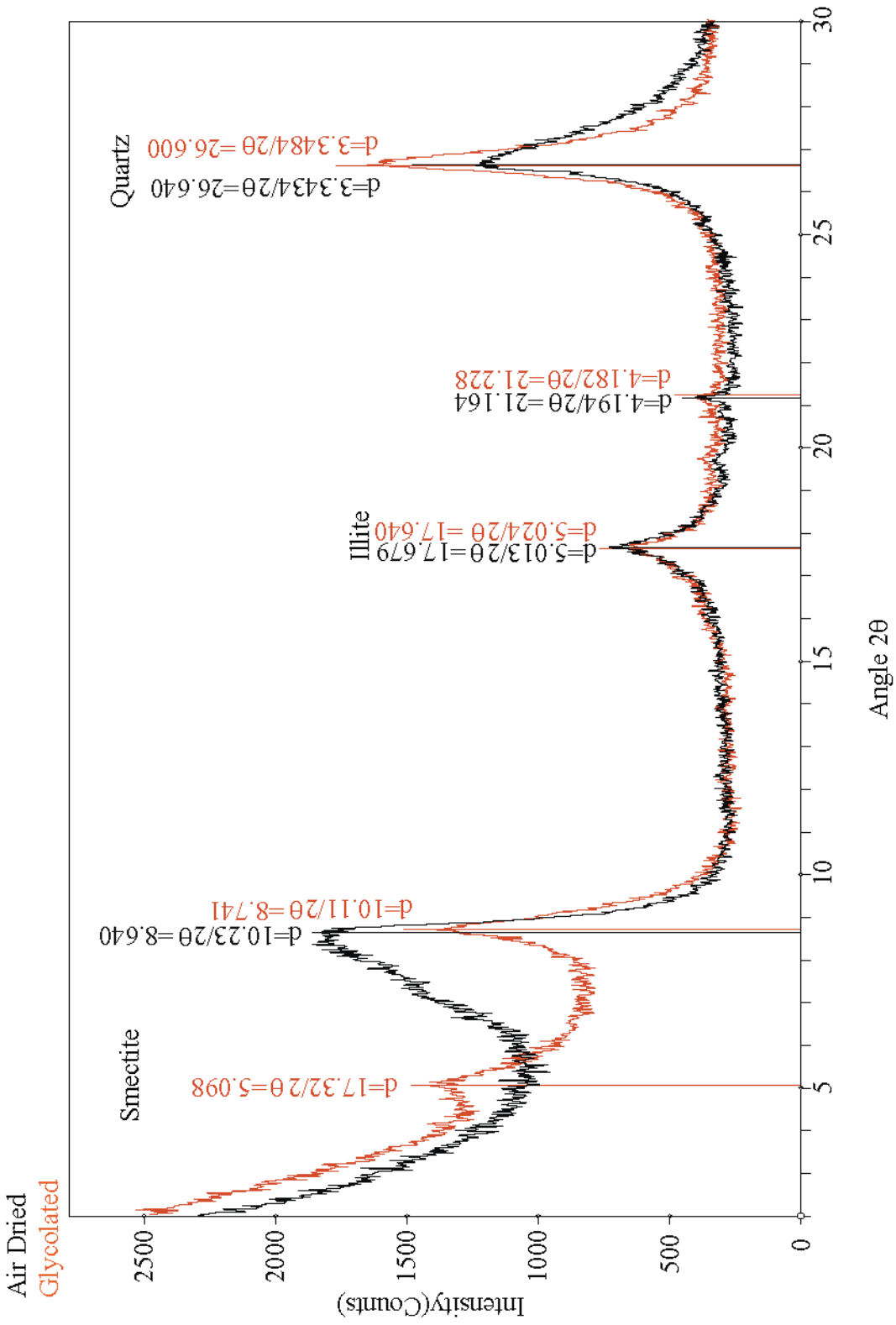

Figure B27. Stratigraphic Section 2: 237.4 m.

Table B1. Relative % Clay by XRD

Interval 1	Depth	Smectite	Illite	Kaolinite
1	2.0	0	71	29
	2.9	7	57	36
	4.1	0	72	28
	4.8	0	53	47
	22.3	19	26	55
	24.6	18	23	59
	51.2	34	0	66
	54.6	33	58	9
2	76.5	17	72	11
	77.2	26	61	13
	84.6	26	60	14
	110.6	100	0	0
	114.2	84	0	16
	129.2	70	6	23
	139.6	95	0	5
	142.5	91	0	9
	151.5	90	0	10
	170.3	31	69	0
3	173.4	19	81	0
	178.0	91	0	9
	179.3	7	93	0
	190.9	17	83	0
	196.0	25	66	9
	206.9	33	57	10
	237.4	13	87	0

APPENDIX C

QEMSCAN FIGURES

QEMSCAN Figures C1-C15 with the following data in Table C1. Note that Table C1 does not contain background in the calculated area % but the figures show values where applicable.

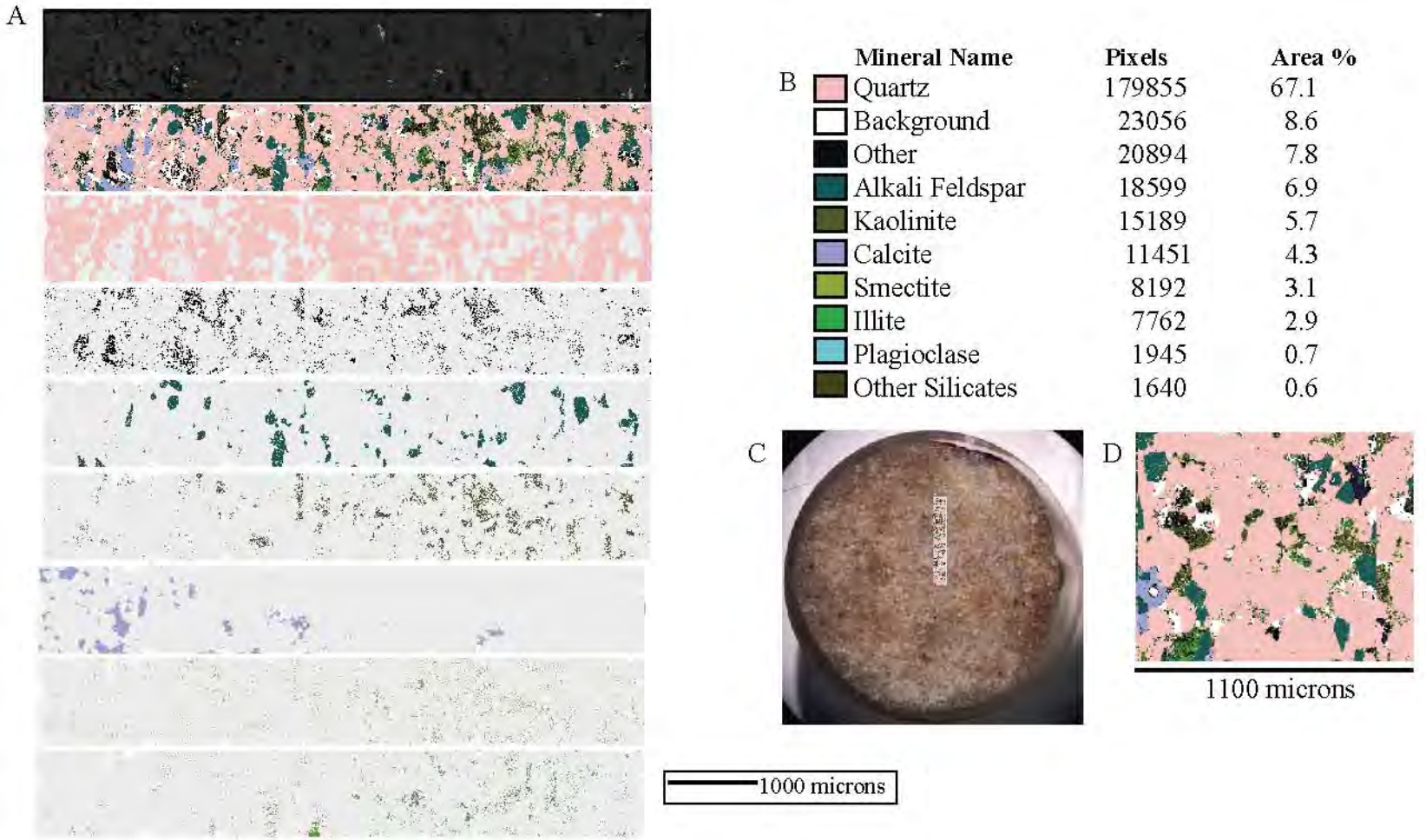

Figure C1. QEMSCAN Data for Epoxy Plug 0 m, 7 mm x 1 mm with 5 μm pixel spacing, a sandstone sample from the top of the Shinarump Member. A) From top: Backscatter image, map of all minerals, each individual mineral in decreasing abundance excluding background, plagioclase, and other silicates. B) Mineral abundances. C) 25 mm diameter, approximate location of measured area. D) Close up view.

A

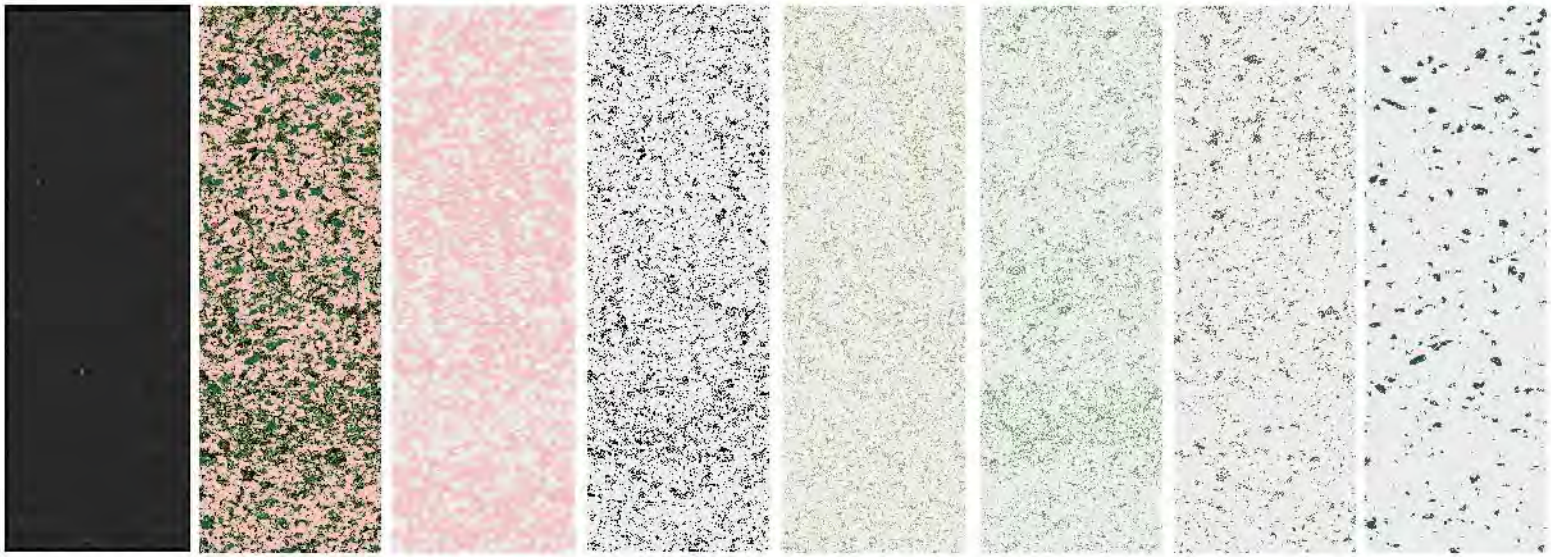

B

Mineral Name	Pixels	Area %
Quartz	258340	51.2
Other	67091	13.3
Smectites	44443	8.8
Illite	43994	8.7
Kaolinite	28089	5.5
Alkali Feldspar	21084	4.1
Other Silicates	20668	4.1
Plagioclase	7564	1.5
Muscovite	3699	0.7
Glauconite	3689	0.7
Chlorite	3175	0.6

C

D

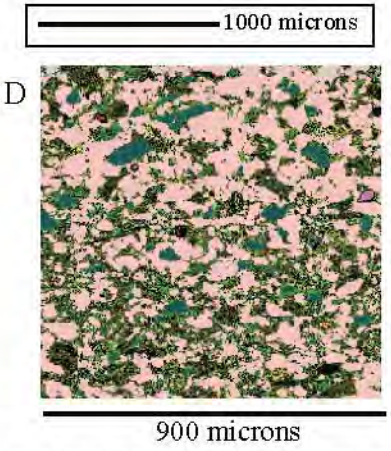

Figure C2. QEMSCAN Data for Epoxy Plug 2 m, 3 mm x 1 mm with 2.5 μm pixel spacing, a paleosol sample from interval 1. A) From left: Backscatter image, map of all minerals, each individual mineral in decreasing abundance excluding other silicates to chlorite. B) Mineral abundances. C) 25 mm diameter, approximate location of measured area. D) Close up view.

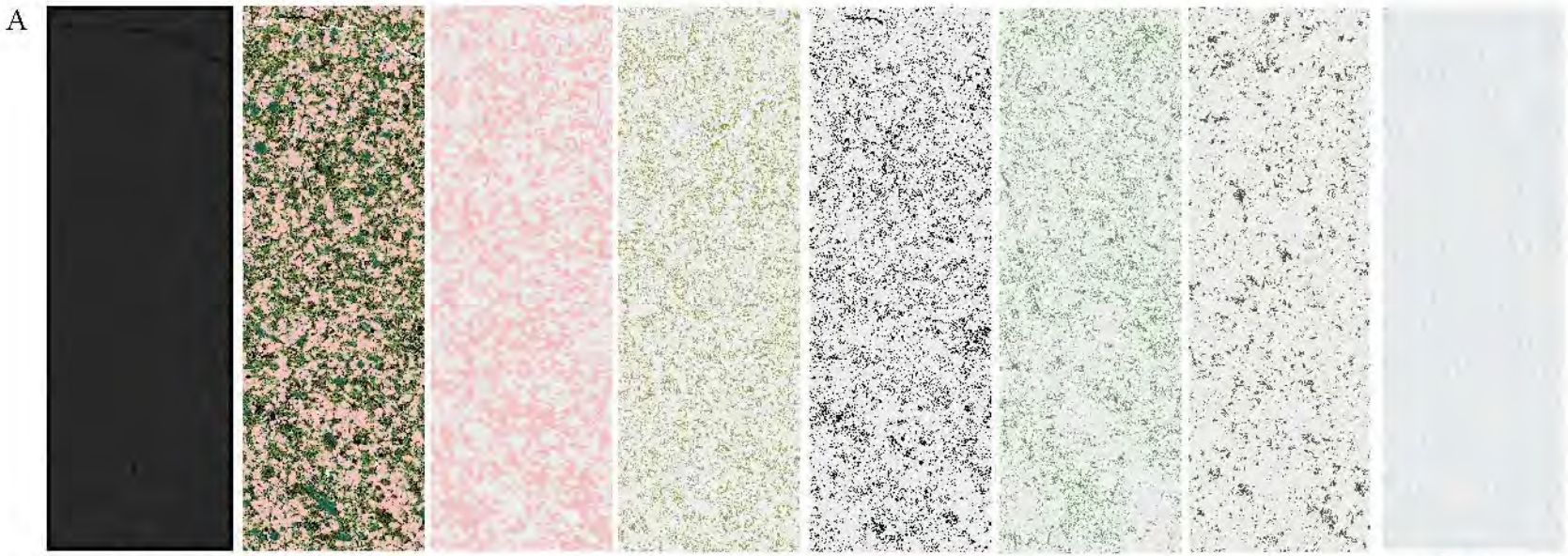

B

Mineral Name	Pixels	Area %
Quartz	209879	41.8
Smectite	73718	14.7
Other	65536	13.0
Illite	56240	11.2
Kaolinite	33849	6.7
Plagioclase	22659	4.5
Other Silicates	20060	4.0
Alkali Feldspar	12176	2.4
Muscovite	3904	0.7

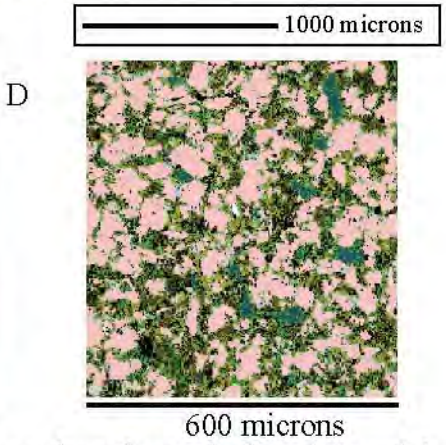

Figure C3. QEMSCAN Data for Epoxy Plug 1.15 m, 3 mm x 1 mm with 2.5 μm pixel spacing, a paleosol sample from interval 1. A) From left: Backscatter image, map of all minerals, each individual mineral in decreasing abundance excluding other silicates to muscovite. B) Mineral abundances. C) 25 mm diameter, approximate location of measured area. D) Close up view.

A

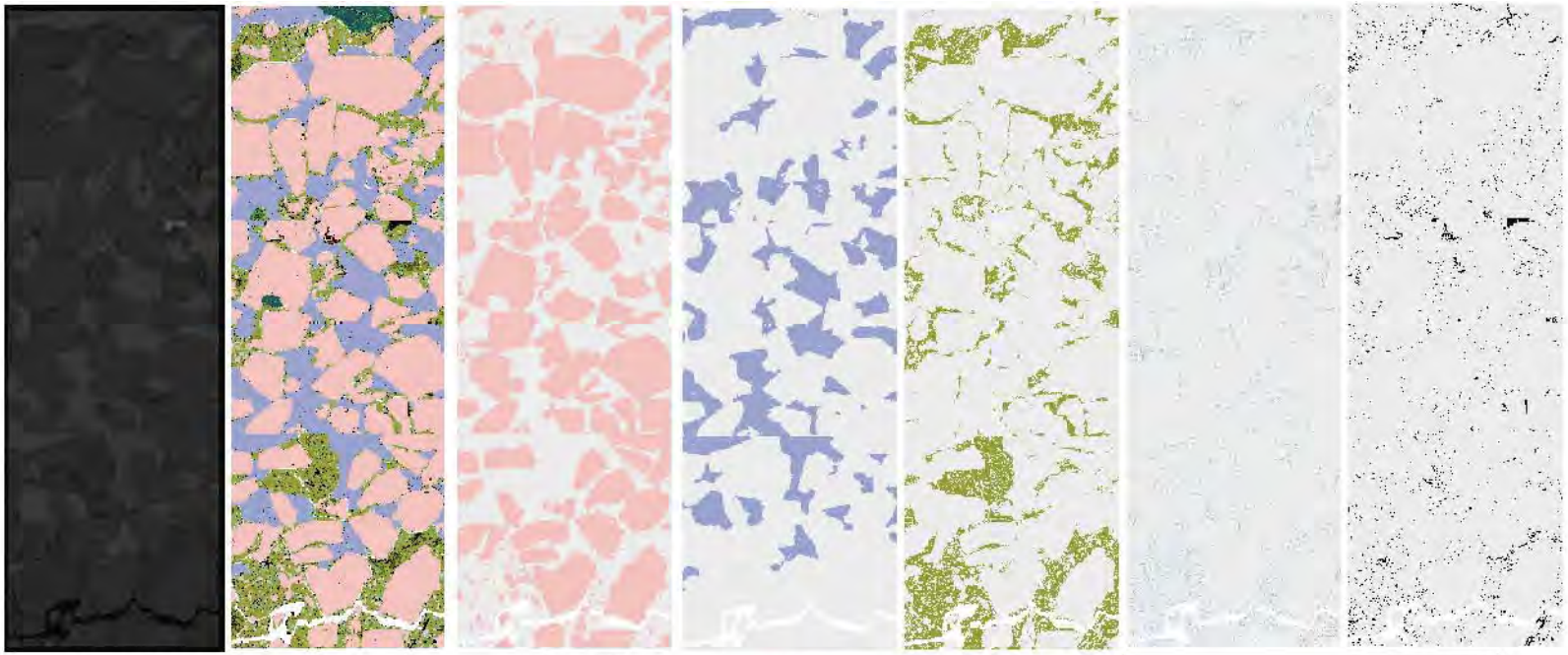

B

Mineral Name	Pixels	Area %
Quartz	106076	55.33
Calcite	40355	21.05
Smectite	30016	15.66
Plagioclase	5949	3.10
Other	4463	2.33
Background	2132	1.11
Kaolinite	2060	1.07
Alkali Feldspar	1563	0.82

C

D

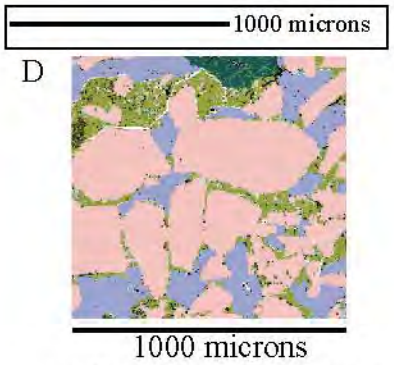

Figure C4. QEMSCAN Data for Epoxy Plug 38.0 m, 3 mm x 1 mm with 4 μm pixel spacing, a sandstone sample from interval 1. A) From left: Backscatter image, map of all minerals, each individual mineral in decreasing abundance excluding background to alkali feldspar. B) Mineral abundances. C) 25 mm diameter, approximate location of measured area. D) Close up view.

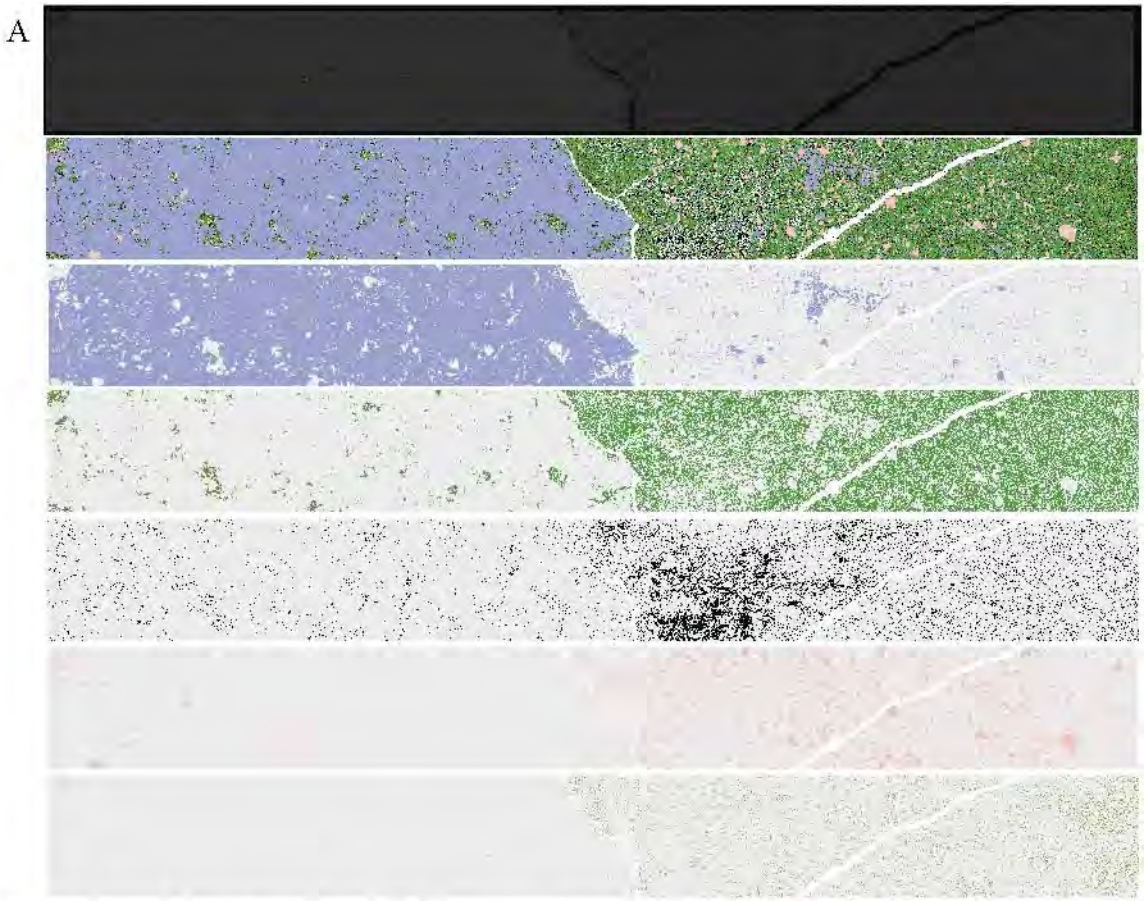

B

Mineral Name	Pixels	Area %
Calcite	283933	49.0
Illite	153346	26.5
Other	51153	8.8
Quartz	46348	8.0
Other Silicates	20015	3.5
Smectite	16331	2.8
Plagioclase	5470	0.9

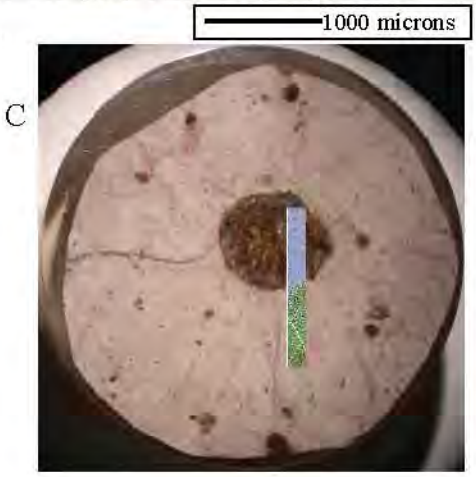

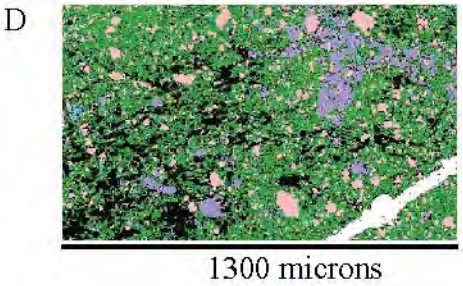

Figure C5. QEMSCAN Data for Epoxy Plug 61.9 m, 9 mm x 1 mm with 4 μm pixel spacing, a paleosol sample from interval 1. A) From left: Backscatter image, map of all minerals, each individual mineral in decreasing abundance excluding plagioclase. B) Mineral abundances. C) 25 mm diameter, approximate location of measured area, black carbonate nodule in center. D) Close up view.

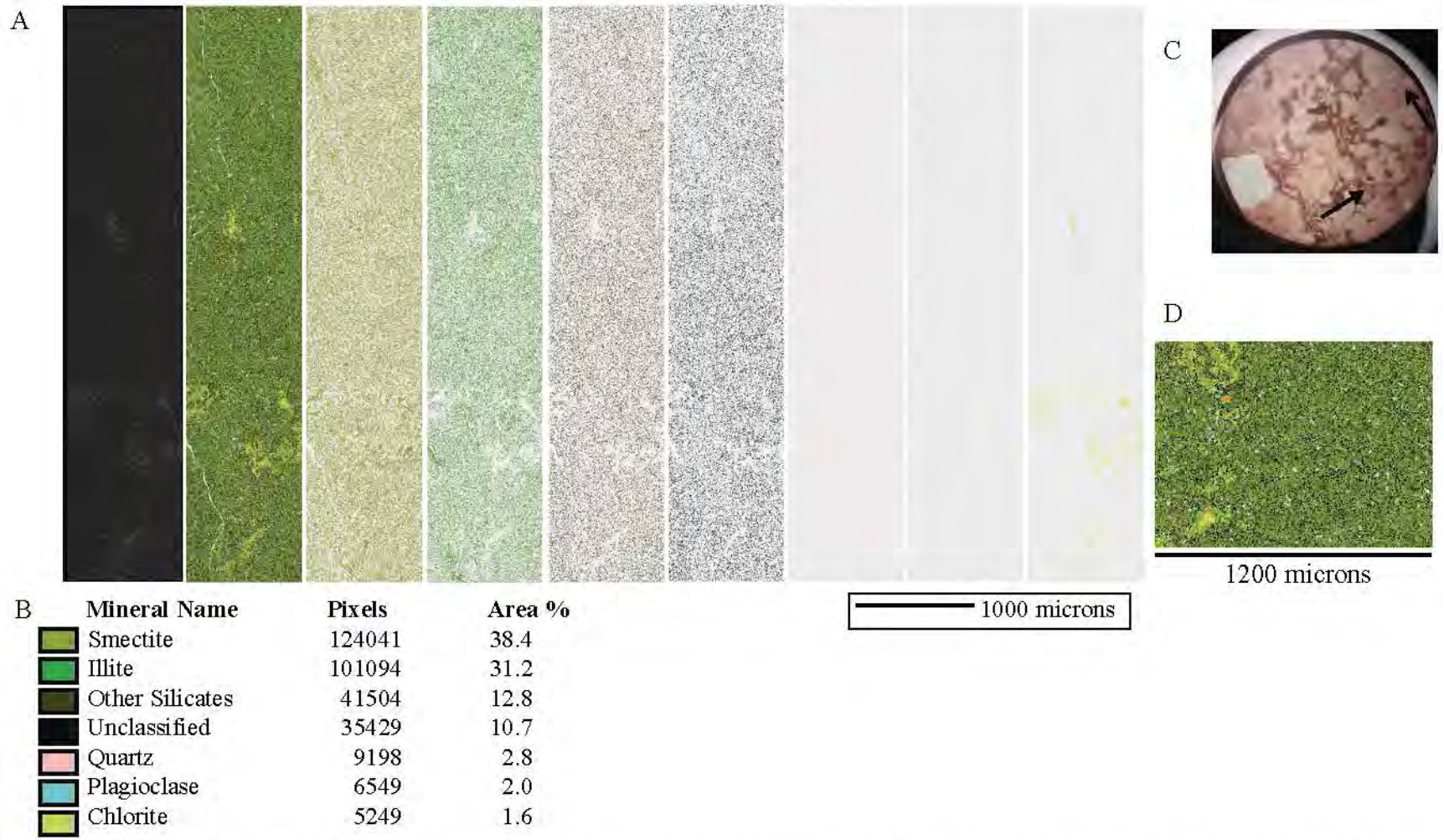

B

Mineral Name	Pixels	Area %
Smectite	124041	38.4
Illite	101094	31.2
Other Silicates	41504	12.8
Unclassified	35429	10.7
Quartz	9198	2.8
Plagioclase	6549	2.0
Chlorite	5249	1.6

Figure C6. QEMSCAN Data for Epoxy Plug 84.6 m, 5 mm x 1 mm with 4μm pixel spacing, a paleosol sample from interval 2. A) From left: Backscatter image, map of all minerals, each individual mineral in decreasing abundance. B) Mineral abundances. C) 25 mm diameter, approximate location of measured area. The arrows point to meniscate backfilled burrows. D) Close up view.

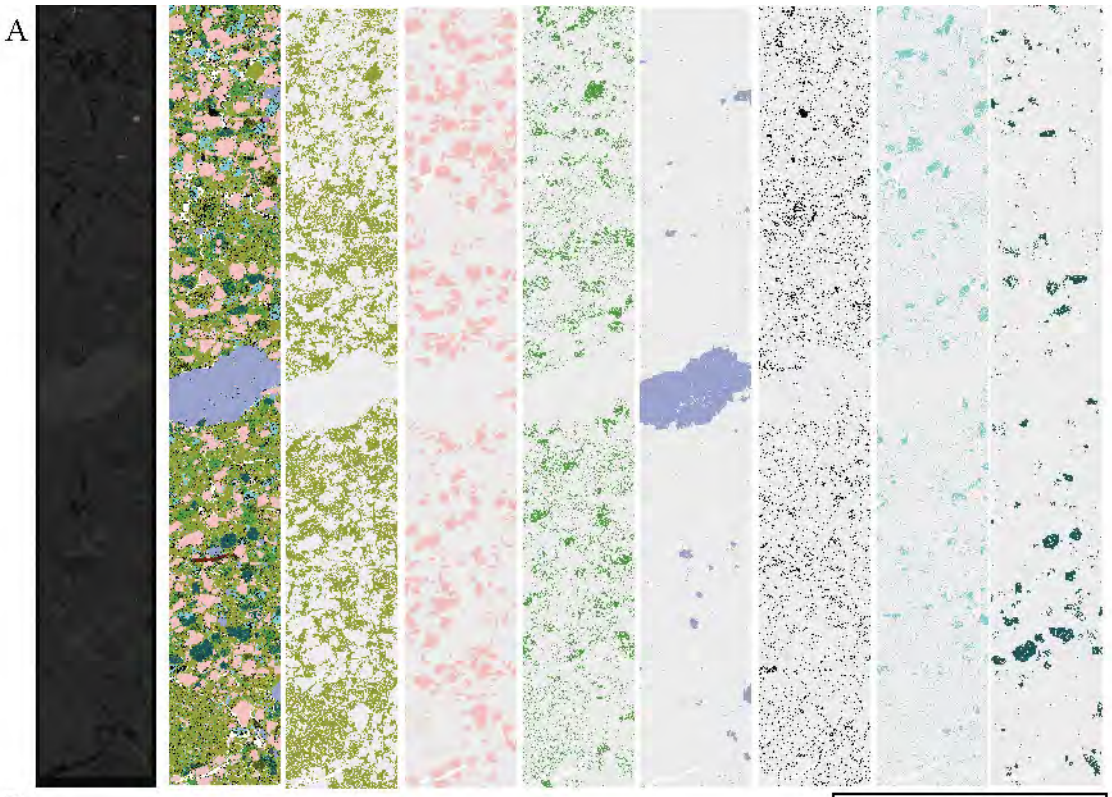

B

Mineral Name	Pixels	Area %
Smectite	102389	35.6
Quartz	63259	22.0
Illite	31081	10.8
Calcite	20394	7.1
Unclassified	18126	6.3
Plagioclase	18083	6.3
Alkali Feldspar	12090	4.2
Background	10182	3.5
Other Silicates	4310	1.5
Kaolinite	3722	1.3
Chlorite	3462	1.2

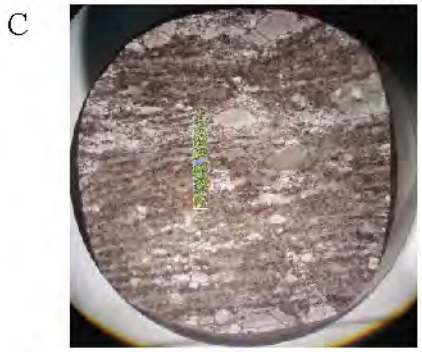

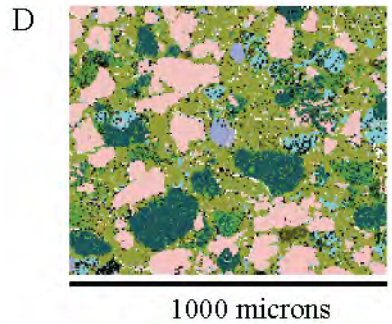

Figure C7. QEMSCAN Data for Epoxy Plug 114.2 m, 7 mm x 1 mm with 5 μm pixel spacing, a sandstone sample from interval 2. A) From left: Backscatter image, map of all minerals, each individual mineral in decreasing abundance excluding background to chlorite. B) Mineral abundances. C) 25 mm diameter, approximate location of measured area. D) Close up view.

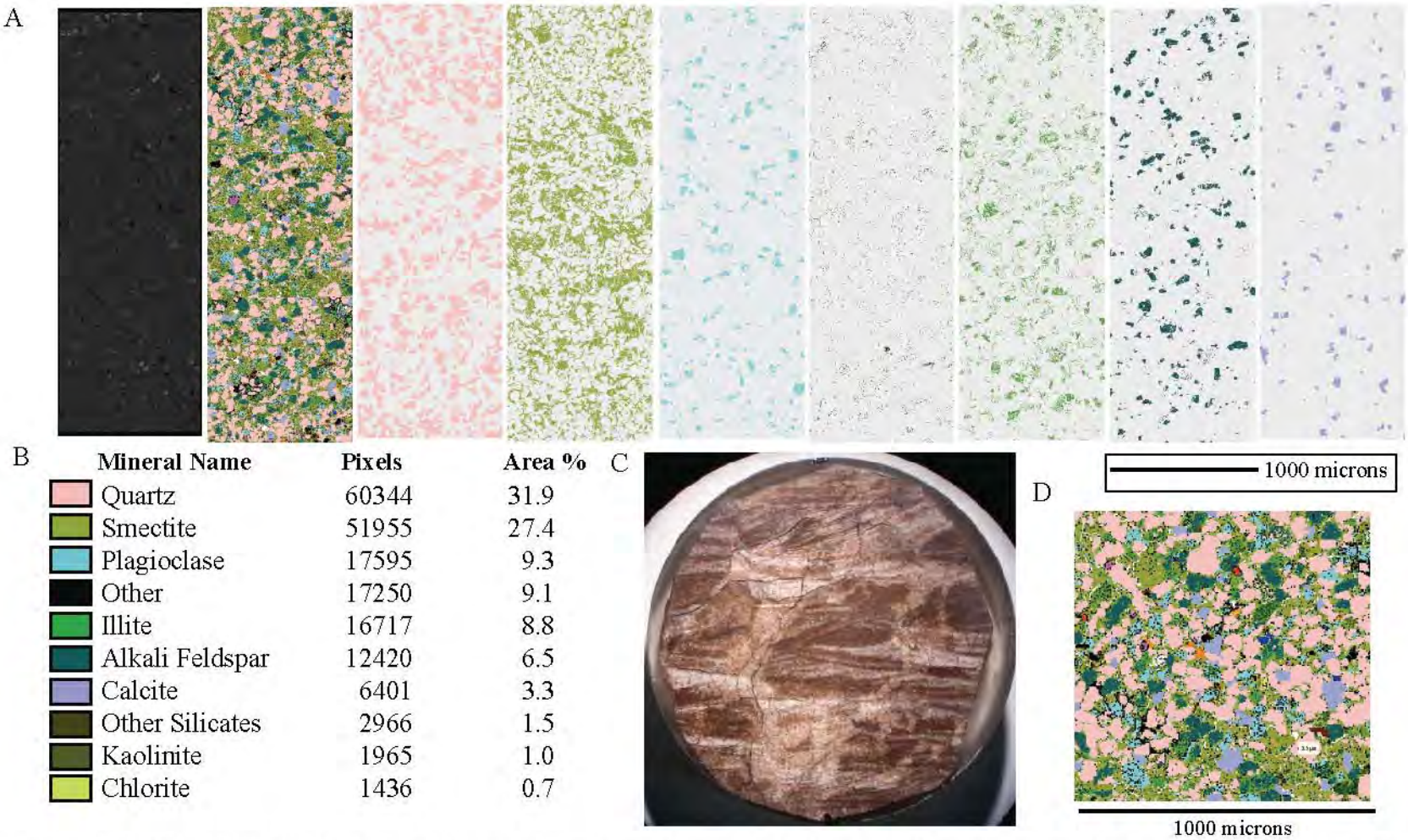

Figure C8. QEMSCAN Data for Epoxy Plug 129.5 m, 3 mm x 1 mm with 4 μm pixel spacing, a muddy sandstone from interval 2. A) From left: Backscatter image, map of all minerals, each individual mineral in decreasing abundance excluding other silicates to chlorite. B) Mineral abundances. C) 25 mm diameter, approximate location of measured area. D) Close up view.

A

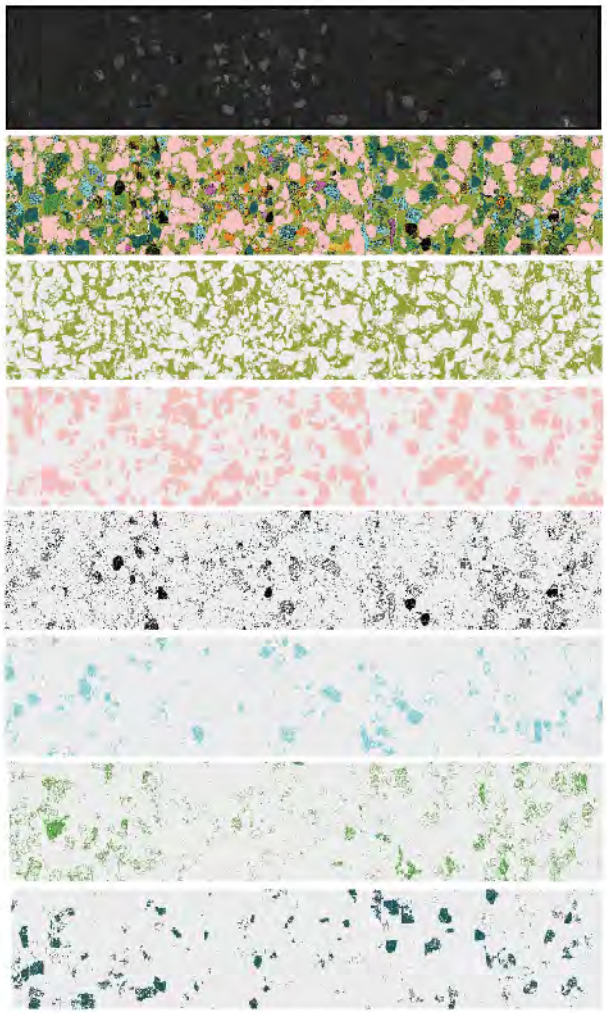

B

Mineral Name	Pixels	Area %
Smectites	48961	34.2
Quartz	46586	32.5
Unclassified	10389	7.2
Plagioclase	9375	6.5
Illite	9308	6.5
Alkali Feldspar	8591	6.0
Other Silicates	2747	1.9
Chlorite	2335	1.6
Background	2103	1.4
Siderite	1928	1.3
Kaolinite	767	0.5

C

1000 microns

D

1000 microns

Figure C9. QEMSCAN Data for Epoxy Plug 139.6 m, 5 mm x 1 mm with 6 μm pixel spacing, a sandstone from interval 2. A) From left: Backscatter image, map of all minerals, each individual mineral in decreasing abundance excluding other silicates to kaolinite. B) Mineral abundances. C) 25 mm diameter, approximate location of measured area. D) Close up view.

A

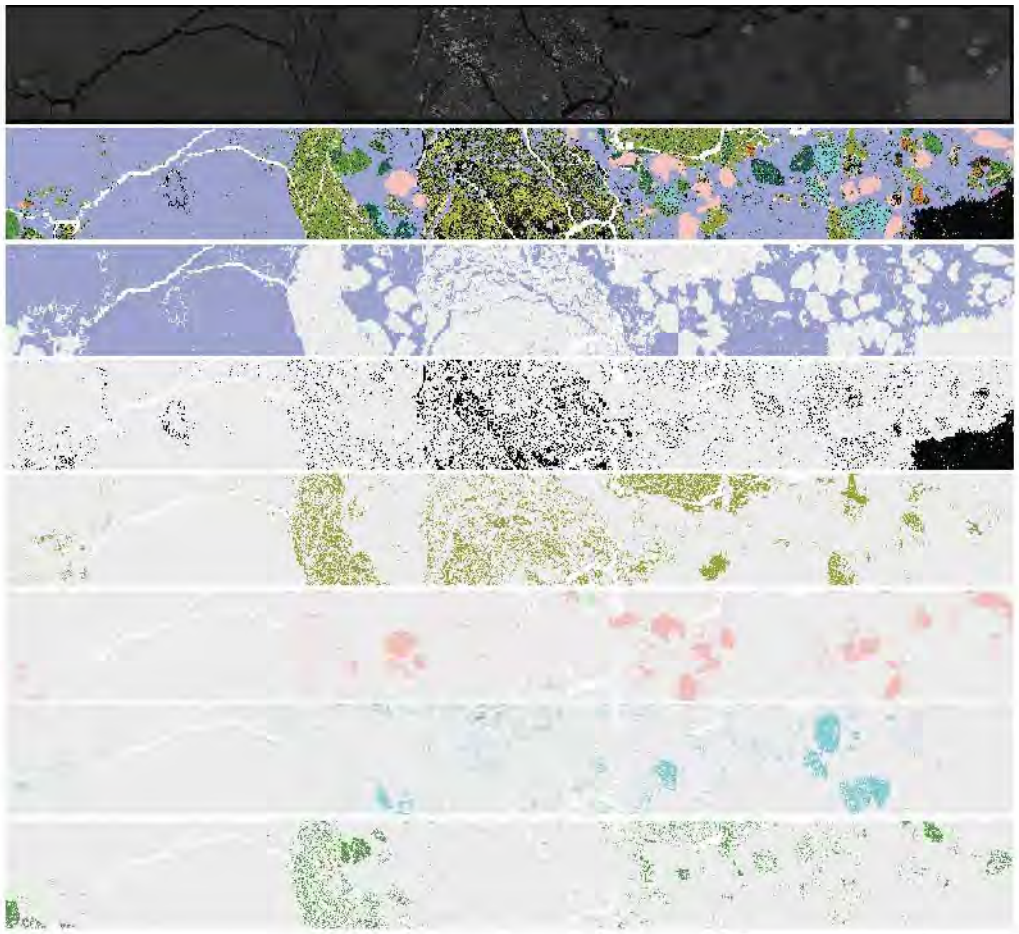

B

Mineral Name	Pixels	Area %
Calcite	192114	52.7
Other	41840	11.5
Smectite	38793	10.6
Quartz	25727	7.1
Plagioclase	17020	4.7
Illite	14415	4.0
Other Silicates	14052	3.9
Chlorite	9490	2.6
Alkali Feldspar	6975	1.9
Background	6662	1.8

D

C

Figure C10. QEMSCAN Data for Epoxy Plug 139.8 m, 6 mm x 1 mm with 5 μm pixel spacing, a conglomeratic sandstone from interval 2. A) From left: Backscatter image, map of all minerals, each individual mineral in decreasing abundance excluding other silicates to background. B) Mineral abundances. C) 25 mm diameter, approximate location of measured area. D) Close up view.

A

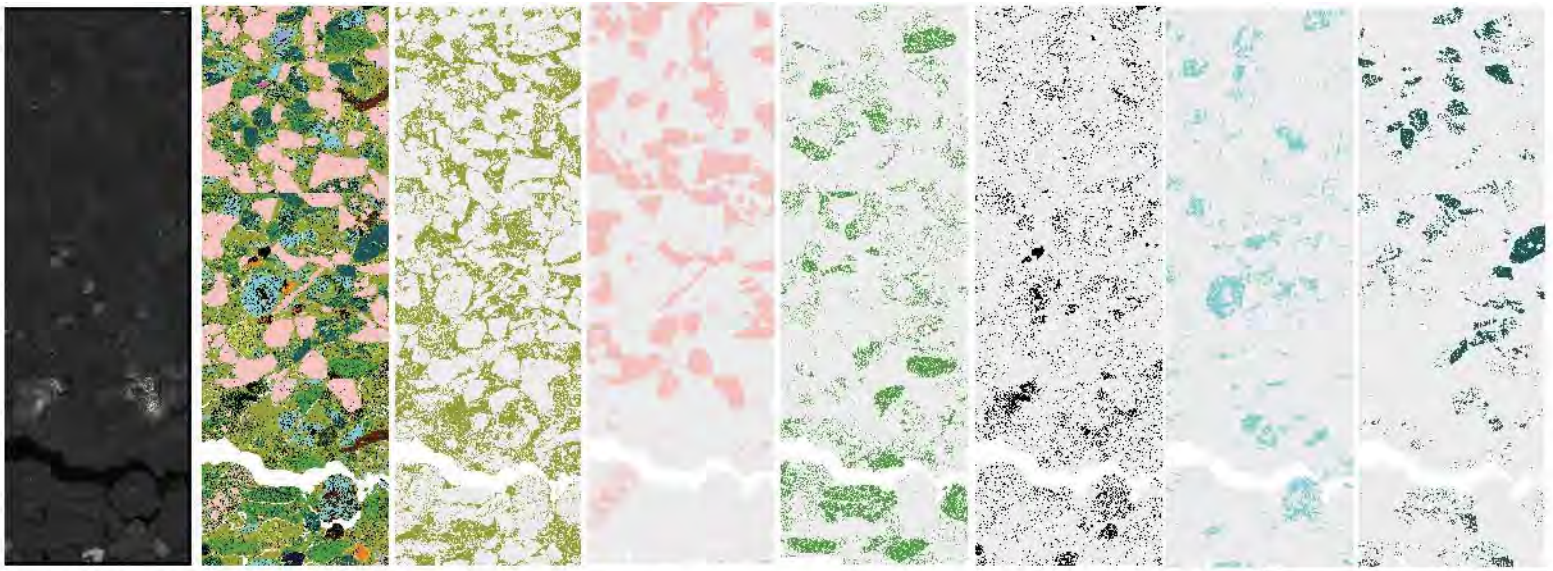

B

Mineral Name	Pixels	Area %
Smectite	147686	30.8
Quartz	117457	24.5
Illite	63409	13.2
Other	42520	8.8
Plagioclase	37436	7.8
Alkali Feldspar	32661	6.8
Other Silicates	12281	2.5
Chlorite	10468	2.1
Background	9731	2.0
Biotite	2944	0.6
Kaolinite	2627	0.5

C

D

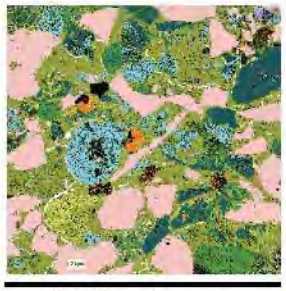

Figure C11. QEMSCAN Data for Epoxy Plug 142.5 m, 3 mm x 1 mm with 2.5 μm pixel spacing, a sandstone sample from interval 2. A) From top: Backscatter image, map of all minerals, each individual mineral in decreasing abundance excluding other silicates to kaolinite B) Mineral abundances. C) 25 mm diameter, approximate location of measured area. D) Close up view.

A

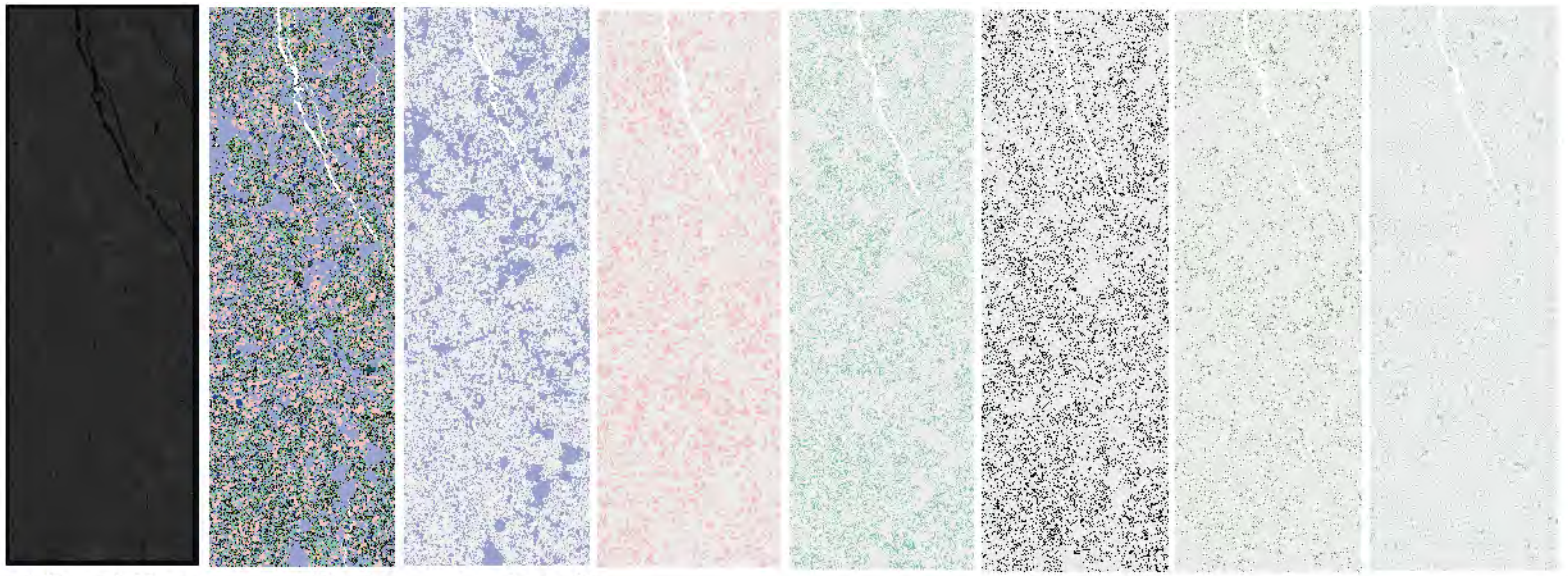

B

Mineral Name	Pixels	Area %
Calcite	119548	34.8
Quartz	77186	22.4
Amphiboles	50419	14.6
Other	47603	13.8
Illite	13121	3.8
Plagioclase	12844	3.7
Dolomite	9799	2.8
Other Silicates	6376	1.8
Smectite	4099	1.1
Alkali Feldspar	2176	0.6
Chlorite	1474	0.4

C

1000 microns

D

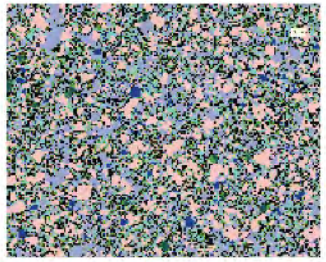

750 microns

Figure C12. QEMSCAN Data for Epoxy Plug 172.3 m, 3 mm x 1 mm with 3 μm pixel spacing, a paleosol sample form interval 3. A) From top: Backscatter image, map of all minerals, each individual mineral in decreasing abundance excluding dolomite to chlorite. B) Mineral abundances. C) 25 mm diameter, approximate location of measured area. D) Close up view.

A B

Mineral Name	Pixels	Area %
Calcite	117419	25.8
Quartz	111493	24.5
Unclassified	80047	17.6
Amphiboles	57583	12.6
Illite	29102	6.4
Plagioclase	16799	3.7
Other Silicates	14948	3.3
Dolomite	12498	2.7
Smectite	7956	1.7
Alkali Feldspar	3280	0.7
Chlorite	2536	0.6


C

Figure C13. QEMSCAN Data for Epoxy Plug 173.4 m, 7 mm x 1 mm with 4 μm pixel spacing, a paleosol sample from interval 3. A) From top: Backscatter image, map of all minerals, each individual mineral in decreasing abundance excluding dolomite to chlorite. B) Mineral abundances. C) 25 mm diameter, approximate location of measured area. D) Close up view.

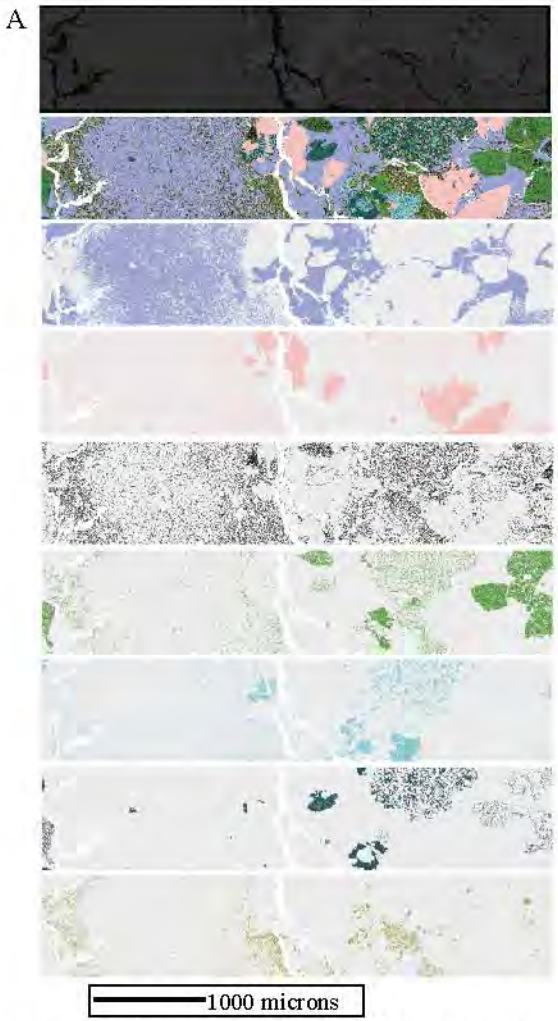

B

Mineral Name	Pixels	Area %
Calcite	85257	42.9
Quartz	32584	16.4
Other	21104	10.6
Illite	20460	10.3
Plagioclase	16078	8.1
Alkali Feldspar	9586	4.8
Smectite	7607	3.8
Background	4892	2.4
Other Silicates	4021	2.0
Chlorite	976	0.4

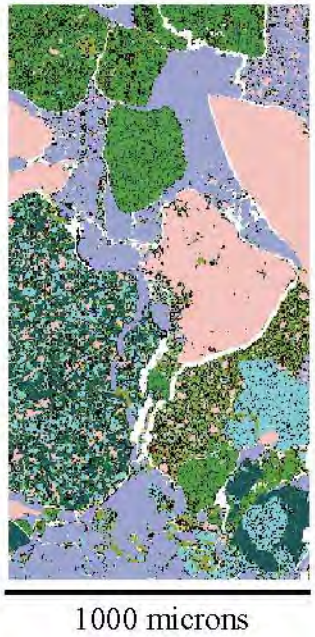

Figure C14. QEMSCAN Data for Epoxy Plug 179.3 m, 5 mm x 1 mm with 5 μm pixel spacing, a carbonate nodular sample from interval 3. A) From top: Backscatter image, map of all minerals, each individual mineral in decreasing abundance excluding background to chlorite. B) Mineral abundances. C) 25 mm diameter, approximate location of measured area. D) Close up view.

A

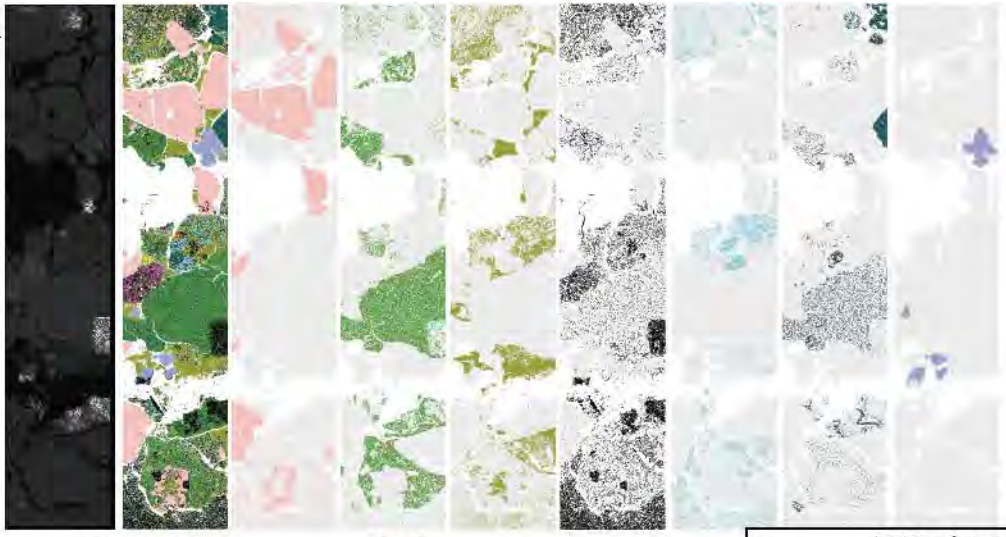

B

Mineral Name	Pixels	Area %
Quartz	101269	22.7
Illite	99150	22.3
Smectite	72347	16.2
Other	68266	15.3
Plagioclase	35920	8.0
Alkali Feldspar	30645	6.9
Calcite	12666	2.8
Other Silicates	8502	1.9
Background	7725	1.7
Apatite	5599	1.2
Other	4281	0.9
Chlorite	4110	0.9

C

D

Figure C15. QEMSCAN Data for Epoxy Plug 190.9 m, 5 mm x 1 mm with 3 μm pixel spacing, a muddy sandstone from interval 3. A) From top: Backscatter image, map of all minerals, each individual mineral in decreasing abundance excluding other silicates to chlorite. B) Mineral abundances. C) 25 mm diameter, approximate location of measured area. D) Close up view.

Table C1. QEMSCAN Data

Interval	Depth (m)	Alkali Feldspar Pixels	Alkali Feldspar Area %	Calcite Pixels	Calcite Area %	Chlorite Pixels	Chlorite Area %	Illite Pixels	Illite Area %	Kaolinite Pixels	Kaolinite Area %
1	0	18599	7	11451	4	0	0	7762	3	15189	6
	2.0	21084	4	0	0	3175	1	43994	9	28089	6
	2.9	12176	2	0	0	0	0	56240	11	33849	7
	6.1	0	0	0	0	101422	18	0	0	18981	3
	38.0	1563	1	40355	21	0	0	0	0	2060	1
2	84.6	0	0	0	0	5249	2	101094	31	0	0
	114.2	12090	4	20394	7	3462	1	31081	11	3722	1
	129.2	12420	7	6401	3	1436	1	16717	9	1965	1
	139.6	8591	6	0	0	2335	2	9308	7	767	1
	139.8	6975	2	192114	53	9490	3	14415	4	0	0
	142.5	32661	7	0	0	10468	2	63409	14	2627	1
3	172.3	2176	1	119548	35	0	0	13121	4	1474	0
	173.4	3280	1	117419	26	2536	1	29102	6	0	0
	179.3	9586	5	85257	43	976	0	20460	10	0	0
	190.9	30645	7	12666	3	4110	1	99150	22	0	0

Table C1. Continued

Interval	Depth (m)	Other Silicates Pixels	Other Silicates Area %	Plagioclase Pixels	Plagioclase Area %	Quartz Pixels	Quartz Area %	Smectite Pixels	Smectite Area %	Unclassified Pixels
1	0	1640	1	1945	1	179855	68	8192	3	20894
	2.0	20668	4	7564	2	258340	52	44443	9	67091
	2.9	20060	4	22659	5	209879	42	73718	15	65536
	6.1	10543	2	19623	3	115323	20	263511	46	44765
	38.0	0	0	5949	3	106076	56	30016	16	4463
2	84.6	41504	13	6549	2	9198	3	124041	38	35429
	114.2	4310	2	18083	7	63259	23	102389	37	18126
	129.2	2966	2	17595	9	60344	32	51955	27	17250
	139.6	2747	2	9375	7	46586	33	48961	35	10389
	139.8	14052	4	17020	5	25727	7	38793	11	41840
	142.5	12281	3	37436	8	117456	25	147686	31	42520
3	172.3	6376	2	12844	4	77186	22	4099	1	47603
	173.4	14948	3	16799	4	111493	25	7956	2	80047
	179.3	4021	2	16078	8	32584	16	7607	4	21104
	190.9	8502	2	35920	8	101269	23	72347	16	72547

Table C1. Continued

Interval	Depth (m)	Unclassified Area %	Apatite Pixels	Apatite Area %	Amphiboles Pixels	Amphiboles Area %	Biotite Pixels	Biotite Area %	Dolomite Pixels	Dolomite Area %
1	0	8	0	0	0.00	0	0.00	0	0.00	0
	2.0	13	0	0	0.00	0	0.00	0	0.00	0
	2.9	13	0	0	0.00	0	0.00	0	0.00	0
	6.1	8	0	0	0.00	0	0.00	0	0.00	0
	38.0	2	0	0	0.00	0	0.00	0	0.00	0
2	84.6	11	0	0	0.00	0	0.00	0	0.00	0
	114.2	7	0	0	0.00	0	0.00	0	0.00	0
	129.2	9	0	0	0.00	0	0.00	0	0.00	0
	139.6	7	0	0	0.00	0	0.00	0	0.00	0
	139.8	12	0	0	0.00	0	0.00	0	0.00	0
	142.5	9	0	0	0.00	0	2944	1	0.00	0
3	172.3	14	0	0	50419	15	0.00	0	9799	3
	173.4	18	0	0	57583	13	0.00	0	12498	3
	179.3	11	0	0	0.00	0	0.00	0	0.00	0
	190.9	16	5599	1	0.00	0	0.00	0	0.00	0

Table C1. Continued

Interval	Depth (m)	Muscovite Pixels	Muscovite Area %	Siderite Pixels	Siderite Area %	Total Pixels	Total Area %
1	0	0.00	0	0.00	0	265527	100
	2.0	3699	1	0.00	0	498147	100
	2.9	3904	1	0.00	0	498021	100
	6.1	0.00	0	4572	1	578740	100
	38.0	0.00	0	0.00	0	190482	100
2	84.6	0.00	0	0.00	0	323064	100
	114.2	0.00	0	0.00	0	276916	100
	129.2	0.00	0	0.00	0	189049	100
	139.6	0.00	0	1928	1	140987	100
	139.8	0.00	0	0.00	0	360426	100
	142.5	0.00	0	0.00	0	469488	100
3	172.3	0.00	0	0.00	0	344645	100
	173.4	0.00	0	0.00	0	453661	100
	179.3	0.00	0	0.00	0	197673	100
	190.9	0.00	0	0.00	0	442755	100

REFERENCES

Abdel-Gawad, A.M. and Kerr, P. F., 1963, Alteration of Chinle Siltstone and Uranium Emplacement, Arizona and Utah: Geological Society of America Bulletin, v. 74, p. 23-46.

Allen, J.L., Johnson, C.L., Heumann, M.J., Gooley, J., and Gallin, W., 2012, New technology and methodology for assessing sandstone composition: A preliminary case study using a quantitative electron microscope scanner (QEMScan), *in* Rasbury, E.T., Hemming, S.R., and Riggs, N.R., eds., Mineralogical and Geochemical Approaches to Provenance: Geological Society of America Special Paper 487, (in press).

Ash, S.R., 1972. Plant megafossils of the Chinle Formation, *in*: Breed, C.S. and Breed, W. J. (eds.), Investigations in the Triassic Chinle Formation. Museum of Northern Arizona Bulletin 47, p. 23-44.

Ash, S.R. and Creber, G.T., 1992, Palaeoclimatic interpretation of the wood structures of the trees in the Chinle Formation (Upper Triassic), Petrified Forest National Park, Arizona, USA: Palaeogeography, Palaeoclimatology, Palaeoecology, v. 96, p. 299-317.

Ash, S.R., 1987, Growth habit and systematlcs of the Upper Triassic plant *Pelourdea poleoensls,* southwestern USA: Review of Palaeobotany and Palynology, v. 51, p. 37-49

Ash, S.R., 2001, New cycadophytes from the Upper Triassic Chinle Formation of the Southwestern United States: Paleobios, v. 21, no. 1, p. 15-28

Ash, S.R., 2001, The fossil ferns of Petrified Forest National Park, and their paleoclimatological interpretations, *in:* Santucci VL, McClelland L, eds., Proceedings of the 6th Fossil Research Conference, National Park Service, p. 3–10.

Ash, S.R., 2003, The Wolverine Petrified Forest: Utah Geological Survey Notes, v. 35, p. 3-6.

Ash, S.R., 2005, Synopsis of the Upper Triassic Flora of Petrified Forest National Park and vicinity, *in:* Nesbitt, S. J., Parker, W. G., and Irmis, R.B., eds. Guidebook to the Triassic Formations of the Colorado Plateau in northern

Arizona: Geology, Paleontology, and History: Mesa Southwest Museum Bulletin 6, p. 59-70.

Beer, J.J., 2005, Sequence stratigraphy of fluvial and lacustrine deposits in the lower part of the Chinle Formation, South Central Utah, United States: Paleoclimatic and Tectonic Implications [Master's Thesis]: University of Minnesota, 169 p.

Basdeska, P.O., 1993, Provenance and diagenesis of the Shinarump Member, Triassic Chinle Formation, Southern Nevada to Southern Utah [Master's Thesis]: Northern Arizona University, 142 p.

Bilodeau, W.L., 1986. The Mesozoic Mogollon highlands, Arizona--an Early Cretaceous rift shoulder: J. Geol., v. 94, p. 724-735.

Blakey, R.C., and Gubitosa, R., 1983, Late Triassic paleogeography and depositional history of the Chinle Formation, southern Utah and northern Arizona, *in:* Reynolds, M.W., and Dolby, E.D., eds., Mesozoic Paleogeography of West-Central United States: SEPM, Rocky Mountain Section, p. 57–76.

Blakey, R.C. and Middleton, L.T., 1986, Triassic-Jurassic continental systems, northern Arizona; *in:* Nations, J.D., Conway, C.M. and Swann, G.A., eds., Geology of central and northern Arizona: Field Trip Guidebook: Boulder, Geological Society of America, Rocky Mountain Section, p. 93-110.

Blakey, R.C., (Personal Communication, October 10th, 2010).

Bown, T.M. and Kraus, M.J., 1981, Lower Eocene alluvial paleosols (Willwood Formation, Northwest Wyoming, U.S.A.) and their significance for paleoecology, paleoclimatology, and basin analysis: Palaeogeography, Palaeoclimatology, Palaeoecology, v. 34, p. 1–30.

Bown, T.M. and Kraus, M.J., 1987, Integration of channel and floodplain suites, I. Developmental sequence and lateral relations of alluvial paleosols: Journal of Sedimentary Petrology, v. 57, no. 4, p. 587-601.

Breecker, D., 2010, Improving paleosol carbonate based estimates of ancient atmospheric CO2: Geochemical News, v. 144.

Brown, C.M., 2003, Sedimentology and sequence stratigraphy of the Chinle Formation, southern Utah, [Master's Thesis]: 217 p. http://scholarworks.sjsu.edu/etd_theses/2396

Cerling, T.E., 1991, Carbon dioxide in the atmosphere: evidence from Cenozoic and Mesozoic paleosols: American Journal of Science, v. 291, p. 377-400.

Clemmensen, L.B., Olsen, H., Blakey, R.C., 1989, Erg-margin deposits in the Lower

Jurassic Moenave Formation and Wingate Sandstone, southern Utah: Geological Society of America Bulletin, v. 101, p. 759-773.

Cleveland, D., Nordt, L., and Atchley, S., 2008, Paleosols, trace fossils, and precipitation estimates of the uppermost Triassic strata in northern New Mexico: Palaeogeography, Palaeoclimatology, Palaeoecology, v. 257, p. 421-444.

Cleveland, D., Nordt, L., Dworkin, S.I., and Atchley, S., 2008, Pedogenic carbonate isotopes as evidence for extreme climatic events preceding the Triassic-Jurassic boundary: Implications for the biotic crisis? Geological Society of America Bulletin, v. 120, p. 1408-1415.

Creber, G.T. and Chaloner, W.G., 1985, Tree growth in the Mesozoic and Early Tertiary and the reconstruction of paleoclimates: Palaeogeography, Palaeoclimatology, and Palaeoecology, v. 52, p. 35-50.

Curtin, T., and Parrish, J.T., 1999, The Pangean megamonsoon in SW Pangea: preliminary results from Middle Triassic lacustrine rocks and paleosols, NW Argentina: Geological Society of America Abstract with Programs, v. 31, no. 7, p. 417–418.

Curtis, C.D., 1990, Aspects of climatic influence on the clay mineralogy and geochemistry of soils, palaeosols, and clastic sedimentary rocks: Journal of the Geological Society, London, v. 147, p. 351-357.

DeBlieux, D.D., Kirkland, J.I., Smith, J.A., McGuire, J., and Santucci, V.L., 2006, An overview of the paleontology of Upper Triassic and Lower Jurassic rocks in Zion National Park, Utah, *in:* Harris, J.D., Lucas, S.G., Spielmann, J.A., Lockley, M.G., Milner, A.R.C., and Kirkland, J.I. eds., The Triassic-Jurassic Terrestrial Transition: New Mexico Museum of Natural History and Science Bulletin 37, p. 490–501.

Demko, T.M., Dubiel, R.F., and Parrish, J.T., 1998, Plant taphonomy in incised valleys: implications for interpreting paleoclimate from fossil plants: Geology, v. 26, p. 1119-1122.

Dickinson, W.R., Gehrels, G.E., 2008, U-Pb ages of detrital zircons in relation to paloegeography: Triassic paleodrainage networks and sediment dispersal across southwest Laurentia: Journal of Sedimentary Research, v. 78, p. 745-764.

Donohoo-Hurley, L.L., Geissman, J.W., and Lucas, S.G., 2007, What do we know about the magentostratigraphy across the Triassic-Jurassic boundary? *in:* Lucas, S.G. and Spielman, J.A., eds., The Global Triassic New Mexico Museum of Natural History and Science Bulletin 41, p. 33-38.

Donohoo-Hurley, L.L., Geissman, J.W., Lucas, S.G., 2010, Magnetostratigraphy of the

uppermost Triassic and lowermost Jurassic Moenave Formation, western United States: Correlation with strata in the United Kingdom, Morocco, Turkey, Italy, and eastern United States: Geological Society of America Bulletin, v. 122, no. 11/12, p. 2005-2019.

Dubiel, R.F., 1987, Sedimentology of the Upper Triassic Chinle Formation, southeastern Utah: paleoclimatic implications: Arizona–Nevada Academy of Science, Journal, v. 22, p. 35–45.

Dubiel, R.F., 1989, Depositional and climatic setting of the Upper Triassic Chinle Formation, Colorado Plateau, *in:* Lucas, S.G., and Hunt, A.P., eds., Dawn of the Age of Dinosaurs in the American Southwest, New Mexico Museum of Natural History, Spring Field Conference Guidebook, p. 171–187.

Dubiel, R.F., 1991, Architectural-facies analysis of nonmarine depositional systems in the Upper Triassic Chinle Formation, southeastern Utah, *in:* Miall, A.D., and Tyler, N., eds., The Three-Dimensional Facies Architecture of Terrigenous Clastic Sediments and Its Implications for Hydrocarbon Discovery and Recovery: SEPM, Concepts in Sedimentology and Paleontology 3, p. 103–110.

Dubiel, R.F., 1992, Sedimentology and Depositional History of the Upper Triassic Chinle Formation in the Uinta, Piceance, and Eagle Basins, Northwestern Colorado and Northeastern Utah: U.S. Geological Survey Bulletin, v. 1787-W, p W1-W25.

Dubiel, R.F., 1993, Triassic paleoclimate and significance of red beds: The New Mexico Museum of Natural History and Science Bulletin, no. 3, p. 30.

Dubiel, R.F., 1994, Triassic deposystems, paleogeography, and paleoclimate of the western interior: SEPM Theme Meeting, Mesozoic Systems of the Rocky Mountain Region, p. 133–168.

Dubiel, R.F., and Brown, J.L., 1993, Sedimentologic analysis of cores from the Upper Triassic Chinle Formation and Lower Permian Cutler Formation, Lisbon Valley, Utah: U.S. Geological Survey Bulletin, v. 2000-E, p. E1–E40.

Dubiel, R.F., Hasiotis, S.T., Demko, T.M., 1999, Incised valley fills in the lower part of the Chinle Formation, Petrified Forest National Park, Arizona: Complete measured sections and regional stratigraphic implications of Upper Triassic rocks: National Park Service Paleontological Research, v. 4, p. 78-84.

Dubiel, R.F., Parrish, J.T., Parrish, J.M., and Good, S.C., 1991, The Pangean megamonsoon—evidence from the Upper Triassic Chinle Formation, Colorado Plateau: Palaios, v. 6, p. 347–370.

Elliot, W.C., Savin, S.M., Dong, H., and Peacor, D.R., 1997, A paleoclimate

interpretation from pedogenic clay minerals from the Piedmont Province, Virginia: Chemical Geology, v. 142, p. 201-211.

Ehrmann, W., 1998, Implications of late Eocene to Early Miocene clay mineral assemblages in McMurdo Sound (Ross Sea, Antarctica) on paleoclimate and ice dynamics: Palaeogeography, Palaeoclimatology, Palaeoecology, v. 139, p. 213-231.

Erwin, D., Kidwell, S., Lawton, T., Mohrig, D., Nordt, L.C., Parrish, J.T., Schmitz, M., and Walton, A., 2012, Transitions The Changing Earth-Life System—Critical Information for Society from the Deep Past: Unpublished Report, 64 p.

Fahn, A. and Werker, E., 1990, Seasonal cambial activity, *in*: Iqbal, M., (ed.), The vascular cambium: John Wiley & Sons: New York, p. 139–154.

Fallin, M.J., Kraus, M.J., Platt, B.F., 2004, Controls on vertical color changes in alluvial paleosols of the Morrison Formation, Coyote Basin, Wyoming: Geological Society of America Abstracts with Programs, v. 36, no. 5, p. 375.

FEI Website. [Online] Available: http://www.fei-naturalresources.com/products/qemscan.aspx [November 2011]

Freeman, K.H., and Goldhaber, M.B., 2011, Future Directions in Geobiology and Low-Temperature Geochemistry, report of Workshop, 27-28 August 2010, Carnegie institution of Washington, Geophysical Laboratory, Washington, D.C., 20 p.

Furin, S., Preto, N., Rigo, M., Roghi, G., Gianolla, P., Crowley, J.L., Bowring, S.A., 2006. High- precision U-Pb zircon age from the Triassic of Italy: implications for the Triassic time scale and the Carnian origin of calcareous nannoplankton and dinosaurs: Geology, v. 34, p, 1009-1012.

Goddard E.N., Trask, P.D., de Ford, R.K., Rove, O.N., Singewald, J.T. and Overbeck, R.M., Rock Color Chart: Geological Society of America, 1979, 6 p.

Good. S.C., Parrish, J.M., and Dubiel, R.F., 1987, Paleoenvironmental implications of sedimentology and paleontology of the Upper Triassic Chinle Formation, Southeastern Utah, *in:* Four Corners Geological Society Guidebook. 10th Field Conference, Cataract Canyon, p. 117-118.

Haberlah, D., Williams, M.A.J., Halverson, G., Hill, S.M., Hrstka, T., Butcher, A.R., McTainsh, G.H., Glasby, P., 2010, Loess and floods: high resolution multi-proxy data of Last Glacial Maximum (LGM) slackwater deposition in the Flinders Ranges, semi-arid South Australia: Quaternary Science Reviews 29, p. 2673–2693.

Haq, B.U., Hardenbol, J., Vail, P.R., 1987, Chronology of Fluctuating Sea Levels since

the Triassic: Science, v. 235, no. 4793, p. 1156-1167.

Hasiotis, S.T., and Dubiel, R.F., 1993, Continental trace fossils of the Upper Triassic Chinle Formation, Petrified Forest National Park, Arizona, *in* Lucas, S.G., and Morales, M., eds., The Nonmarine Triassic: New Mexico Museum of Natural History & Science Bulletin, no. 3, p. 175–178.

Hasiotis, S.T., and Dubiel, R.F., 1994, Ichnofossil tiering in Triassic alluvial paleosols: Implications for Pangean continental rocks and paleoclimate, *in:* Beauchamp, B., Embry, A.F., and Glass, D., eds., Pangea: Global environments and resources: Canadian Society of Petroleum Geologists Memoir 17, p. 311–317.

Hazel, J.E., Jr., 1994, Sedimentary response to intrabasinal salt tectonism in the Upper Triassic Chinle Formation, Paradox Basin, Utah: U.S. Geological Survey Bulletin, 2000-F, p. 34.

Heckert, A.B., and Lucas, S.G., 2002, Revised Upper Triassic stratigraphy of the Petrified Forest National Park: New Mexico Museum of Natural History and Science Bulletin, v. 21, p.1-36.

Irmis, R.B., Mundil, R., Martz, J.W., and Parker, W.G., 2011, High-resolution U-Pb ages from the Upper Triassic Chinle Formation (New Mexico, USA): support a diachronous rise of dinosaurs: Earth and Planetary Science Letters, v. 309, p. 258-267.

Imis, R.B., 2005, The vertebrate fauna of the Upper Triassic Chinle Formation in Northern Arizona, *in:* Nesbitt, S.J., Parker, W.G., and Irmis, R.B. eds., Guidebook to the Triassic formations of the Colorado Plateau in northern Arizona: Geology, Paleontology, and History, Mesa Southwest Museum Bulletin 9, p. 63-88.

Kent, T.R. and Irving, E., 2010, Influence of inclination error in sedimentary rocks on the Triassic and Jurassic apparent pole wander path for North America and implications for Cordilleran tectonics: Journal of Geophysical Research, v. 115, p. 1-25.

Karl, T.R. and Trenberth, K.E., 2003, Modern Global Climate Change: Science, v. 302, no. 5651, p. 1719-1723.

Kent, D.V. and Olsen, P.E., 1997, Magnetostratigraphy and paleopoles from the Late Triassic Dan River-Danville basin: interbasin correlation of continental sediments and a test of the tectonic coherence of Newark rift basins in eastern North America: Geological Society of America Bulletin, v. 109, no. 3, p. 366-377.

Kraus, M.J. and Middleton, L.T., 1987, Dissected paleotopography and base-level changes in a Triassic fluvial sequence: Geology, v. 15. p. 18-21.

Kraus, M.J. and Aslan, A., 1993, Eocene hydromorphic paleosols: significance for interpretation ancient floodplain processes: Journal of Sedimentary Petrology, v. 63, no. 3, p. 453-463.

Kraus, M.J., 1999, Paleosols in clastic sedimentary rocks: their geologic applications: Earth-Science Reviews, v. 47, p. 41–70.

Kutzbach, J.E. and Gallimore, R.G., 1989, Pangaean Climates: Megamonsoons of the Megacontinent: Journal of Geophysical. Research, v. 94, no. D3, p. 3341-3357.

Mack, G.H., James, W.C., and Monger, H.C., 1993, Classification of paleosols: Geological Society of America Bulletin, v. 105, p. 129-136.

Martz, J.W., and Parker, W.G., 2010, Revised Lithostratigraphy of the Sonsela Member (Chinle Formation, Upper Triassic) in the Southern Part of Petrified Forest National Park, Arizona: PLoS ONE, v. 5, no. 2.

Matthews, W.J., Hampson, G.J., Trudgill, B.D., Underhill, J.R., 2007, Controls on fluviolacustrine reservoir distribution and architecture in passive salt-diapir provinces: Insights from outcrop analogs: AAPG Bulletin, v. 91 no. 10, p.1367-1403.

McCarthy, F., 2000, What Does Our Perspective on Deep Time Have to Offer in a New Millennium?: Palaios, v. 15. no. 1 p. 1-2.

Milner, R.C., 2006, Plant Fossils from the Owl Rock or Church Rock Members, Chinle Formation, San Juan County, Utah. From Harris et al., eds., The Triassic-Jurassic Terrestrial Transition, New Mexico Museum of Natural History and Science Bulletin, 37.

Mitchell, J.F.B., Lowe, J., Wood, R.A. and Vellinga, M., 2006, Extreme events due to human-induced climate change: Philosophical Transactions: Mathematical, Physical, and Engineering Sciences, v. 364, no. 1845.

Morton, N., and Hesselbo, S., eds., 2008, Details of voting on proposed GSSP and ASSP for the base of the Hettangian Stage and Jurassic System: International Subcommission on Jurassic Stratigraphy Newsletter, v. 35, part 1, December, 76 p.

Moore, D.M. and Reynolds, R.C. Jr., 1989, X-Ray Diffraction and the Identification and Analysis of Clay Minerals: Oxford, Oxford University Press, 332 p.

Mundil, R., 2007, Critical view of the calibration of the Triassic time scale: New Mexico Museum of Natural History and Science Bulletin, v. 41, p. 314-315.

Murray, P.A., 1990, Stratigraphy of the Upper Triassic Petrified Forest Member (Chinle Formation) in Petrified Forest National Park, Arizona, USA: The Journal of Geology, v. 98, no. 5, p. 780-789.

Mutti, M. and Weissert, H., 1995, Triassic monsoonal climate and its signature in Ladinian-Carnian Carbonate Platforms (Southern Alps, Italy): Journal of Sedimentary Research, v. B65, no. 3. p. 357-367.

Muttoni, G., Kent, D.V., Olsen, P.E., Di Stefano, P., Lowrie, W., Bernasconi, S.M., Hernandez, F.M., 2004, Tethyan magnetostratigraphy from Pizzo Mondello (Sicily) and correlation to the Late Triassic Newark astrochronological polarity time scale: Geological Society of America Bulletin, v. 116, p. 1043-1058.

Nesbitt, H.W., and Young, G.M., 1989, Formation and Diagenesis of Weathering Profiles: The Journal of Geology, v. 97, no. 2, p. 129-147.

Parker, W.G., Brinkman, D.L., Fox, M., Gauthier, J.A., Joyce, W.G., and Murray, L.K., 2006, New additions to the fauna of the Upper Triassic Chinle Formation of Utah, *in:* W.G. Parker, S.R. Ash and R.B. Irmis, eds., A Century of Research at Petrified Forest National Park: Geology and Paleontology. Museum of Northern Arizona Bulletin 62, p. 166–167.

Parker, W. G., and Clements, S., 2004, First year results of the ongoing paleontological inventory of Petrified Forest National Park, Arizona, *in:* Van Riper, III, C. and Cole, K. eds., The Colorado Plateau: Cultural, Biological, and Physical Research: University of Arizona Press, Tucson, p. 201-210

Parrish, J.T., 1993, Climate of the supercontinent Pangea: Journal of Geology, v. 101, p. 215– 253.

Parrish, J.T., 1985, Latitudinal distribution of land and shelf and absorbed solar radiation during the Phanerozoic: U.S. Geological Survey Open File Report, 85-31, 21 p.

Parrish, J.M., 1989, Vertebrate paleoecology of the Chinle Formation (Late Triassic) of the southwestern United States: Palaeogeography, Palaeoclimatology,, Palaeoecology, v. 72, p. 227-247.

Parrish, J.M., 2001, Interpreting Pre-Quaternary Climate from the Geologic Record: Columbia University Press, New York, 348 p.

Parry, W.T., Jasumback, M., and Wilson, P.N., 2002, Clay Mineralogy of Phyllic and Intermediate Argillic Alteration at Bingham, Utah: Economic Geology, v. 97, no. 2, p. 221-239.

Pirrie, D., Butcher, A.R., Power, M.R., Gottlieb, P., and Miller, G.L., 2004, Rapid

quantitative mineral and phase analysis using automated scanning electron microscopy (QemSCAN): Potential application in forensic geosciences, *in* Pye, K., and Crodt, D.J., eds., Forensic Geoscience: Principles, Techniques and Applications: Geological Society [London] Special Publication 232, p. 123–136.

Pipiringos, G.N. and O'Sullivan, R.B., 1978, Principal unconformities in Triassic and Jurassic rocks, Western Interior United States; a preliminary survey, *in:* Unconformities, correlations, and nomenclature of some Triassic and Jurassic rocks, Western Interior United States: U.S. Geological Survey Professional Paper, 1035-A, p. A1-A29.

Prochnow, S.J., Nordt, L.C., Atchley, S.C., Hudec, M., and Boucher, T.E., 2005, Triassic paleosol catenas associated with a salt-withdrawal minibasin in southeastern Utah, U.S.A.: Rocky Mountain Geology, v. 40, no. 1, p. 25-49.

Prochnow, S.J., Nordt, L.C., Atchley, S.C., and Hudec, M.R., 2006, Multi-proxy paleosol evidence for middle and Late Triassic Climate trends in eastern Utah: Paleogeography, Palaeoclimatology, Palaeoecology, v. 232, p. 53-72.

Ramezani, J., Hoke, G.D., D.E. Fastovsky, Bowring, S.A., Therrien, F., Dworkin, S.I., Atchley, S.C., and Nordt, L.C., 2011, High-precision U-Pb zircon geochronology of the Late Triassic Chinle Formation, Petrified Forest National Park (Arizona, USA): Temporal constraints on the early evolution of dinosaurs: GSA Bulletin, v. 123, no. 11/12, p. 2142-2159.

Retallack, G.J., 1990, Soils of the Past: An Introduction to Paleopedology: Boston, Unwin Hyman, 520 p.

Retallack, G.J., 2005, Pedogenic carbonate proxies for amount and seasonality of precipitation in paleosols: Geology, v. 33, no. 5, p. 333-336.

Riggs, N.R., Stewart, J.H., Haxel, G.B., and Conway, C.M., 1993, Sources of Chinle Formation volcanic detritus: Where and how big were they: Rocky Mountain Section GSA, v. 25, i. 5, p. 138-139.

Robert, C., Kennett, J.P., 1994, Antarctic subtropical humid episode at the Paleocene–Eocene boundary: clay–mineral evidence: Geology, v. 22, p. 211–214.

Robinson, P.L., 1971, A problem of faunal replacement on Permo-Triassic continents: Paleontology, v. 14, no. 1, p. 131-153.

Schaetzl, R. and Anderson, S., 2005, Soils, Genesis, and Geomorphology: Cambridge University Press, New York, 817 p.

Schaltegger, U., Guex, J., Bartolini, A., Schoene, B., and Ovtcharova, M., 2008, Precise

U-Pb age constraints for end-Triassic mass extinction, its correlation to volcanism and Hettangian post-extinction recovery: Earth and Planetary Science Letters, v. 267, p. 266-275.

Schoene, B., Guex, J., Bartolini, A., Schaltegger, U., and Blackburn, T.J., 2010, Correlating the end-Triassic mass extinction and flood basalt volcanism at the 100 ka level: Geology, v. 38, n. 5, p. 387-390.

Schultz, L.G., 1963, Clay minerals in Triassic Rocks of the Colorado Plateau: U.S. Geological Survey Bulletin 1147-C, p. C1-C47.

Schwartz, H.L. and Gillette, D.D., 1994, Geology and Taphonomy of the Coelophysis Quarry, Upper Triassic Chinle Formation, Ghost Ranch, New Mexico: Journal of Paleontology, v. 68, no. 5, p. 1118-1130.

Sellwood, B.W. and Valdes, P.J., 2006, Mesozoic climates: General circulation models and the rock record: Sedimentary Geology, v. 190, p. 269-287.

Smith, R.M.H. and Swart, R., 2002, Changing Fluvial Environments and Vertebrate Taphonomy in Response to Climatic Drying in a Mid-Triassic Rift Valley Fill: The Omingonde Formation (Karoo Supergroup) of Central Namibia: Palaios, v. 17, no. 3, p. 249-267.

Sroden, J. and Eberl, D.D., 1984, Illite: Reviews in Mineralogy, v. 13, p. 495-544.

Stewart, J.H., 1986, Late Triassic paleogeography of the southern Cordillera: The problem of a source for voluminous volcanic detritus in the Chinle Formation of the Colorado Plateau region: Geology, v. 14, p. 567-570.

Stewart, J.H., Poole, F.G., and Wilson, R.F., 1972, Stratigraphy and origin of the Chinle Formation and related upper Triassic strata in the Colorado Plateau region: U.S. Geological Survey, Professional Paper 690, p. 336.

Tanner, L.H., 2000, Palustrine-lacustrine and alluvial facies of the (Norian) Owl Rock Formation (Chinle Group), Four Corners Region, southwestern U.S.A.: Implications for Late Triassic paleoclimate. Journal of Sedimentary Research, v. 70, p. 1280-1289.

Tanner, L.H., Lucas, S.G., 2006. Calcareous paleosols of the Upper Triassic Chinle Group, Four Corners region, southwestern United States: climatic implications: Geological Society of America Special Paper 416, p. 53–74.

Tanner, L.H., Hubert, J.F., Coffey, B.P., and McInerney, D.P., 2001, Stability of atmospheric *p*CO2 levels across the Triassic/Jurassic boundary: Nature, v. 411, p. 675–677.

Therrien, F. and Fastovsky, D.E., 2000, Paleoenvironments of Early Theropods, Chinle Formation (Late Triassic), Petrified Forest National Park, Arizona: Palaios, v. 15, no. 3, p. 1994-211.

Tribble, J.S. and Yeh, H., 1994, Origin of smectite and illite-smecite in the Barbados accretionary complex: Oxygen isotopic evidence: Geology, v. 22, p. 219-222.

Vail, P.R., Mitchum, R.M. Jr, Thompson III, S., 1977, Seismic Stratigraphy and Global Changes of Sea Level, Part 4: Global Cycles of Relative Changes of Sea Level, *in:* Payton, C.E., ed., Seismic Stratigraphy Applications to Hydrocarbon Exploration, AAPG Memoir 26, p. 83-97.

Van Der Voo, R., Mauk, F.J., and French, R.B., 1976, Permian–Triassic continental configurations and the origin of the Gulf of Mexico: Geology, v. 4, p. 177–180.

Van Houten, F.B., 1964, Origin of Red Beds-Some Unsolved Problems. Problems in palaeoclimatology; proceedings, p. 647-661.

Whiteside, J.H., Grogan, D.S., Olsen, P.E., Kent, D.V., 2011, Climatically driven biogeographic provinces of Late Triassic tropical Pangea: PNAS, v. 108, no. 22, p. 8972-8977.

Wilkinson, B.H. 2005., Humans as geologic agents: A deep-time perspective: Geology, v. 33, no. 3, p. 161-164.

Witzke, B.J., 1990, Paleoclimatic constraints for Paleozoic paleolatitudes of Laurentia and Euramerica, *in:* McKerrow, W.S., and Scotese, C.R., eds., Paleozoic palaogeography, and biogeography: Geological Society (London) Memoir, p. 57-73.

Wilson, K.M., Pollard, D., Hay, W.W., Thompson, S.L. and Wold, C.N., 1994, General circulation model simulations of Triassic climates: preliminary results. In: Pangea: Paleoclimate, Tectonics and Sedimentation during Accretion, Zenith and Breakup of a Supercontinent, Klein, G.D., ed., Special Paper 288, Geological Society of America, Boulder, Colorado, p. 91-116.

Woody, D.T., 2006, Revised stratigraphy of the Lower Chinle Formation (Upper Triassic) of Petrified Forest National Park, Arizona, *in:* Parker, W.G., Ash, S.R, Irmis, R.B., eds. A Century of Research at Petrified Forest National Park 1906-2006: Museum of Northern Arizona Bulletin, no. 62, p. 17–45.

Zachos, J.C., Dickens, G.R., Zeebe, R.E., 2008, An early Cenozoic perspective on greenhouse warming and carbon-cycle dynamics: Nature, v. 451, p 279-283.

Ziegler, A.M., Scotese, C.R., and Barrett, S.F., 1983, Mesozoic and

Cenozoic paleogeographic maps, *in:* Brosche, P., and Sundermann, J., eds., Tidal Friction and the Earth's Rotation, II: Berlin, Springer-Verlag, p. 240–252.

Zuber, J.D., and Parnell, R.A., 1989, A new paleoclimatic indicator from Triassic Paleosols, Chinle Formation, Petrified Forest National Park, Arizona: Geological Society of America Abstracts with Programs, v. 21, i. 5, p. 163.